The influence of depth limited water conditions on the rock slope stability

Abstract

The hydraulic stability of the armour layer of rubble mound breakwaters has been widely discussed in literature and several empirical formulas have been proposed for design purposes. Nevertheless, few studies focused on the armour stability in case of water depth limited water conditions. Then, the aim of the present research is to provide more insights into the stability of the armour layer ranging from intermediate till extremely shallow water conditions. To this end, a 2D physical experiments have been carried out at the EUropean Maritime and Environmental Research (EUMER) laboratory of the University of Salento (Lecce), in presence of a 1V:30H foreshore. Tests aimed to investigate both the nearshore hydrodynamics and the hydraulic armour stability under different irregular waves attack. Experimental results are also compared with the damage evaluated from the empirical formulations available in literature, in order to investigate the predicted damage level in the shallowness range analyzed.

Cover image: 3D damage progression of a rubble mound breakwater, induced by the wave motion.

Stefano Marino

The influence of depth-limited water conditions on the rock slope stability

POLITECNICO DI BARI

D.R.R.S

Doctor of Philosophy in Environmental and Building Risk and Development

Coordinator: Prof. Michele Mossa

XXXV CYCLE
Curriculum: ICAR/02

DICATECh

Department of Civil, Environmental, Building Engineering and Chemistry

Stefano Marino

The influence of depth-limited water conditions on the rock slope stability

Prof. Leonardo Damiani[1]
Prof. Vito Iacobellis[1]
Prof.ssa Alessandra Saponieri[2]

[1]Department of Civil, Environmental, Building Engineering and Chemistry
[2]Department of Engineering for Innovation, University of Salento

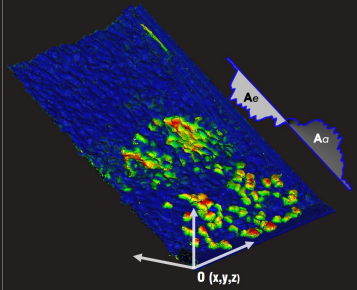

Politecnico di Bari

LIBERATORIA PER L'ARCHIVIAZIONE DELLA TESI DI DOTTORATO

Al Magnifico Rettore

del Politecnico di Bari

Il sottoscritto STEFANO MARINO nato a FOGGIA il 15/06/1991 residente a FOGGIA in VIA ROVELLI 28/A e-mail stefano.marino@poliba.it iscritto al 3° anno di Corso di Dottorato di Ricerca in Rischio e Sviluppo Ambientale, Territoriale ed Edilizio ciclo XXXV ed essendo stato ammesso a sostenere l'esame finale con la prevista discussione della tesi dal titolo:

The influence of depth-limited water conditions on the rock slope stability

DICHIARA

1) di essere consapevole che, ai sensi del D.P.R. n. 445 del 28.12.2000, le dichiarazioni mendaci, la falsità negli atti e l'uso di atti falsi sono puniti ai sensi del codice penale e delle Leggi speciali in materia, e che nel caso ricorressero dette ipotesi, decade fin dall'inizio e senza necessità di nessuna formalità dai benefici conseguenti al provvedimento emanato sulla base di tali dichiarazioni;
2) di essere iscritto al Corso di Dottorato di ricerca Rischio e Sviluppo Ambientale, Territoriale ed Edilizio ciclo XXXV, corso attivato ai sensi del "*Regolamento dei Corsi di Dottorato di ricerca del Politecnico di Bari*", emanato con D.R. n.286 del 01.07.2013;
3) di essere pienamente a conoscenza delle disposizioni contenute nel predetto Regolamento in merito alla procedura di deposito, pubblicazione e autoarchiviazione della tesi di dottorato nell'Archivio Istituzionale ad accesso aperto alla letteratura scientifica;
4) di essere consapevole che attraverso l'autoarchiviazione delle tesi nell'Archivio Istituzionale ad accesso aperto alla letteratura scientifica del Politecnico di Bari (IRIS-POLIBA), l'Ateneo archivierà e renderà consultabile in rete (nel rispetto della Policy di Ateneo di cui al D.R. 642 del 13.11.2015) il testo completo della tesi di dottorato, fatta salva la possibilità di sottoscrizione di apposite licenze per le relative condizioni di utilizzo (di cui al sito http://www.creativecommons.it/Licenze), e fatte salve, altresì, le eventuali esigenze di "embargo", legate a strette considerazioni sulla tutelabilità e sfruttamento industriale/commerciale dei contenuti della tesi, da rappresentarsi mediante compilazione e sottoscrizione del modulo in calce (Richiesta di embargo);
5) che la tesi da depositare in IRIS-POLIBA, in formato digitale (PDF/A) sarà del tutto identica a quelle **consegnate**/inviate/da inviarsi ai componenti della commissione per l'esame finale e a qualsiasi altra copia depositata presso gli Uffici del Politecnico di Bari in forma cartacea o digitale, ovvero a quella da discutere in sede di esame finale, a quella da depositare, a cura dell'Ateneo, presso le Biblioteche Nazionali Centrali di Roma e Firenze e presso tutti gli Uffici competenti per legge al momento del deposito stesso, e che di conseguenza va esclusa qualsiasi responsabilità del Politecnico di Bari per quanto riguarda eventuali errori, imprecisioni o omissioni nei contenuti della tesi;
6) che il contenuto e l'organizzazione della tesi è opera originale realizzata dal sottoscritto e non compromette in alcun modo i diritti di terzi, ivi compresi quelli relativi alla sicurezza dei dati personali; che pertanto il Politecnico di Bari ed i suoi funzionari sono in ogni caso esenti da responsabilità di qualsivoglia natura: civile, amministrativa e penale e saranno dal sottoscritto tenuti indenni da qualsiasi richiesta o rivendicazione da parte di terzi;
7) che il contenuto della tesi non infrange in alcun modo il diritto d'Autore né gli obblighi connessi alla salvaguardia di diritti morali od economici di altri autori o di altri aventi diritto, sia per testi, immagini, foto, tabelle, o altre parti di cui la tesi è composta.

Luogo e data, Bari, 24/04/2023

Firma

Politecnico di Bari

Il sottoscritto, con l'autoarchiviazione della propria tesi di dottorato nell'Archivio Istituzionale ad accesso aperto del Politecnico di Bari (POLIBA-IRIS), pur mantenendo su di essa tutti i diritti d'autore, morali ed economici, ai sensi della normativa vigente (Legge 633/1941 e ss.mm.ii.),

CONCEDE

- al Politecnico di Bari il permesso di trasferire l'opera su qualsiasi supporto e di convertirla in qualsiasi formato al fine di una corretta conservazione nel tempo. Il Politecnico di Bari garantisce che non verrà effettuata alcuna modifica al contenuto e alla struttura dell'opera.
- al Politecnico di Bari la possibilità di riprodurre l'opera in più di una copia per fini di sicurezza, back-up e conservazione.

Luogo e data, Bari 24/04/2023 Firma

Politecnico di Bari

Department of Civil, Environmental, Land, Building Engineering and Chemistry
Ph.D. Program Risk Environmental, Territorial and Building Development
SSD: ICAR/02– Hydraulic and Maritime Constructions and Hydrology

Final Dissertation

THE INFLUENCE OF DEPTH-LIMITED WATER CONDITIONS ON THE ROCK SLOPE STABILITY

by

Stefano Marino

Supervisors:

Prof. Leonardo Damiani
Prof. Vito Iacobellis
Prof.ssa Alessandra Saponieri

Coordinator of Ph.D. Program:

Prof. Michele Mossa

Course n°35, 01/11/2019-31/01/2023

Politecnico di Bari

Department of Civil, Environmental, Land, Building Engineering and Chemistry
Ph.D. Program Risk Environmental, Territorial and Building Development
SSD: ICAR/02–Hydraulic and Maritime Constructions and Hydrology

Final Dissertation

THE INFLUENCE OF DEPTH-LIMITED WATER CONDITIONS ON THE ROCK SLOPE STABILITY

by

Stefano Marino:

Referees:

Prof. Marcello Di Risio

Prof. Mariano Buccino

Supervisors:

Prof. Leonardo Damiani

Prof. Vito Iacobellis

Prof.ssa Alessandra Saponieri

Coordinator of Ph.D. Program:

Prof. Michele Mossa

Course n°35, 01/11/2019-31/01/2023

D.R.R.S

POLITECNICO DI BARI

Doctor of Philosophy in Environmental and Building Risk and Development

Coordinator: Prof. Michele Mossa

XXXV CYCLE
Curriculum: ICAR/02

DICATECh
Department of Civil, Environmental, Building Engineering and Chemistry

The influence of depth-limited water conditions on the rock slope stability

Prof. Leonardo Damiani[1]
Prof. Vito Iacobellis[1]
Prof.ssa Alessandra Saponieri[2]

[1]Department of Civil, Environmental, Building Engineering and Chemistry
[2]Department of Engineering for Innovation, University of Salento

Ph.D. Candidate: Stefano Marino

POLITECNICO DI BARI

D.R.R.S

Dottorato in Rischio e Sviluppo ambientale, territoriale ed edilizio

Coordinatore: Prof. Michele Mossa

XXXV CICLO
Curriculum: ICAR/02

DICATECh
Dipartimento di Ingegneria Civile, Ambientale, del Territorio, Edile e di Chimica

L'effetto sulla stabilità idraulica di un'opera di difesa costiera in massi a gettata, in presenza di acque limitate dalla profondità

Prof. Leonardo Damiani[1]
Prof. Vito Iacobellis[1]
Prof.ssa Alessandra Saponieri[2]

[1]Department of Civil, Environmental, Building Engineering and Chemistry
[2]Department of Engineering for Innovation, University of Salento

Dottorando: Stefano Marino

Index

INDEX I

LIST OF FIGURES 1

LIST OF TABLES 5

LIST OF SYMBOLS 6

EXTENDED ABSTRACT 9

ABSTRACT ESTESO 11

1. INTRODUCTION 14

1.1 Background and aim of the research 14

1.2 Thesis outline 17

2. LITERATURE REVIEW 20

2.1 Waves breaking criteria 20

2.2 Wave heights in depth-limited water conditions 22

2.2.1 Waves period in depth-limited water conditions and shallowness classification 26

2.3 Hydraulic stability of rubble mound breakwater 28

3. LABORATORY EXPERIMENTAL CAMPAIGN 40

3.1 Experimental design 40
3.1.1 Facilities and equipment 40
3.1.2 Physical scaled model 41
3.1.3 Test program 47
3.2 Data acquisition 51
3.2.1 Wave measurements 51
3.2.2 Pore Pressure measurements 54
3.2.3 Damage measurement 57
3.2.3.1 Overview of the available techniques for slope damage measurement 61
3.2.4 Photogrammetric damage measurement system 66
3.2.4.1 Photogrammetric technique 66
3.2.4.2 Acquisition campaign and 3D structure reconstruction 69
3.2.4.3 Laser profiler and photogrammetric 2D data interpolation 75
4. RESULTS AND DISCUSSION 78
4.1 Data Analysis 78
4.1.1 Wave analysis 78
4.1.2 Damage analysis 83
4.1.2.1 Validation of photogrammetric technique for damage evaluation 84
4.1.3 Pressure analysis 91
4.2 Waves in depth limited water conditions 95

4.3 Comparison with the existing hydraulic stability formulae in depth limited water conditions 98

5 CONCLUSION AND FUTURE REMARKS 110

ACKNOWLEDGMENTS 113

BIBLIOGRAPHY 115

ANNEX 1 – LONGITUDINAL SECTIONS OF THE WAVE FLUME 124

List of figures

Figure 1 Water depth around Europe, a categorical description Bosch et al. (2018). 15

Figure 2. Maximum crest angle physically possible. 20

Figure 3. Sketch of wave breaking parameters H_b and h_b Miche (1944). 21

Figure 4. Classification of breaking types EurOtop (2018)..... 22

Figure 5 The foreshore sketch that is represented in this study. Three possible locations for structures on the sea bed are indicated, as well as the spectral period at toe structure, $T_{m-1,0,t}$ and the water depth at the same point h_t. The offshore conditions are indicated by the offshore spectral wave characteristic period ($T_{m-1,0,o}$) and height ($H_{m0,o}$) respectively Hofland et al. (2017)..... 26

Figure 6 a) Wave Flume; b) The flume control room. 40

Figure 7 Top panel: longitudinal section of 2D wave flume; Bottom panel: Plan view of the wave flume. 41

Figure 8 Grading curves of the rocks used to build the physical model. 42

Figure 9: An hand-made instrument used to measure the stones dimensions. 44

Figure 10: Left panels show the aspect ratio and the right ones the Blockiness of the rocks used for building the armour layer of the tested structures. 45

Figure 11 Few steps of the set-up of the first layout. 47

Figure 12 Rubble-mound structure layouts: (a) WL1; (b) WL2; (c) WL3; (d) WL4. 47

Figure 13 Gravel spending beach at the end of the wave flume. 49

Figure 14: Shallowness classification of the performed experimental tests. 49

Figure 15 Wave probes acquisition card (AC) 51

Figure 16 Horizontal section of the 2D wave flume showing the first wave gauge configuration. 52

Figure 17: Wave run-up gauge..... 54

Figure 18: Installation phase inside the core of the rubble mound breakwater of pore pressure sensors. 55

Figure 19 Side view of the breakwater, specifically the relative distances between the pressure sensors are reported along with the two S.W.L. tested. 55

Figure 20 Wave impacting the rock armour slope. 57

Figure 21 Reference coordinate system. 58

Figure 22 Laser bed profiler system. 59

Figure 23 Top: example of mean initial (red curve) and final (black curve) profiles measured after wave attack (Test WL1-02 with $H_{m0,o} = 0.25$ m and $T_{m-1,0} = 2.57$ s).Bottom: the blue curve represents the spatial evolution of slope elevation changes (*dz*) with respect to the initial profile 60

Figure 24 Methodological workflow. 65

Figure 25 Deviation map reporting both absolute and relative distances between pre and post corresponding points. 68

Figure 26 Photogrammetric acquisition set up 70

Figure 27 Result of one of the photogrammetric reconstruction report that highlight that each point of the breakwater has been acquired by > 9 images 71

Figure 28 Example of point clouds pre and post wave test. 72

Figure 29 An example of the application of the zero-up crossing method for the test WL1-04 with Hs=0.302 m and Tm =1.795 s measured at the offshore gauge (WG1). 79

Figure 30 Temporal evolution of the free surface elevation η(t) (m); b) Wave spectra of the free surface elevation and computed at three different points along the wave flume from offshore till the structure toe (WG1-WG5-WG7) 80

Figure 31 a) – b) Comparison between the spectral wave period with and without the structure in place, offshore ($T_{m-1,0,o}$) and at the breakwater toe ($T_{m-1,0,t}$), respectively; c) comparison between the spectral wave height at the breakwater toe ($H_{m-1,0,t}$), with and without structure; d) comparison between the height measured without the structure and the height retrieve by applying a reflection coefficient evaluated offshore 82

Figure 32 Example of cross shore structure profiles acquired by laser profiler (blue lines) and extracted from images (red lines) before (left panel) and after (right panel) the wave test WL1-02 (see Table 11). 83

Figure 33 Example of comparison between the average profiles before (red curve) and after (black curve) the wave attack measured by the laser profile (left panel) and extracted from photogrammetry (right panel), for the test WL1-02 (see Table 11)..... 84

Figure 34 Top: Deviation maps, representing the absolute distances (top) and the distances computed in z (bottom), with the relative scalar fields, for the test WL1-02 ($H_{m0,o}$ = 0.25 m, $T_{m-1,0}$ = 2.57 s). Bottom: z-difference point Gaussian distribution for each test..... 89

Figure 35 Sensitivity analysis with respect to the Savitzy-Golay filter (top), the Morlet filter (middle) and the Zero phase digital filter (bottom). 92

Figure 36 Example of temporal variation of the adimensionalised internal setup for: a) an irregular test b) a regular test. 93

Figure 37 Left: Temporal variation p'(t) (meter of water column) of the horizontal filtered pressure signals for a time frame of 50 s for an irregular test; Right, Pressure spectra retrieved from the pressure time series for all the pressor devices placed on the same distance from the bottom. 94

Figure 38 Example of pore pressure damping trend inside the core of the breakwater for an irregular test, together with the mean wave heights measured by the 2 wave gauges (WG6 - WG7) placed at the structure toe. 95

Figure 39 The effect of the water depth-limited conditions on the ratio $H_{m0,o}/H_{m0,t}$. 96

Figure 40 The influence of the relative depth in different shallowness conditions, on the spectral breaker parameter $\xi_{m-1,0}$..... 97

Figure 41 The measure evolution of the spectral wave period at the breakwater toe $T_{m-1,0,t}$ as a function of the relative depth (on the left) and with a slope correction (on the right) (Hofland et al. (2017)). 98

Figure 42 Slope armour damage S as a function of the stability number $Ns = H/\Delta D_{n50}$, with $H = H_{m0,t}$. .. 99

Figure 43 The influence of the shallow water conditions on the ratio $H_{2\%,t}/H_{s,t}$..... 100

Figure 44 Top: Wave height distribution evaluated at two different locations along the wave flume for test serie WL4 with Hm0,o=0,25 m and Tp = 2,83 s; Bottom: Wave height distribution retrieved at two different locations along the wave flume for test serie WL1 with Hm0,o=0,25 m and Tp = 2,83 s.. 101

Figure 45 The experimental data compared to stability numbers with different wave characteristics, $H_{2\%}$, H_s and H_{m0}, respectively from left to the right. 102

Figure 46 Comparison between observed and predicted stability numbers (Van Gent et al. (2004) Eq.(2. 15)). The solid black line represents a perfect agreement between the results. 103

Figure 47 The experimental damage data classified in terms of water depth h_t and rock armour diameter D_{n50},plotted by using the equation (2. 17) reported in Van Gent et al. (2004). 104

Figure 48 Top: Present data compared to design formula and data by Van Gent et al. (2004) (2. 16); Bottom: Data in the deeper water conditions tested (Test Serie WL1 and WL2), compared to design formula..... 105

Figure 49 The experimental damage data classified in terms of water depth h_t and rock armour diameter D_{n50},plotted by using the equation (2. 19) reported in Eldrup et al. (2019). 106

Figure 50 The experimental dam age data classified in terms of water depth h_t and rock armour diameter D_{n50},plotted by using the equation (2. 21) reported in Etemad et al. (2020). 107

List of tables

Table 1 Classification of water conditions based on the relative depth parameter Van Gent (2000). ... 27

Table 2 Damage classification for a rubble mound breakwater, van der Meer (1988). ... 32

Table 3 Main parameters for the existing formulae previous exposed. The different datasets on which have been calibrated are reported Thompson & Shuttler (1975), van der Meer (1988), Van Gent et al. (2004), Vidal et al. (2006),Herrera et al. (2017) and Eldrup & Andersen (2019). ... 37

Table 4 - Rock's characteristics. ... 42

Table 5. The values of LT and BLc for each armour stones used during the tests. ... 45

Table 6. Rock grading classification based on CIRIA, CUR, CUTMEF (2007). ... 45

Table 7 Main parameters of the tests performed. ... 50

Table 8 Absolute distances of wave gauges from the wave paddle. ... 53

Table 9 Main parameters of the tests performed in order to measure pore pressures ... 56

Table 10 Physical model parameters and photogrammetric characteristics (R_h=height resolution, E_{rep}=reprojection error, d_{points}=point density). ... 74

Table 11 Results from the application of both measurement techniques and relative standard statistics (E_r and R^2). ... 86

Table 12 Time estimation for retrieving the level of damage of the structure by applying both the photogrammetry and laser profiler method. ... 90

List of symbols

Name	Symbol	Unit
Gravitational acceleration	g	m/s^2
Mass density of the armour rock	ρ_r	kg/m^3
Mass density of the water	ρ_w	kg/m^3
Relative mass density, $\Delta = \rho_r / \rho_w - 1$	Δ	-
Offshore water depth	h	m
Water depth at the breaker point	h_b	m
Water depth at structure toe	h_t	m
Number of waves	N_w	-
Breaker index Miche (1944)	γ_b	-
Wave celerity	c	m/s
Significant wave height at breaker point	H_b	m
Statistical wave height (offshore)	$H_{z,o}$	m
Statistical wave height (structure toe)	$H_{z,t}$	m
Significant wave height in the time domain	H_s	m
Root- mean square wave height	H_{rms}	m
Significant wave height in deep water (offshore)	$H_{s,o}$	m

Significant wave height at the slope's toe	$H_{s,t}$	m
Spectral wave height in deep water $H_{mo} = 4(m_0)^{1/2}$	$H_{m0,\,o}$	m
Spectral wave height at the slope's toe	$H_{m0,\,t}$	m
n^{th} moment of the frequency spectrum	m_n	-
Mean wave period	T_m	s
Spectral wave period in deep water (offshore)	$T_{m-1,0,\,o}$	s
Spectral wave period at the slope's toe	$T_{m-1,0,\,t}$	s
Significant wave period	T_s	s
Peak wave period	T_p	s
Wave steepness based on significant wave characteristics, $s_{om} = 2\pi H_s/(gT_m^2)$	s_{om}	-
Wave steepness based on spectral wave characteristics, $s_{om-1,0} = 2\pi H_{m0}/(gT_{m-1,0}^2)$	$s_{om-1,0}$	-
Mean Breaker parameter, $\xi_m = \tan\alpha/(s_{om})^{0.5}$	ξ_m	-
Spectral Breaker parameter, $\xi_{m-1,0} = \tan\alpha/(s_{om-1,0})^{0.5}$	$\xi_{m-1,0}$	-
Seaside/leeside slope angle of the breakwater	α	-
Foreshore angle	Θ or m	-
Mean sieve diameter, 15% of mass not exceeded	D_{15}	m

Mean sieve diameter, 50% of mass not exceeded	D_{50}	*m*
Mean sieve diameter, 85% of mass not exceeded	D_{85}	*m*
Mean mass of the armour rock grading (50% value by mass)	M_{50}	*kg*
Nominal Diameter of the armour rock	D_{n50}	*m*
Nominal diameter of the structure core	$D_{n50,\ core}$	*m*
Weight of individual armour units	W_r	*kg*
Effective coefficient of friction between armour units	μ	-
Notional permeability	*P*	-
Length to thickness ratio, LT=L/d	*LT*	-
Reference coordinate system of the wave flume	*x-y-z*	*m*
Dimensions of the smallest box that can enclose a rock	*X-Y-Z*	*m*
Blockiness coefficient = 100% rock volume * 1/XYZ	*Blc*	-
Area of the erosion area	A_e	m^2
Level of damage retrieved from the erosion profile, $S = A_e/D_{n50}^2$	*S*	-

Extended abstract

The hydraulic stability of the armour layer of rubble mound breakwaters has been widely discussed in literature and several empirical formulas have been proposed for design purposes. Nevertheless, few studies focused on the armour stability in case of water depth limited water conditions. Then, the aim of the present research is to provide more insights into the stability of the armour layer ranging from intermediate till extremely shallow water conditions. To this end, a new 2D physical experiments have been carried out at the EUropean Maritime and Environmental Research (EUMER) laboratory of the University of Salento (Lecce), in presence of a 1V:30H foreshore. Tests aimed to investigate both the nearshore hydrodynamics and the hydraulic armour stability under different irregular waves attack. Experimental results are also compared with the damage evaluated from the empirical formulations available in literature, in order to investigate the predicted damage level in the shallowness range analyzed.

Furthermore, an innovative method, based on photogrammetry, for the measurement of the damage of rock slope structures (i.e. depth and extension of the damaged area) has been developed. The approach has been tested and validated during the experimental campaign. Photogrammetric outputs have been compared with the laser derived profiles, under different structures layouts and hydrodynamic conditions. Results have proven to be highly accurate (relative error lower than 5%), with time and cost-effective equipment (standard digital camera) and simple acquisition and processing procedures.

Also the results of the impact of depth-limited water conditions on wave-induced dynamic pressures in a rubble mound breakwater are presented. Physical model tests performed in the wave flume allowed to assess the effects of such conditions on the attenuation of pore pressures through a porous body of the structure.

Key words: rubble mound breakwaters, hydraulic stability, physical model, shallow foreshore, depth limited water conditions.

Abstract esteso

Le aree costiere sono in rapido sviluppo come poli di attrazione per le attività economico-turistiche, commerciali e, come tali, sede di un notevole fenomeno di urbanizzazione. Diventa cruciale, dunque, la gestione e la protezione di queste aree al fine di prevenire il rischio di inondazione e aumentare la resilienza delle infrastrutture e della popolazione che ivi risiede. Al fine di perseguire tale obiettivo, risulta necessario intervenire attraverso la progettazione di nuove opere di difesa costiera o l'adeguamento di quelle esistenti. Le conoscenze attuali spesso si scontrano con i nuovi limiti e le sfide imposte dai fenomeni indotti dal cambiamento climatico (e.g., innalzamento del livello medio del mare, maggiore frequenza e intensità degli eventi estremi). In tal senso, lo studio dei fenomeni di interazione onda/struttura, hanno lo scopo di approfondire la conoscenza dei processi di idrodinamica sotto-costa in presenza di strutture di difesa a gettata, attraverso modellazione fisica e numerica, e, in particolare, di investigare la stabilità delle suddette strutture in condizioni di acque basse, per le quali la letteratura di riferimento presenta alcune limitazioni. In tal senso, il presente lavoro è stato finalizzata allo studio della stabilità idraulica di un'opera di difesa costiera di massi a gettata, attraverso modellazione fisica bidimensionale (2D), in presenza di un fondale di pendenza 1V:30H, svolta presso il canale di moto ondoso sito presso il Laboratorio EUropean Maritime Environmental Research (EUMER) dell'Università del Salento (Lecce). Durante le attività sperimentali, sono state effettuate: i) le misure del danno subito della struttura, variando i layouts della stessa e le condizioni idrodinamiche al contorno; ii) la calibrazione e validazione di un metodo basato sulle tecniche di fotogrammetria per la valutazione del danno della struttura; iii) l'acquisizione di misure di pressione al fine di ricostruire il campo delle pressioni all'interno della scogliera indotto dal moto ondoso.

Key words: stabilità idraulica, modellazione fisica, fondale a debole pendenza, condizione di acque a profondità limitata, opere di difesa costiera in massi a gettata.

CHAPTER 1
INTRODUCTION

"I stand upon my desk to remind myself that we must constantly look at things in a different way." (Dead Poets Society, 1989).

1. Introduction

1.1 Background and aim of the research

In the field of coastal engineering, the topic of wave-structure interaction has been extensively investigated over the years. Many studies have been focused on wave overtopping, reflection, run-up and hydraulic stability of coastal structures.

The rising sea water level induced by the climate change requires further research developments towards a thorough comprehension about wave coastal structure interaction (Glavovic et al. (2022)). It is well known that storms intensity and frequency are gradually increasing (Pörtner et al. (2022)), thus reducing the efficacy of coastal defence structures, which often prove to be inadequate or even face the risk of failure during short-duration, extreme storms (Saponieri et al. (2018)). Hence, the rehabilitation or the design of new structures is often required, in order to assure the protection against flooding of coastal urbanized areas.

Rubble mound breakwaters can be counted among the most widespread and explored coastal defence structures CIRIA, CUR, CUTMEF (2007). A breakwater, placed in deep or shallow waters, aims to protect port, basins or beaches against flooding and erosion phenomena. Their principal task is to reduce the energy of the approaching waves by forcing their breaking. They are generally built with different layers of material (mainly sand and gravel), armoured by rocks or concrete armour units. Often, to reduce the environmental and economical impact of such structures, they are built as submerged or low crested, even allowing a small amount of overtopping on the leeside (Ahrens (1989); Argente et al. (2018); Burcharth et al. (2006); Vidal (1992)).

In the surf zone, wave breaking occurs over the seabed bathymetry seaward of the structures toe. In contests characterized by a steep bathymetry (e.g., Mediterranean sea as depicted in Figure 1), this phenomenon usually happens at depths of around 3-4 m, close to the coast.

The design of such structures in limited depth water conditions, namely the estimation of the wave characteristics at structure toe ($H_{mo,t}$ and $T_{m1-0,t}$), is not an easy task. The

presence of a gentle foreshore induces wave breaking and the release of the bound long waves that play an important role in the wave structure interaction process (Smith et al. (2003)). Indeed, in many countries, especially in northern Europe (e.g., Belgium, Netherlands), mound breakwaters and others coastal defence structures (i.e., coastal dikes) are realized in limited depth (~ 1 m), since the seabed bathymetry is characterized by gentle slope, and a design depth of 3 or 4 m would be placed too far from the coast, thus reducing the protective effect of the structure.

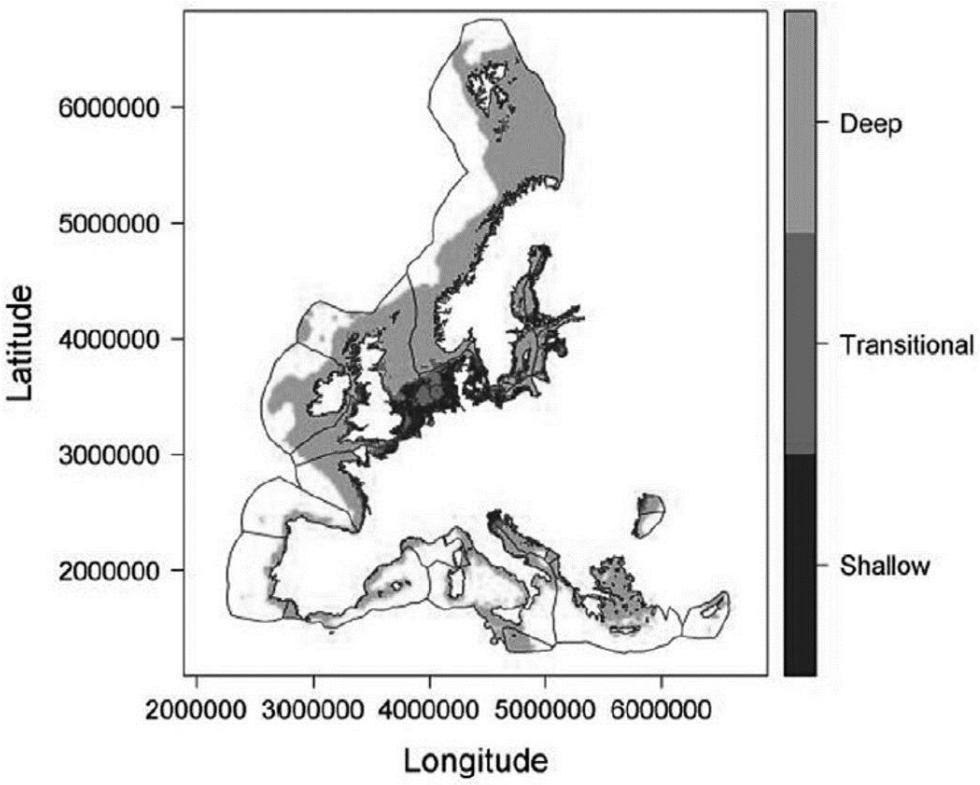

Figure 1 Water depth around Europe, a categorical description Bosch et al. (2018).

Therefore, in the last decades, different studies have been conducted aimed at investigating the influence of shallow water conditions on wave structure interaction, which encompasses phenomena from medium to local scale (Van Gent (2000); Van

Gent et al. (2004); Van Gent & Smith (1999)). Nowadays, these topics are still an open field of research, about which many authors have provided new insights (Altomare et al. (2016); Eldrup & Andersen (2019); Lashley et al. (2021)).

In this contest, the synergy between the numerical and physical tools is essential to address future challenges of climate change, whose effects on coastal systems and infrastructures could be predicted by the integration of these two (Frostick et al. (2019)). Indeed, despite the use of numerical models is increasingly being frequent (e.g., SPH, OpenFOAM), due to the progressive growth of informatics expertise, physical laboratory experiments and field campaigns remain the most affordable methodologies. In fact, laboratory facilities have faced many improvements in the last decades, above all: i) the development of advanced technologies and equipment, which provide the opportunity to observe 3D phenomena under controlled boundary conditions, and ii) the exploitation of non-intrusive techniques, automated data acquisition and analysis systems, which are able to provide a big amount of data with high spatial and temporal resolution, useful for validating numerical models.

In particular, the present work will address the problem of the hydraulic stability of a conventional multi layered rubble mound breakwaters in case of depth limited water conditions. The aim of the research is to provide more insights about the stability of the armour layer, ranging from intermediate till extremely shallow water conditions. To this end, new 2D physical experiments have been carried out at the EUropean Maritime and Environmental Research (EUMER) laboratory of the University of Salento (Lecce), in presence of a 1V:30H foreshore. Tests aimed to investigate both the nearshore hydrodynamics and the hydraulic armour stability under different irregular wave loading.

1.2 Thesis outline

The Ph.D thesis has been structured as follows:

- Chapter 1 details the background and the goals of the present research;
- Chapter 2 supplies a review of the literature related to the design of coastal structures in depth-limited water conditions, mainly: i) wave transformations in presence of shallow foreshore are described and the main methods developed to estimate wave characteristics ($H_{mo,t}$ and $T_{m1-0,t}$) is such conditions are reported; ii) a general description of hydraulic stability of mound breakwaters is provided; iii) the main hydraulic stability formulas for the design of rock armours in shallow water conditions are examined;
- Chapter 3 deals with: i) the description of the physical model tests of a double-layer rock armours breakwater placed in shallow water with a mildly slope foreshore of 1V:30H; ii) data acquisition and mainly the techniques and the methodological workflow used to measure the damage of the structure;
- Chapter 4 reports the results of the experimental campaign (wave, pressure and damage measurements). The comparison of the damage results with the main available formulations in literature Van Gent et al. (2004).
- Chapter 5 provides the main conclusions of the study and future research.

CHAPTER 2
LITERATURE REVIEW

"Sea waves are generated by the wind and propagate over the surface.
When they approach the shore, they break and disappear
People have amused themselves in watching
wave breaking at the shore."(Y. Goda, 1975)

2. Literature review

2.1 Waves breaking criteria

Since the present work deals with the wave structure interaction in shallow waters, it becomes necessary to describe the main phenomenon (e.g., breaking) that occur to the waves when they approach a sloping seabed during the propagation towards the coast. A wave crest becomes unstable and starts breaking when the particle velocity exceed the velocity of the wave crest (the wave celerity *c*). this breaking condition corresponds to a crest angle of about 120° (Figure 2). This phenomenon is also truthful in deep waters.

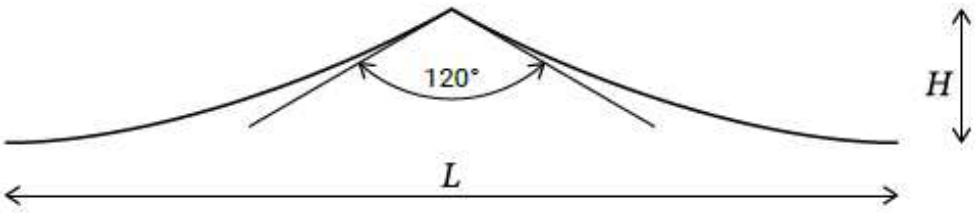

Figure 2. Maximum crest angle physically possible.

The historic work of Miche (1944) expressed the limiting wave steepness based on Stokes wave theory:

$$\left[\frac{H}{L}\right]\max = 0.142\tanh\left(kh\right) \tag{2. 1}$$

this quantity is almost equal to 1/7 in deep water condition, when this limit is exceeded, steepness induced wave breaking (recognizable as white capping) occurs. Instead , in shallow water the Miche formulation becomes:

$$\gamma_b = \left[\frac{H}{h}\right]\max = \frac{H_b}{h_b} \cong 0.88 \tag{2. 2}$$

where γ_b is the breaker index and H_b and h_b are the wave height and the water depth at the braker point respectively. The breaker index shows that in the shallow near-shore zone wave-breaking of individual waves starts when the wave height becomes greater than a certain fraction of the water depth. This is called depth-induced breaking since the limiting wave height is governed by a water depth limitation (Figure 3).

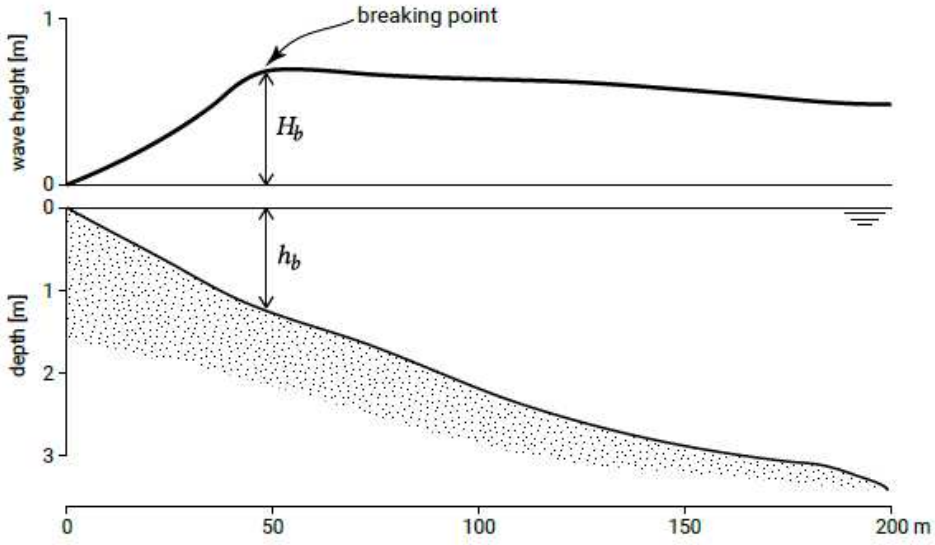

Figure 3. Sketch of wave breaking parameters H_b and h_b Miche (1944).

The above breaking wave relations were derived for a horizontal bottom. In reality the bottom is sloping, which affect the breaker index.

In the work of Battjes (1974) the study of the process of wave breaking on a slope was faced, depending on the wave significant properties and the angle of the bed slope.

The breaking takes place in various different ways and it is governed by the Iribarren parameter which was generally defined as follows:

$$\xi_m = \frac{\tan\alpha}{\sqrt{H_{s,o}/L_{m,o}}} \tag{2. 3}$$

where, $tan\alpha$ is the bed slope while $H_{s,o}$ and $L_{m,o}$ are the wave characteristics evaluated offshore.

Based on the values of ξ_m , in Figure 4 a distinction among the types of breakers was made. Generally is possible to distinguish, spilling, plunging, surging and collapsing breakers as depicted.

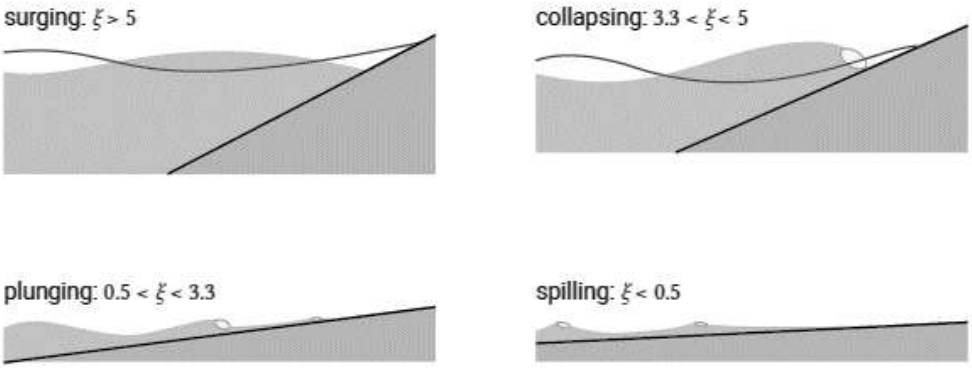

Figure 4. Classification of breaking types EurOtop (2018).

2.2 Wave heights in depth-limited water conditions

As stated in section 2.1 the waves behaviour drastically change according to the water conditions. In fact, in deep water, the free surface elevation over time usually follows a Gaussian process and it was achieved to be statistically described by a Rayleigh distribution Longuet-Higgins (1952), as reported in the following expression:

$$f_{\mathrm{H}} = P\{\mathrm{H} < H\} = 1 - exp\left[-\left(\frac{H}{H_{rms}}\right)^2\right]$$

(2. 4)

In this way, all the quantiles of the empirical cumulative distribution function of the individual waves were theoretically correlated, since fixed ratios exist between them, for instance, $H_{s,o}/H_{rms} \approx 1.416$.

In shallow water, the situation is completely different. Wave transformations (e.g., shoaling) distorts the wave profile, the crest height becomes predominant, and the flat shallow troughs are almost unrecognizable. Then, the surface elevation no longer follows a Gaussian process and the knowledge of the statistical wave characteristics is more complicated. The situation is aggravated by the wave breaking which causes the release of the bound spectral components.

So, over the years, many authors struggled to derive a method able to calculate the wave heights distribution in shallow water even in case of waves breaking (Collins (1970); Dally (1992), (1990); Dally & Dean (1986); Kuriyama (1996); Mase & Iwagaki (1982)). The idea of these studies, was to cut-off the portion of wave height distribution beyond the breaker height that is governed by the water depth and other factors.

The distribution of the wave heights in the surf zone (where wave breaking occur) was originally estimated by a numerical model developed by Goda (1975). The proposed model incorporated: i) the above cited breaking model; ii) the estimation of the wave set-up by means the theory of Longuet-Higgins (Longuet-Higgins (1952)) through the application the radiation stress concept. The applied formula to retrieve the differential equation for the amount of the wave setup $\bar{\eta}$ is reported as follows:

$$\frac{d\bar{\eta}}{dx} = -\frac{1}{(\bar{\eta} + h)} \frac{d}{dx}\left[\frac{1}{8} H_{rms}^2 \left(\frac{1}{2} + \frac{2kh}{sinh2kh}\right)\right]$$

(2. 5)

iii) the formula of the surf beat amplitude. The numerical model was accurately validated through the comparison with both laboratory and field observation data.

Later on Thornton & Guza (1983), developed a theoretical model able to describe the transformation of random wave heights in the surf zone based on energy flux balance. The model was calibrated and validated against a set of experimental and field data acquired. The author stated that the random nature of the wave heights was well described by applying a Rayleigh distribution both in deep water and nearshore. In the model was assumed that the energy dissipation rate was mainly due to wave breaking and bed friction.
An interesting semi empirical adaptations of the Rayleigh distribution of the wave heights was furnished in Glukhovskiy (1966) which generalized the Rayleigh distribution by substituting the exponent 2 (2. 4) with a function of the ratio between the wave height and water depth.

Battjes & Groenendijk (2000) based on the observations of many wave heights Rayleigh distributions on shallow foreshores, noticed a clear transition between higher and lower waves, since that were able to demonstrate that the Composite Weibull Distribution (CWD) was valid for the modelling of depth-limited waves. The CWD is a simple combination of two Weibull distribution whose continuity is guaranteed by imposing the condition $f_1(H_{tr}) = f_2(H_{tr})$(2. 6).

$$f_H = P\{H \leq H\} = \begin{cases} f_1(H_{tr}) = 1 - exp\left[-\left(\frac{H}{H_1}\right)^{k_1}\right] & H \leq H_{tr} \\ f_2(H_{tr}) = 1 - exp\left[-\left(\frac{H}{H_2}\right)^{k_2}\right] & H \geq H_{tr} \end{cases}$$

(2. 6)

Where, k_1 and k_2 are the shape parameters of the distribution equal to 2 and 3.6 respectively, H_1 and H_2 are scale parameters and H_{tr} is the transitional wave height which depends on the bed slope and the local water depth (h) as reported in (2. 7).

$$H_{tr} = (0.35 + 5.8\, tan\theta)h$$

(2. 7)

The H_{rms} was then related to wave energy parameters namely, variance of the surface elevation (m_o) and spectral wave height ($H_{m1\text{-}0}$) thus overcoming the limitations of previously method especially in shallow waters.

$$H_{rms} = (2.69 + 3.24\,\sqrt{m_0}/_h)\sqrt{m_0} \tag{2. 8}$$

Through this parameters, Battjes & Groenendijk (2000) provided a table with different normalised characteristic wave height: $H_{1/3}/ H_{rms}$, $H_{1/10}/H_{rms}$, $H_{2\%}/H_{rms}$, $H_{1\%}/H_{rms}$, and $H_{0.1\%}/H_{rms}$.

A simple and used empirical method was proposed by Goda (2000). The author, starting from the assumption that the wave characteristics in the breaking zone are influenced by many parameters (e.g., seabed slope, wave steepness), retrieved a series of graph. In order to evaluate spectral wave height ($H_{m1\text{-}0,t}$) for a given steepness and various sloping bathymetries, ranging from 1V:10H to 1V:100H. However, the approach doesn't take into account the effect of long waves generate by wave breaking nor a variation of the wave period.

Recently, Lashley et al. (2021) on the basis of the work of Goda (2000), developed a prediction methodology able to retrieve the spectral wave height at both vertical and sloping structures toes with a shallow foreshore, by means a simple linear relationship.

$$\frac{H_{m1-0,t}}{H_{m1-0,o}} = M\,\frac{h_t}{H_{m1-0,o}} + C \tag{2. 9}$$

With $M=0.35(\tan\theta^{0.10}/s_{0m1\text{-}0}{}^{0.2})$ and $C= 0.95(\tan\theta)^{0.15} - 0.30$ the slope and the intercept of the relationship respectively. Although the formulation is only limited to the range for which was validated since not much data are available with shallow foreshores, it presents the great advantage to relate the wave at structure toe, necessary for design

purposes, to readily available parameters such as offshore wave height, wave steepness and the foreshore slope.

2.2.1 Waves period in depth-limited water conditions and shallowness classification

Over the last years, the influence of the spectral wave period (T_{m1-0}) on different processes related to wave-structure interactions (e.g., hydraulic stability, wave run-up, wave overtopping) was achieved by Hofland et al. (2017). Particularly interesting is the situation depicted in Figure 5 , when the structure is placed in shallow foreshore. In fact in such cases the $T_{m10,t}$ is strongly influenced by the generation of low-frequencies waves (Munk (1951)), making it difficult to evaluate.

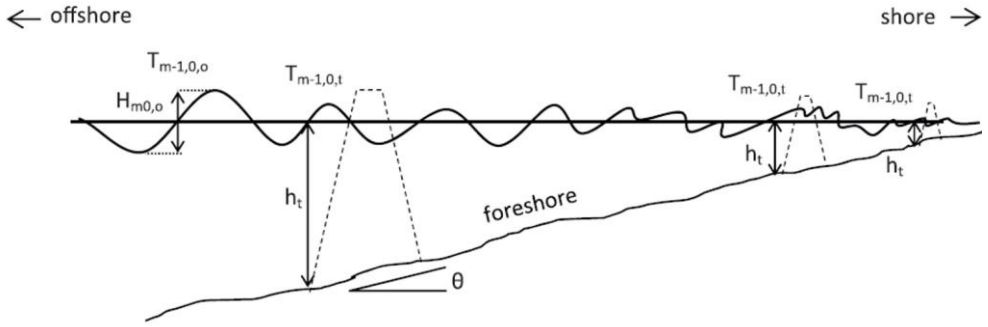

Figure 5 The foreshore sketch that is represented in this study. Three possible locations for structures on the sea bed are indicated, as well as the spectral period at toe structure, $T_{m-1,0,t}$ and the water depth at the same point h_t. The offshore conditions are indicated by the offshore spectral wave characteristic period ($T_{m-1,0,o}$) and height ($H_{m0,o}$) respectively Hofland et al. (2017).

Recently, a straightforward formulation was presented in Hofland et al. (2017), validated against different experimental dataset available in literature (Altomare et al. (2016); Chen et al. (2016); Van Gent (2000))

$$\ddot{h} = \frac{h_t}{H_{m0,o}} \left(\frac{cot\theta}{100} \right)^{0.2} \tag{2. 10}$$

$$\frac{T_{m1-0,t}}{T_{m1-0,o}} = 6 \exp(-4\ddot{h}) + \exp(-\ddot{h}) + 1 \tag{2. 11}$$

Mainly, it depends on two parameters, the offshore spectral wave period ($T_{m1-0,o}$) and $\ddot{h}$ that is a function both of relative depth and foreshore slope as reported in ((2. 11)
Since in the present work, the foreshore plays a key role in the phenomenon investigated, it is important to provide a consistent definition. In the field of coastal engineering a clear description of the foreshore is reported in Hofland et al. (2017) as, "*the part of the seabed bathymetry seaward of the structure toe that is characterized by depth induced wave processes such as depth induced wave breaking*".
The shallowness of the foreshore is characterized by the ratio between the spectral wave height offshore ($H_{m0,o}$) and the water depth at the toe of the structures (h_t); this parameter is called relative depth (Table 1).

Table 1 Classification of water conditions based on the relative depth parameter Van Gent (2000).

Relative depth	**Water conditions**
$H_{m0,o}/h_t < 0.4$	Deep
$0.4 < H_{m0,o}/h_t < 0.75$	Intermediate
$0.75 < H_{m0,o}/h_t < 1.5$	Shallow
$1.5 < H_{m0,o}/h_t < 3$	Very Shallow
$H_{m0,o}/h_t > 3$	Extremely Shallow

Similarly, in Hofland et al. (2017) another shallowness classification was reported based on the inverse of the relative depth. Furthermore the author provided a detailed illustration of each category, mainly:

- Deep with $H_{m0,o}/h_t<0.4$ (or $h_t/H_{m0,o}>4$), in this condition no depth-induced wave breaking nor shoaling occurs;
- Shallow $0.75<H_{m0,o}/h_t<1.5$ (or $1< h_t/H_{m0,o}<4$), it occurs when depth starts to influence wave propagation, the wave spectrum is almost identical to the one offshore, with a single peak, even if some minor peaks are recognizable at the low frequencies.
- Very shallow $1.5<H_{m0,o}/h_t<3$ (or $0.3< h_t/H_{m0,o}<1$), now the water depth has a strong influence on the wave characteristics. In fact the wave height can be reduced of 50%-60% of the offshore heights. The spectrum has totally changed its aspect, the wave energy at frequencies around 0,4Hz-0.5 Hz is almost dissipated, on contrary, a big amount the energy is appeared at the low frequencies;
- Extremely shallow $H_{m0,o}/h_t>3$ ($h_t/H_{m0,o}<0.3$), in this last case, all the high frequencies of the original wave spectrum has been dissipated, the only energetic content is related to the infragravity waves (low frequencies).

2.3 Hydraulic stability of rubble mound breakwater

The design of a rubble mound breakwater is governed by multiples variables:
Hydraulic parameters: both statistical and spectral wave characteristics. The former ones are the significant wave height ($H_{s,t}$) measured at the toe of the structure and the wave mean period (T_m) , whereas the latter ones are the spectral wave height ($H_{mo,t}$) and the spectral wave period ($T_{m1,0}$) (or the peak period, T_p). Generally, the wave characteristics are presented through a single parameter called wave steepness, $s = \frac{2\pi H}{gT^2}$. It is calculated by using the deep-water wavelength $L_{m,o} = gT^2/2\pi$. Sometimes, the resulting wave steepness is fictious because the wave characteristics

are taken in front of the structure. The steepness is noted with two symbols, i.e., s_{op} or s_{om} depending if it accounts for statistical or spectral characteristics. The surf similarity parameter is used to describe the type of breaking on the structure, it is defined as follow $\xi_m = tan\alpha/\sqrt{s_m}$ On the base of the steepness the breaker parameter could be defined in different way. The main hydraulic responses of the structure are wave run-up, wave run-down, wave overtopping, wave reflection and wave transmission. These phenomena are related to the parameters listed before.

Structural parameters: as defined in van der Meer (1988) they can be classified in four groups related to: 1) waves, 2) rocks, 3) cross–section and 4) response of the structure. A relation between the wave characteristics and the structure is defined by the stability number $N_s = H/\Delta D_{n50}$ where H (statistic or spectral) is measured at toe structure, $\Delta = \frac{\rho_r}{\rho_w} - 1$ is the relative buoyant and ρ_r and ρ_w the mass density respectively of rock and water; D_{n50} is the nominal diameter of the armour layer.

The response of the structure could be described in term of damage as $S = A_e/Dn_{,50}^2$, where A_e is the erosion area and Dn_{50} is the rock nominal diameter of the armour. In Campos et al. (2020) an extensive literature review of the breakwater damage descriptor is reported.

Some of the early research on hydraulic stability of rock armoured rubble mound breakwaters were performed in the 1930s. Iribarren (1938) and Hudson (1959) were some of the first to investigate the hydraulic stability of rock armoured rubble mound breakwaters. The physically based Iribarren's formula could be applied to determine the weight of individual armour units (W_r) just once the effective coefficient of friction between armour units (μ) had been determined. Hudson (1959) found out that the W_r, was strongly depended on the μ estimation which, in turn, was hard to estimate especially in small scale tests. Then a new formula (2. 12) was developed by Hudson (1959) able to estimate the required weight of the rock material based on front slope angle ($\cot\alpha$), rock diameter(D_{n50}), wave height ($H_{s,t}$), the reduced relative density ($\Delta =$

$\rho_r/\rho_w - 1$) and a dimensionless parameter that depends on the damage level of the armour layer (K_D).

$$N_s = \frac{H_{s,t}}{\Delta D_{n50}} = (K_D cot\alpha)^{1/3} \quad (2.\ 12)$$

The description of the wave breaking type was first introduced by Iribarren & Nogales (1952) by the surf similarity parameter, also known as the Iribarren number. Battjes (1974) used the surf similarity parameter to separate the wave breaking types into three categories: spilling, plunging, and surging or collapsing breakers. The same descriptions are used to describe the wave breaking type on the front slope of the breakwater.

Since the pioneering work of Hudson (1959), several studies have been conducted to define the design of breakwaters, mostly aimed at evaluating their hydraulic stability by means of the calculation of the stability number (Ns), given the designed level of structure damage (S). The parameter N_s, as previously seen, is a function of both wave and rocks characteristics, from which the mean weight of the individual armour unit can be estimated.

The dimensionless damage S is typically quantified through the evaluation of rock displacements. Physically, it corresponds to the number of elements, enclosed within an ideal cube with a side equal to D_{n50}, dislocated by waves. Despite the damage depends on many factors (i.e. porosity, shape and grading of the armour stones), S is actually defined as the eroded area (A_e Broderick (1984)) normalized by the square of the nominal mean stones diameter, Eq. (2. 13).

$$S = \frac{A_e}{D_{n50}^2} \quad (2.\ 13)$$

Thus, given the design level of damage (S), the D_{n50} of the armour rock can be derived under different hydrodynamic conditions and structure layouts (Thompson & Shuttler (1975); van der Meer (1988); Van Gent et al. (2004)).

In Thompson & Shuttler (1975) were reported tests with irregular waves in deep water wave conditions from which they established a stability formula. Later on, this extensive work was extended by van der Meer (1988) who performed a new large experimental campaign aimed at investigating the influence of many parameters e.g., wave period porosity, number of waves, wave steepness, type of armour layer) on the structure stability, mainly in deep water conditions, without any depth-induced wave breaking.

The formulae by van der Meer (1988) is widely used in design practice (e.g.,CIRIA, CUR, CUTMEF (2007)) and in research, to estimate the required size of the rock armour units for conventional rubble mound breakwaters (2. 14).

$$\frac{H_{s,t}}{\Delta D_{n50}} = 6.2P^{0.18}\left(\frac{S}{\sqrt{N}}\right)^{0.2}\xi_m^{-0.5} \qquad with\ \xi_m < \xi_{mc}$$
$$\frac{H_{s,t}}{\Delta D_{n50}} = 1.0P^{-0.13}\left(\frac{S}{\sqrt{N}}\right)^{0.2}cot\alpha^{0.5}\xi_m^{P} \quad with\ \xi_m \geq \xi_{mc}$$

(2. 14)

Where P is the notional permeability factor (recently re-analysed in Eldrup et al. (2019)), S the damage level, N the number of waves (storm duration), $\xi_m = \tan\alpha/\sqrt{(2\pi H_{s,t}/(gT_m^2))}$, is the surf similarity parameter (Battjes (1974)) and T_m is the mean wave period measured in the time domain.

The range of applicability of Eq.(2. 15) depends on the value assumed by the critical breaker parameter ξ_{mc} which has the following expression:

$$\xi_{mc} = \left(\frac{6.2}{1.0}P^{0.31}\sqrt{tan\alpha}\right)^{1/(P+0.5)}$$

(2. 15)

then, if $\xi_m < \xi_{mc}$ the first equation is valid for plunging waves whereas the second one should be used for surging waves. Furthermore, for design purposes in van der Meer (1988) was introduced a damage classification for a classical rubble mound breakwater which distinguish three different level of damage, based the armour slope (cotα) of the structure investigated, as reported in Table 2.

Table 2 Damage classification for a rubble mound breakwater, van der Meer (1988).

Armour slope	Level of damage		
	Initial	Intermediate	Failure (under layer visible)
1V : 1.5H	2	3 to 5	8
1V : 2H	2	4 to 6	8
1V : 3H	2	6 to 9	12
1V : 4H	3	8 to 12	17
1V : 6H	3	8 to 12	17

A limitation of such formulations lays in their application range, in fact, equations (2. 14) are not applicable both in very shallow water and with heavy wave breaking conditions as stated in van der Meer (2021).

The design of such structures in limited-depth water conditions, namely the estimation of the armour rock nominal diameter (D_{n50}), is not an easy task. Generally, the presence of a gentle foreshore induces wave breaking and the release of the bound long waves that play an important role in the wave structure interaction process Smith et al. (2003), making hard the evaluation of the wave characteristics at structure toe (namely $H_{mo,t}$ and $T_{m1-0,t}$) necessary for the design process. In this contest, Smith et al. (2003) addressed the study of the hydraulic stability of a rock slope in shallow waters through

an experimental campaign conducted with a foreshore slope θ = 1V:100H and with different wave conditions (e.g., single and double-peaked spectra and breaking wave). Experimental results showed that the empirical formulations used in van der Meer (1988) are very sensitive to the choice of input parameters (statistical or spectral wave characteristics). Indeed, the author suggested that in Eq. (2. 14), the spectral wave period ($T_{m1-0,t}$) has to be used instead of the mean one (T_m) (Van Gent & Doorn (2001)) since it allows a more accurate evaluation of the structure stability. The work by Smith et al. (2003), was later on extended by Van Gent et al. (2004), who introduced in the analysis, new stability data acquired in shallow water conditions, in presence of a steeper foreshore 1V:30H. Tests were aimed to re-calibrate the formulations proposed by van der Meer (1988), including conditions with shallow foreshores (2. 16).

$$\frac{H_{s,t}}{\Delta D_{n50}} = 8.4P^{0.18}\left(\frac{S}{\sqrt{N}}\right)^{0.2}\xi_m^{-0.5}\left(\frac{H_{2\%,t}}{H_{s,t}}\right)^{-1} \qquad with\ \xi_m < \xi_{mc}$$
$$\frac{H_{s,t}}{\Delta D_{n50}} = 1.3P^{-0.13}\left(\frac{S}{\sqrt{N}}\right)^{0.2}cot\alpha^{0.5}\xi_m^{P}\left(\frac{H_{2\%,t}}{H_{s,t}}\right)^{-1} \qquad with\ \xi_m \geq \xi_{mc} \tag{2. 16}$$

In Eq. (2. 16) it is worth highlighting that: i) the coefficients 6.2 and 1.0 (2. 14) were replaced by 8.4 and 1.3 for plunging and surging breaker conditions, respectively, since the use of the spectral wave characteristics ($T_{m1-0,t}$ and $H_{m0,t}$) led to a better fitting of the data analysed (standard deviation σ =0.107); ii) the author proposed to take into account in Eq. (4), the ratio $H_{2\%,t}\backslash H_{s,t}$, instead than replacing it with a coefficient equal to 1.4 Smith et al. (2003). This consideration is above all valid in shallow water conditions when the Reyleigh wave heights distribution is no more guaranteed. Furthermore, in Van Gent et al. (2004) an alternative stability formula was shown (2. 17), not depending by either the wave spectral period $T_{m-1,0}$, or the notional permeability P but simply by structure characteristics (armour slope, both nominal rocks diameter of armour and core $D_{n50,core}$).

$$\frac{S}{\sqrt{N}} = \left(0.57\ \frac{H_{s,t}}{\Delta D_{n50}}\sqrt{tan\alpha}\,\frac{1}{1 + D_{n50,core}/D_{n50}}\right)^{5}$$

(2. 17)

Recently, Herrera et al. (2017), achieved a new design formula (2. 18), based on new tests conducted with a double armour layer with a 1V:50H foreshore and for breaking waves.

$$S = 0.066\left(\frac{H_{m0,t}}{\Delta D_{n50}}\right)^{6}$$

(2. 18)

The authors found out that the best fit for the Eq. (2. 18) is obtained for a spectral wave height ($H_{m0,t}$) measured at a distance of three times h_t (h_t the water depth at the slope toe) seaward from the structure toe.

In Eldrup & Andersen (2019) the hydraulic stability of a conventional rubble mound breakwater in shallow waters was investigated, mainly focusing on the effects of nonlinear waves. To this aim, new experimental tests were performed with both foreshore slopes 1V:30H and 1V:100H. The tests on the gentler foreshore included mildly nonlinear waves in deep and shallow water, while the steeper foreshore included highly nonlinear waves in shallow water. The authors revisited the stability design formulae Eq. (2. 16) and later achieved a new reliable formulation (2. 19) based both on the newly acquired data and a shallow water conditions dataset provided in Eldrup et al. (2019); Van Gent et al. (2004).

$$\frac{H_{m0,t}}{\Delta D_{n50}} = 1.6^{P}\xi_{m-1,0}^{(0.4P-0.67)}4.5\left(\frac{S}{\sqrt{N}}\right)^{0.2}\xi_{m}^{-0.5} \qquad with\ \xi_{m-1,0} < \xi_{mc}$$

$$\frac{H_{m0,t}}{\Delta D_{n50}} = P^{0.17}min\{cot\alpha, 2\}^{0.23}3.1\left(\frac{S}{\sqrt{N}}\right)^{0.2} \qquad with\ \xi_{m-1,0} \geq \xi_{mc}$$

(2. 19)

The critical surf similarity parameters needed to separate plunging and surging conditions were redetermined as in Eq. (2. 20).

$$\xi_{mc-1,0} = \left(\frac{0.69P^{0.17}min\{cot\alpha, 2\}^{0.23}}{1.6^{P}}\right)^{1/(0.4P-0.67)} \tag{2. 20}$$

On the basis of previous findings, the equations (2. 19) were derived using wave spectral parameters, $H_{m0,t}$ and $T_{m1-0,t}$, respectively. In fact, the authors found that for these nonlinear waves the wave height ratio $H_{1/3}/H_{m0} \gg 1$ was found while for the mildly nonlinear waves $H_{1/3}/H_{m0} \approx 1$ was showed. Goda (2000) describes that the difference between H_{m0} and $H_{1/3}$ increases as the nonlinearity of the waves increases. Furthermore, the formulae achieved a scatter reduction of the test analysed (Eldrup et al. (2019); Van Gent et al. (2004)), although, as underlined by the authors: i) the validity should be accomplished by performing tests with different foreshore slope and in various water conditions (from deep to extremely shallow); ii) the constant stability in case of $\xi_{m-1,0} \gg 10$ has to be verified

Despite, through the years, the hydraulic stability of rubble mound breakwaters has been thoroughly investigated, it still remains an open research field. In fact, new approaches have been recently explored, for instance in Etemad-Shahidi et al. (2020), a multi-variable regression model (namely M5 Bonakdar et al. (2015); Wang & Witten (1996)) has been employed on a experimental dataset of 791 points available in literature, in order to retrieve a compact formula suitable from deep to shallow water conditions (2. 21).

$$\begin{aligned} \frac{H_{s,t}}{\Delta D_{n50}} &= 4.5C_P N^{-1/10} S^{1/6} \xi_{m-1,0}^{(-7/12)} (1-3m) \qquad with\ \xi_{m-1,0} < 1.8 \\ \frac{H_{s,t}}{\Delta D_{n50}} &= 3.9C_P N^{-1/10} S^{1/6} \xi_{m-1,0}^{(-1/3)} (1-3m) \qquad with\ \xi_{m-1,0} \geq 1.8 \end{aligned} \tag{2. 21}$$

Where m is the foreshore slope and C_p is the coefficient of permeability that has been introduced to replace the notional permeability P (2. 22).

$$C_P = \left[1 + (D_{n50,core}/D_{n50})^{3/10}\right]^{3/5} \quad (2.\ 22)$$

Ultimately, in Losada (2021) the classical methodology Thompson & Shuttler (1975); van der Meer (1988) used to study the damage evolution of slope coastal structures, has been questioned. In fact, in order to partially overcome the epistemic uncertainty concealed in the current damage evolution model, a new predictive method, based on a sigmoid function, has been proposed.

Hereunder, the Datasets used to calibrate the hydraulic stability formulae previously showed, are reported along with the range of the main parameters investigated (Table 3). The review analysis presented, shows that a few tests have been performed in the depth-limited water conditions with a 1V:30H foreshore, as the one that will be later explained. Specifically, in Eldrup & Andersen (2019) 12 tests have been found and in Van Gent et al. (2004) ∼40 split in experiments with permeable and impermeable core.

Table 3 Main parameters for the existing formulae previous exposed. The different datasets on which have been calibrated are reported Thompson & Shuttler (1975), van der Meer (1988), Van Gent et al. (2004), Vidal et al. (2006),Herrera et al. (2017) and Eldrup & Andersen (2019).

	Formulae				
	Van der Meer (1988)	Van Gent et al. (2004)	Herrera et al. (2017)	Eldrup et al. (2019)	Etemad et al. (2020)
Dataset	Van der Meer (1988); Thompson and Shuttler (1975)	Van der Meer (1988); Van Gent et al. (2004)	Herrera et al. (2017)	Van Gent et al. (2004); Eldrup et al. (2019)	Van der Meer (1988); Thompson and Shuttler (1975); Van Gent et al. (2004); Vidal et al. (2006)
Parameter					
structure slope angle , cotα	1,5 - 6	1,5 -6	1,5	1,5 - 2	1,5 - 6
foreshore slope angle, cotθ	/	30 - 100	50	30 -100	30 - 100
D_{n50} [m]	0,0164 - 0,21	0,02 - 0,036	0,0318	0,044	0,0164 - 0,21
$D_{n50,core}$ [m]	0 - 0,0063	0,01	0,0068	0,015	0 - 0,0063
$D_{n50,core}/D_{n50}$	0 - 1	0,0 - 0,5	0,21	0,34	0,0 - 0,5
Relative mass density, Δ	0,92 - 2,05	0,92 - 1,75	1,7	/	0,92 - 2,05
Notional permeability, P	0,1 - 0,6	0,1 - 0,5	0,42	0,42	0,1 - 0,6
Breaker parameter, $\xi_{m-1,0}$	0,64 - 8,05	1,29 - 15,73	/	2,41 - 6,77	0,64 - 15,73
wave steepness, $s_{om-1,0}$	0,002 - 0,069	0,001 - 0,038	/	/	0,001 - 0,092
Stability number, N_s	0,79 - 4,38	0,7 - 4,27	1 - 2,5	1,20 - 3,22	0,7 - 4,38
slope damage, S	0,32 - 33	0,35 - 62	0 - 18	0 - 12	0,1 - 62
Number of waves, Nw	500 - 5000	492 - 5172	1000	1000	492 - 5172
Number of tests, N	567 (298)	207 (567)	45	68 (207)	1199

CHAPTER 3
LABORATORY EXPERIMENTAL CAMPAIGN

"Bisogna inventare nuove tecniche - che siano irriconoscibili - che non assomiglino a nessuna operazione precedente. Per evitare così la puerilità e il ridicolo. Costruirsi un mondo proprio con cui non siano possibili confronti. Per cui non esistano precedenti misure di giudizio. Le misure devono essere nuove, come la tecnica."
(P.P. Pasolini, Teorema, 1968)

3. Laboratory Experimental Campaign

3.1 Experimental design

3.1.1 Facilities and equipment

The EUropean Maritime and Environmental Research Laboratory (EUMER) of the university of Salento (Lecce, Italy) is provided with a wave basin and a wave flume.
A 2D physical model tests have been performed in the wave flume. The flume is 45 m long, 1.4 m wide and 2 m deep (Figure 7). The wave generation is performed by a single piston type paddle (maximum stroke 0.5 m) equipped with an active wave reflection absorption system. The paddle is controlled remotely with the HR Merlin software. The program allows the user to generate both regular and irregular waves including a predefined list of wave spectra. (e.g. JONSWAP, Pierson-Moskowitz) (Figure 6). To control and fix exactly the water depth a point gauge is generally set at the end of the flume which allows a very accurate measurement (uncertainty of about 0.1 mm).

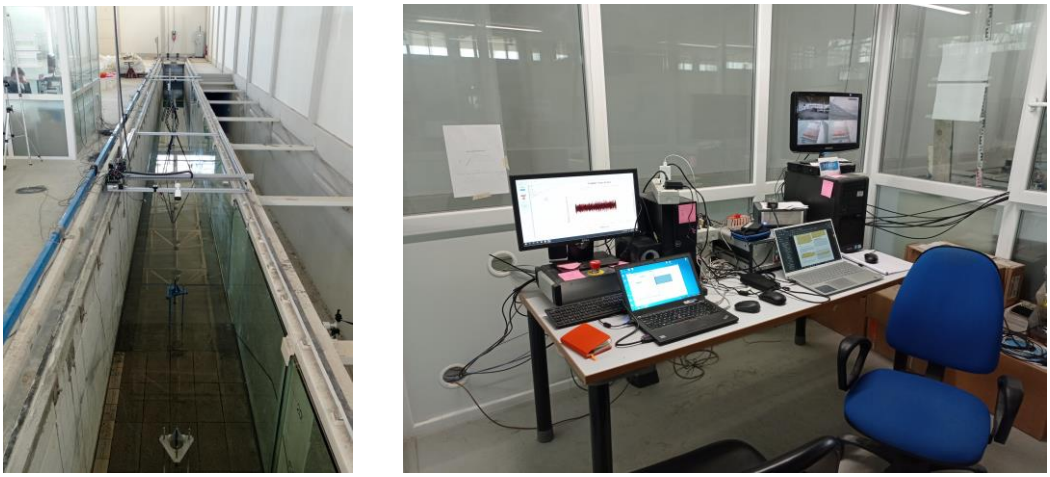

Figure 6 a) Wave Flume; b) The flume control room.

3.1.2 Physical scaled model

Starting from the wave generator, the flume has a flat bottom of 14.80 m followed by a short 1V:5H slope and a 1V:30H concrete foreshore of approximately 14.30 m Figure 7. The slope of the foreshore has been designed, accordingly with the laboratory facilities, to create depth-limited water conditions. Subsequently, a 3.80 m flat bed made of bricks has been built upon which it is placed the rock slope. The rock slope is 1V:2H, the crest is 1.66 m high above the flume bottom and 0.2 m wide.

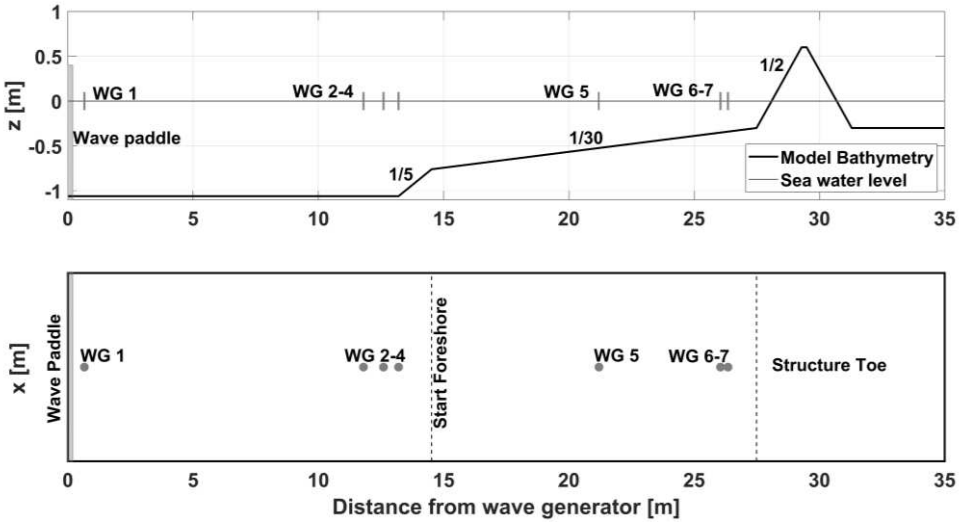

Figure 7 Top panel: longitudinal section of 2D wave flume; Bottom panel: Plan view of the wave flume.

The model cross section is a non-overtopping rubble mound breakwater without a toe berm. The structure tested is protected with a double-layer randomly placed armour made of natural rocks with “standard rough angular shape” provided by a local quarry. Four different rock gradings have been tested and their main characteristics are summarized in Table 4. The rocks have been collected and sieved before the use to obtain the grading curve (Figure 8). The density of the material is $\rho = 2576$ kg/m^{3}and the global porosity n has been assumed equal to 0.4 as reported in Burcharth & Andersen (1995) for a conventional breakwater composed of armour, filter layers, and

core. The porosity has been considered as the suggested value based on the grading curves (see, CIRIA, CUR, CUTMEF (2007)).Specifically, to guarantee a right fully turbulent flow both at the armour layer and inside the breakwater core the Reynolds number ($R_{eD} = 3{,}9*10^4 >> R_{e,crit}$ and $R_{ep} = 2{,}1*10^4 >> 300$ Eq. (3. 1)) has been calculated to verify that no scale effects occur according to Jensen et al. (2014; Jensen & Klinting (1983), with $R_{e,crit} = 3*10^4$ (Dai & Kamel (1969)).

$$R_e = \frac{\sqrt{gH_s}D_{n50}}{\nu} > R_{e,crit} \tag{3. 1}$$

Table 4 - Rock's characteristics.

	WL1	WL2	WL3 and WL5	WL4
Dn_{50} – armour [m]	0.046	0.034	0.024	0.0138
Dn_{50} – under layer [m]	0.024	-	-	-
Dn_{50} – core [m]	0.01	0.01	0.01	0.01
D_{85}/D_{15}	1.26	1.27	1.20	1.28

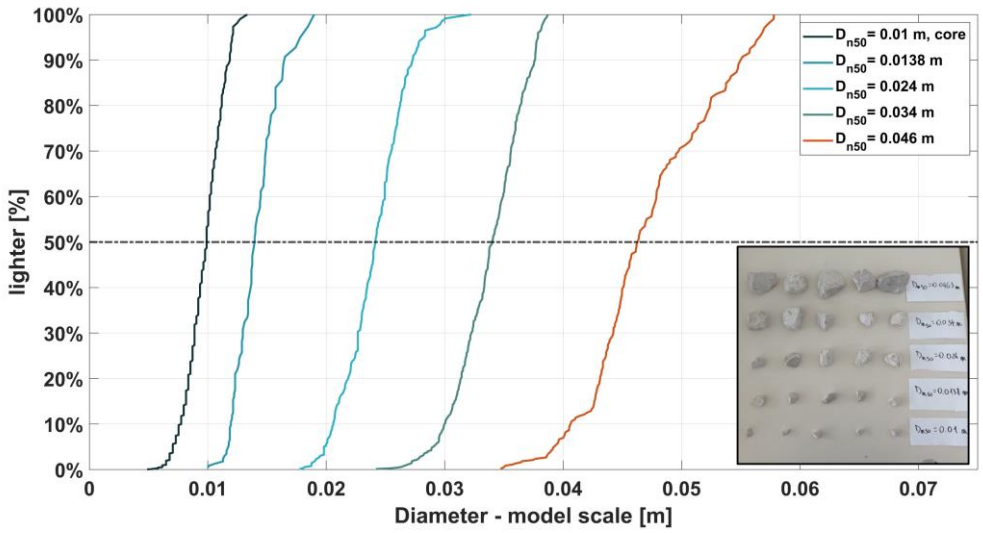

Figure 8 Grading curves of the rocks used to build the physical model.

The shape of rough angular rocks in the armour has been characterized using the length-to-thickness ratio *LT* (3. 2) also called aspect ratio, and the Blockiness coefficient (*BLc*) (3. 3) described by CIRIA, CUR, CUTMEF (2007).

$$LT = \frac{L}{d} \tag{3. 2}$$

$$Blc = \left(\frac{M_{50}}{\rho_r}\frac{1}{XYZ}\right) \tag{3. 3}$$

LT (-) is defined as the maximum length *L* (m) of the stone divided by the minimum distance, *d* (m), between parallel lines through which the particle would just pass.
Blockiness, *BLc* (%) is defined as the volume of a stone divided by the volume of the enclosing XYZ orthogonal box with a minimum volume. Blockiness is a shape descriptor, related to compactness, and it is well correlated with the packing behaviour of individually placed stones. This is because higher blockiness promotes stone positioning with more sub-parallel face alignments, giving higher density, greater numbers of contact points and thus greater interlock. *BLc* is determined by measuring the maximum X, intermediate Y, and minimum rectangular dimensions Z of the smallest hypothetical box that would enclose the block, and by weighing. To help the X, Y, and Z dimensions, Z is set parallel to d and X and Y are then defined by the axes of the perpendicular plane with projected minimum area. The instrument shown in Figure 9 has been realized and used to measure these parameters.


a)

b)

Figure 9: An hand-made instrument used to measure the stones dimensions.

Figure 10 shows the value of *LT* (-) and *BLc* (%) for WL1, WL2 and WL3 (summarized in Table 5) gained through the average of 20 samples taken randomly from the relative grain population.

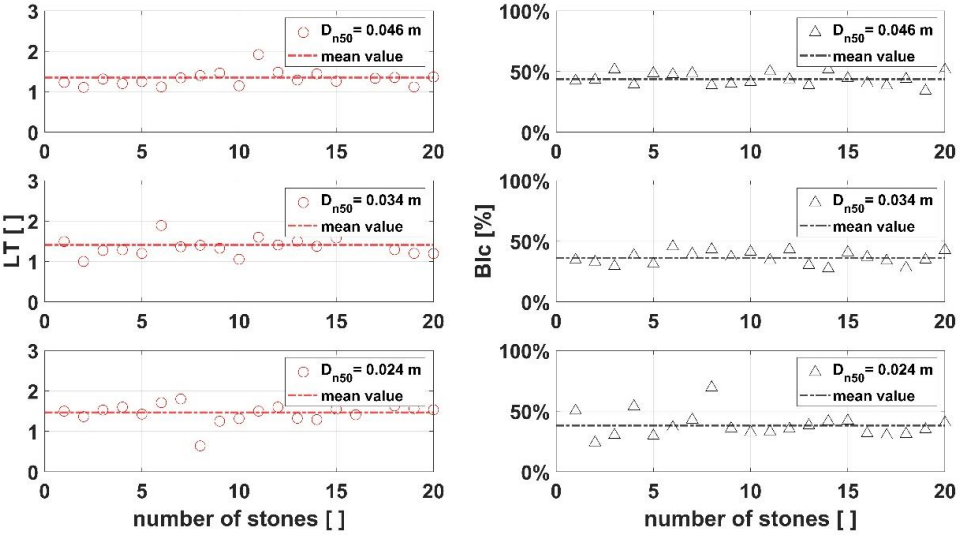

Figure 10: Left panels show the aspect ratio and the right ones the Blockiness of the rocks used for building the armour layer of the tested structures.

Table 5. The values of LT and BLc for each armour stones used during the tests.

D_{n50} armour [m]	LT [-]	Blc [%]
0.046	1.35	43.79
0.034	1.41	36.28
0.024	1.46	38.18

Finally, it can be stated that the rocks used in this experimental campaign show a narrow-gradation according to the Rock Manual's indicator of uniformity (Table 8) and a suitable shape and blockiness in relation to the purpose of this research.

Table 6. Rock grading classification based on CIRIA, CUR, CUTMEF (2007).

Grading width	D_{85}/D_{15}	M_{85}/M_{15}
Narrow or single sized gradation	Less than 1.5	1-7 – 2.7
Wide gradation	1.5 - 2.5	2.7 - 16
Very wide or quarry run gradation	2.5 - 5.0	16 - 125

The profile of the breakwaters has been traced on both the side of the flume (Figure 11), then the structures has been built up and arranged following the profile. A sliding small wooden slat of about 5 mm has been fixed on the seabed in front of the first stones of the toe to prevent the sliding of the rocks over the smooth surface.

Figure 11 Few steps of the set-up of the first layout.

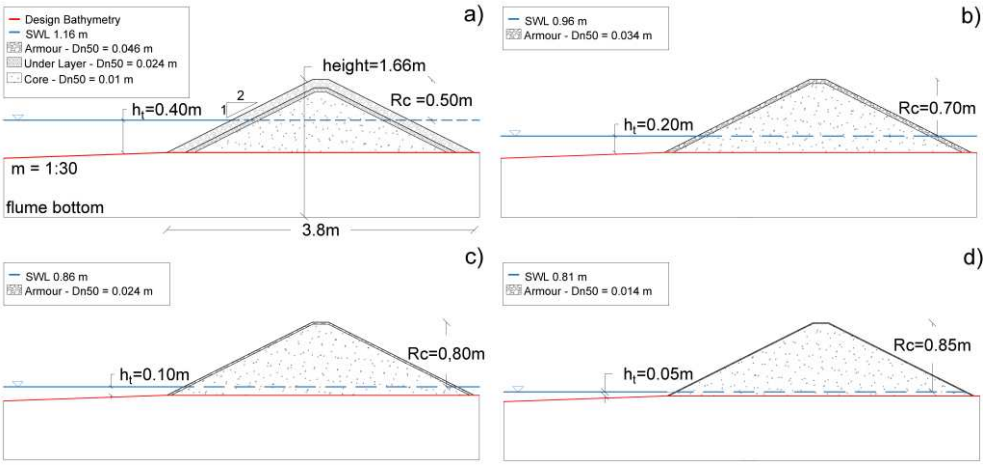

Figure 12 Rubble-mound structure layouts: (a) WL1; (b) WL2; (c) WL3; (d) WL4.

3.1.3 Test program

Globally, 34 tests have been carried out and the minimum duration of each ones has been equal to the needed time toe create 1000 waves, in order to re-produce a sea state statistically relevant Frostick et al. (2019). Furthermore, since that the present experimental campaign aims at investigate the breakwater stability, 3000 individual waves have been generated to the scope. The waves have been generated, employing

a JONSWAP wave spectrum with an enhancement factor $\gamma = 3.3$. Different water conditions have been covered, ranging from deep to extremely shallow, and for each relative water depth (h_r), the tests have been grouped in two series of constant spectral wave steepness ($s_{om-1,0} = 2\pi H_{m0}/(gT_{m-1,0})$,respectively equal to 0.024 and 0.048. The tests have been classified in Figure 14 on the basis of the wave steepness and the shallowness criteria reported in Van Gent & Smith (1999). In Figure 14 with respect to the Dataset of Van Gent et al. (2004) it stands out that the present experimental campaign has provided new stability data in very and extremely shallow waters ($h_r >$ 3). Precisely, among the 34 tests, 8 have been performed in intermediate waters (*WL1*), 10 both in shallow (*WL2*), and very shallow (*WL3*-*WL5*), and 6 in extremely shallow (*WL4*) water conditions (Table 7), since no reflection analysis is suitable in depth-limited conditions (e.g., Altomare et al. (2016)), the same tests have been repeated without the structure in place, to accurately measure the incident wave characteristics at the slope toe. As far as the flume reflection is concerned, in order to avoid some undesirable effect in the wave elevation measurement, a gentle absorbing beach (slope ~1V:8H, Figure 13) has been built at the end of the channel (Marcou (1954)). Indeed, in wave flumes and wave basins it is of paramount importance to have absorbing system, such as spending beach, able to reduce the reflection of the incident waves to avoid scale effects. The efficient design of a highly absorbing beach leads to the correct reproduction of both coastal and nearshore physical phenomena.

Figure 13 Gravel spending beach at the end of the wave flume.

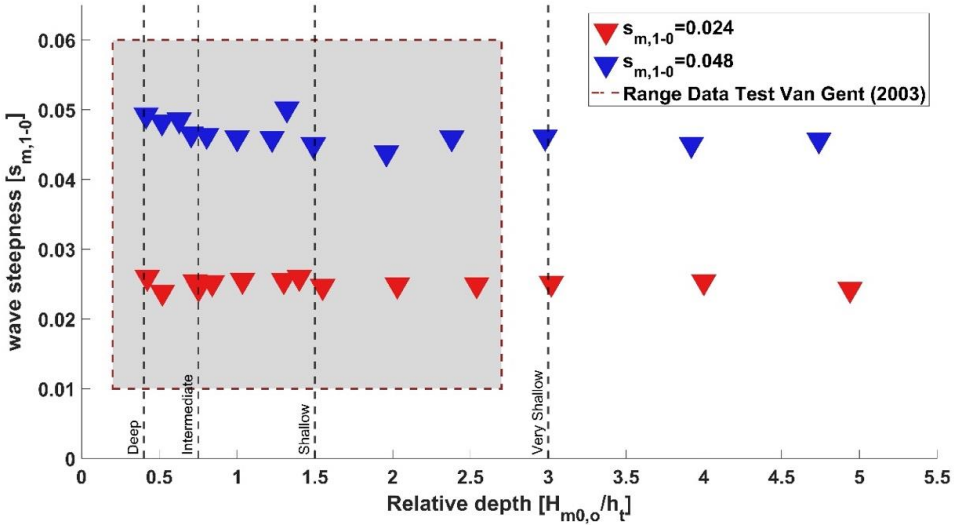

Figure 14: Shallowness classification of the performed experimental tests.

The main wave characteristics of the tests are reported in Table 7, namely the relative water depth (h*r*), the water depth at breakwater toe (h_t); the spectral wave steepness ($s_{om-1,0}$), the breaker parameter ($\xi_{m-1,0} = \tan\alpha/(s_{mo-1,0})^{0.5}$), the stability number (N_s) and the measured slope damage (S). It is important to highlight that for 22 tests the damage has been measured also after 3000 waves. Additionally, before running a test series, the structure has been exposed to a low energy sea state (*shake-down test*) in order to compact the armour rocks (Hudson (1975); Hughes (1993); Tørum et al. (1979)). Moreover, for the sake of completeness, some repeatability tests have been realized to be sure about the reliability of the data acquired, even though scatter in the results is possible, especially in damage measurement.

Table 7 Main parameters of the tests performed.

Main parameters	**WL1**	**WL2**	**WL3-WL5**	**WL4**
Number test (N_w =1000 + 3000)	8+4	10+9	10+5	6+4
Water depth - h_t (m)	0.4	0.2	0.1	0.05
Relative depth - $H_{m0,o}/h_t$ (-)	0.42-0.75	0.71-1.40	1.49-2.54	2.98-4.94
Wave steepness - $s_{m0-1,0}$ (-)	0.024-0.048	0.024-0.048	0.024-0.048	0.024-0.048
Breaker parameter - $\xi_{m0-1,0}$ (-)	2.8-3.4	3.5-7.1	6.1-17.7	11.1-19.6
Slope damage - S (-)	1.8-20	1.5-11.05	1.2-19	1.3-8.2
Stability number - $H_{m0,t}/\Delta D_{n50}$ (-)	2.21-3.8	2.67-2.9	2.36-3.9	2.76-4.1
Grading slope material - D_{85}/D_{15}	1.26	1.27	1.20	1.28
Core material - $D_{n50core}/D_{n50}$	0.21	0.29	0.41-0.71	0.71

3.2 Data acquisition

3.2.1 Wave measurements

The wave surface elevation along the flume has been evaluated using of 8 wave gauges. The wave probe operates by measuring the resistance of the water between a pair of parallel rods. Resistance between the rods is proportional to the immersion depth. Each probe is connected to an acquisition card (AC) that is inside a box that can contain up to 8 ones as shown in Figure 15. The current is converted to an output voltage ($\Delta V = R*i$) that is directly proportional to the immersed depth, where R is the wire electrical resistance that is a function of the wire length and section and i is the electrical intensity.

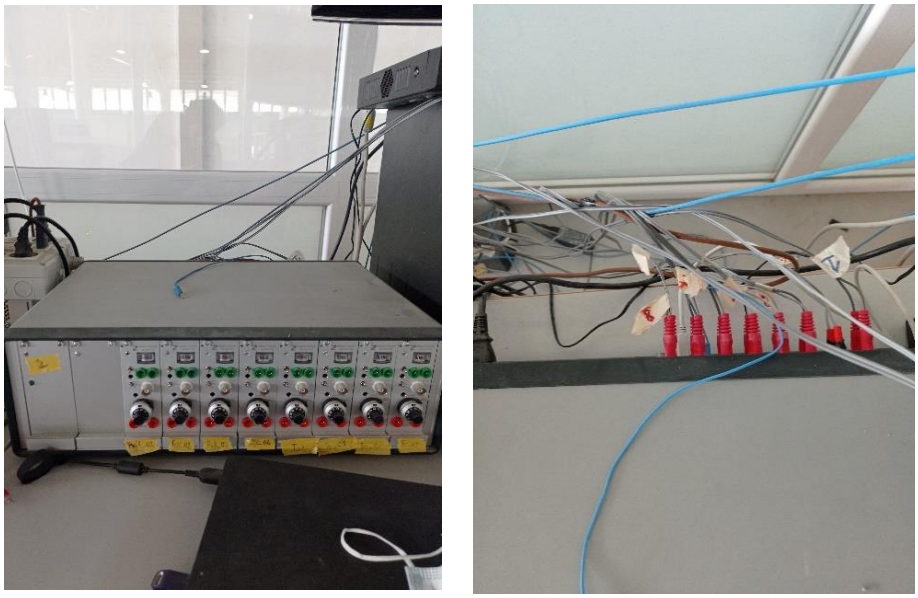

Figure 15 Wave probes acquisition card (AC)

The wave probes, following a standard procedure, have been cleaned and calibrated every morning before the beginning of the tests. Indeed, environmental factors, as the temperature, the presence of limestone in the water, etc. could modify the signal measure from day by day.

The probes have been located as follow:

- 1 wave probe (WG1) offshore to measure the wave generated at the paddle.
- 3 wave probes (WG 2-4) before the foreshore to measure the foreshore reflection.
- 1 probe (WG5) on the foreshore to evaluate the development of the spectrum for limited depth conditions.
- 2 probes (WG 6-7) at the toe of the structures to measure the wave parameters at the toe of the breakwater.
- 1 probe (WG8) along the slope to measure run-up.

The wave gauges were placed as shown in Figure 16, while in Table 8 detailed information about their position are reported. The absolute distance refers to the length that occur between a probe and the wave paddle. The wave characteristics at the toe of the structure were measured at the *WG7* place at 0.45 m from the slope.

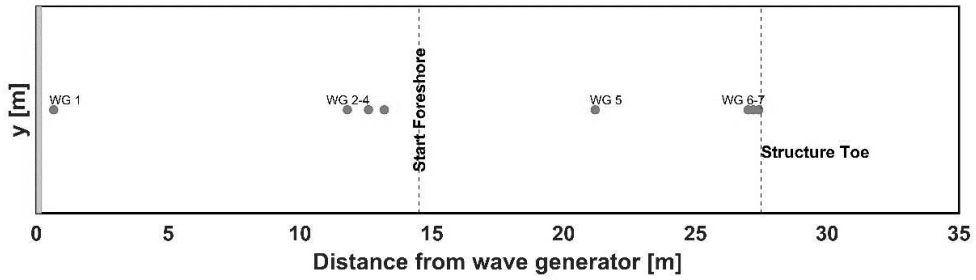

Figure 16 Horizontal section of the 2D wave flume showing the first wave gauge configuration.

Table 8 Absolute distances of wave gauges from the wave paddle.

Name	ID	Absolute distance (m)
Offshore	WG1	0.66
Refl1	WG2	11.8
Refl2	WG3	12.6
Refl3	WG4	13.2
Foreshore	WG5	21.2
Toe1	WG6	28.20
Toe2	WG7	28.65
Run-up	WG8	-along the structure slope

During the calibration tests, performed without structure, clearly the run up gauge has been relocated exactly at the structure toe. The wave measurements that have been performed without the breakwater will be used in the further analysis.

As said, the wave run-up has been measured during almost all the tests (despite several signals are cut). The longest wave gauge available has been rest on the slope to detect at least $\pm 3H_{m0}$ from the sea water level (SWL). A wooden stand has been bonded to the wall in order to avoid unwanted movements and to guarantee at least 0.15 m from the wall to avoid side-effect (Figure 17). To correctly perform the test, for the first two water depths (0.40 m and 0.20 m at the toe of the slope) have been used standard wave probes, whereas for the other two (0.10 m and 0.05 m at the toe of the slope) the smallest ones have been used.

Figure 17: Wave run-up gauge.

3.2.2 Pore Pressure measurements

Pressure sensors have been used to measure the dynamic pressure induced by the wave's flow inside the rubble mound breakwater during the tests, simultaneously with the incident wave characteristics (Scaravaglione et al. (2022)). The dynamic pressure inside the breakwater has been measured by means of 8 pressure sensors, (KELLER model Series 25 Y, furnished by HR Wallingofrd https://equipit.hrwallingford.com/high-performance-pressure-sensors). All the sensors (hereinafter referred to as $P_{t,i}$) have been protected with a wire mesh (Figure 18) before being placed accurately in the central section of the structure and mainly, inside the core and at the interface between core and filter layer. The purpose is to evaluate the temporal and spatial variation of the pore pressure across the structure in both vertical and horizontal directions and along the filter slope, examining the global pressure fields inside the breakwater. The sampling frequency for the pressure sensors has been set to 1000 Hz and then down sampled at 40 Hz for the analysis.

Figure 18: Installation phase inside the core of the rubble mound breakwater of pore pressure sensors.

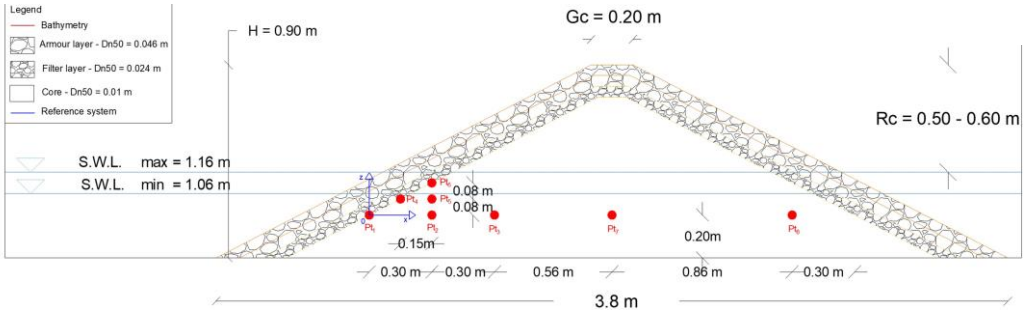

Figure 19 Side view of the breakwater, specifically the relative distances between the pressure sensors are reported along with the two S.W.L. tested.

As previously stated, the entire experimental campaign has been aimed at investigating the rock slope hydraulic stability of a rubble mound breakwaters. Among the tests performed, 7 irregular plus 13 regular experiments, have been used in order to investigate the pore pressure distribution inside the structure (Table 9). All tests have been generated employing a JONSWAP wave spectrum with an enhancement factor $\gamma = 3.3$. Two offshore sea water levels have been tested, equal respectively to 1.16 m and 1.06 m and corresponding to a water depth at the structure toe of 0.4 m and 0.3 m respectively.

It is straightforward to verify that the tests have been performed in transitional water conditions according to the classification proposed using the relative depth (h_{toe}/L_{toe}).

Table 9 Main parameters of the tests performed in order to measure pore pressures

	Test Series 1 Irr. waves	**Test Series 2 Reg.waves**	**Test Series 3 Reg.waves**	**Test Series 4 Reg.waves**
Number test [-]	7	7	3	3
Number of waves [-]	1000	50	50	50
Toe water depth - h_t [m]	0.4	0.4	0.4	0.3
Water condition - h_t / L_{toe} [-]	transitional	transitional	transitional	transitional
Wave height input H_{m0}-H_z [m]	0.16-0.30	0.2	0.3	0.3
Wave period input, T_p-T_z [s]	1.60-2.83	1.4-2.60	1.72-2.19	1.72-2.19
Wave steepness - s_{m0} (-)	0.02-0.04	0.019-0.065	0.040-0.065	0.040-0.065
Surf Similarity parameter - ξ_{m0} (-)	2.20-2.58	1.96-2.54	1.86-2.02	2.22-2.23

For each water level a static pressure measure has been acquired to better control the dumping inside the breakwater.

3.2.3 Damage measurement

The armour damage level of the structure's slope is defined as the ratio between the cross sectional eroded area A_e (m^2) and the nominal diameter of the armour layer Dn_{50} (m) as clearly reported in van der Meer (1988) and here in (2. 13).
The eroded area has been retrieved by measuring the cross-shore profile of the structure before and after each test (Figure 20). The wave flume has been emptied in order to measure the damage.

Figure 20 Wave impacting the rock armour slope.

The measurements have been made with a laser bed profiling system that is a widespread laboratory technique, traditionally used for measuring the damage of rubble mound breakwater induced by wave action Campos et al. (2020). The EUMER Laboratory is equipped with a bed profiling system by HR Wallingford

(www.hrwallingford.com/equipment) , endowed with different kinds of probes able to fit a wide range of applications (e.g., rubble mound breakwater damage, beach/dune profiles evolution, bedforms). The system consists of a vertical position-controlled laser probe, driven by a small electric motor with a mechanical transmission actuating a rod. Both the probe and the rod are installed on a carriage which ensures an accurate positioning in the vertical (*z*), longitudinal (*x*) and transversal (*y*) directions (Figure 21).

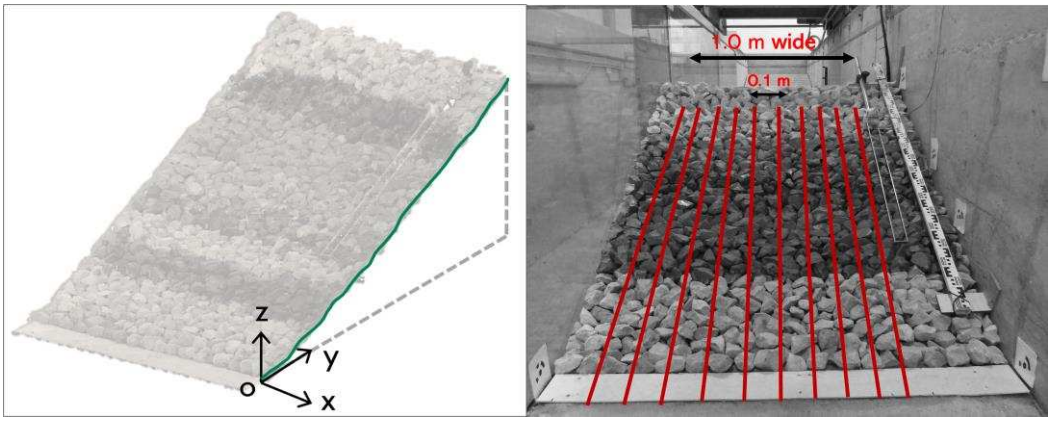

Figure 21 Reference coordinate system.

The profiler system is remotely controlled, providing the possibility to fix some parameters, like the starting point and the acquisition frequency (Figure 22). The probe can move with a constant velocity up to 25 mm/s, both along the z-axis and y-axis, such as to maintain a constant measurement distance (80 mm) above the slope. It can proceed also horizontally (x-direction), up to 50 mm/s. The laser provides high accuracy measurements, reaching a mean resolution in both y and z directions of ±0.5 mm (Atkinson & Baldock (2016)).

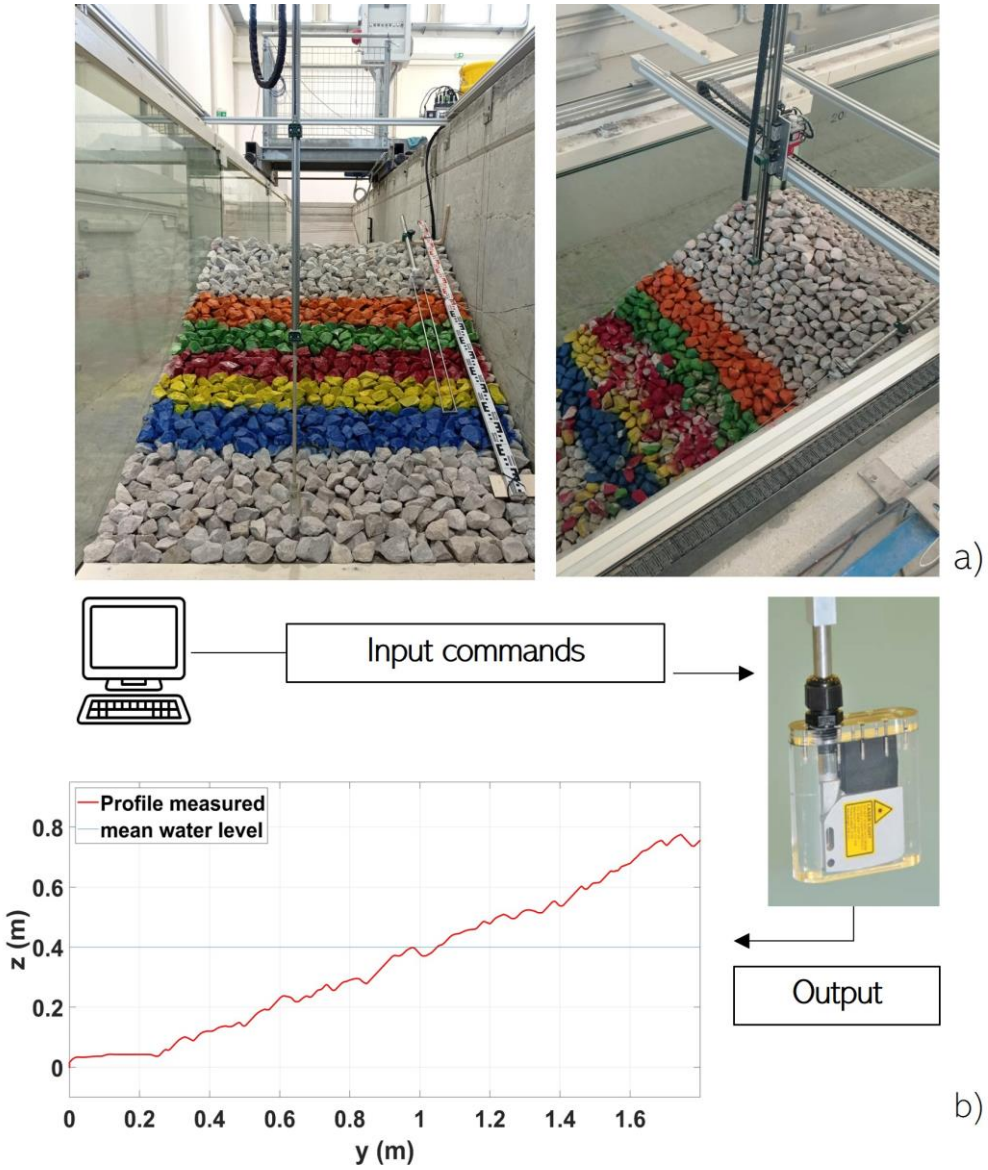

Figure 22 Laser bed profiler system.

According to the procedure described in Van Gent et al. (2004) the eroded area (A_e) has been retrieved by measuring the cross-shore profiles of the rock slope, before and after each wave test, along 0.1 m equally-spaced transects. In Figure 23 an example of

initial (red line) and final (black line) profiles of the structure measured by the laser profiler (*lp*) is reported. Both profiles represent the mean elevation (*z*), with respect to the flume bottom (z = 0) calculated over ten measured transversal sections. The absolute difference between the average initial and final profiles (d_z, blue line) is also reported. Mainly, the eroded (A_e) and accretion (A_a) areas have been calculated as the integral function of the area under the dz positive and negative values, respectively.

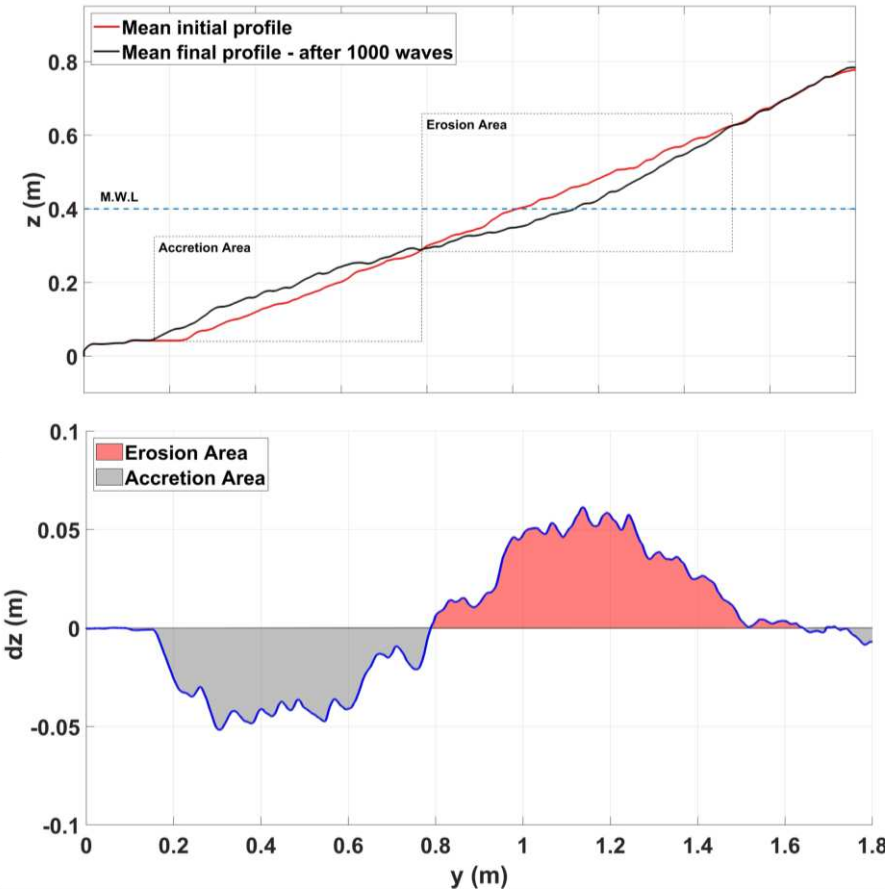

Figure 23 Top: example of mean initial (red curve) and final (black curve) profiles measured after wave attack (Test WL1-02 with $H_{m0,o}$ = 0.25 m and $T_{m-1,0}$ = 2.57 s).Bottom: the blue curve represents the spatial evolution of slope elevation changes (*dz*) with respect to the initial profile

3.2.3.1 Overview of the available techniques for slope damage measurement

As previously stated, the damage *S* can be retrieved by measuring the eroded area due to wave action. Usually, the temporal evolution of the structure can be measured through different techniques (e.g., counting method, mechanical profilers, scanning methods) . Even though the profiling system is an affordable and common instrument to assess rock slope damage, other methodologies are available, mainly based on visual and photographic methods. In fact, as highlighted in Vidal et al. (2004), the assessment of the damaged area can be achieved at the end of the experiments, by counting the displaced stones. According to the sediment mass balance, this method is based on the hypothesis that the averaged eroded area is equal to the settled one. Then, given the number of removed stones (*N*), the armour porosity (*P*), and the flume width (*L*), the eroded transversal area is estimated as follows:

$$A_e = \frac{N D_{n50}^3}{(1-P)L} \tag{3. 4}$$

The counting method is commonly supported by validating the results through digital images of the structure slope, which are frontally taken. The different colors of stone layers enable the retrieval of the eroded transversal area by image processing, from which the number of pixels of both damaged and undamaged zones can be detected.
However, such methods show some drawbacks as the damage increases. When the number of removed stones is high, the counting method becomes tedious and prone to human error. Likewise, if the eroded area is too deep, heavily affecting the under layers, the use of digital images has proven to return results less accurate than other techniques most used for instance the profiling system. In fact, as stated by Campos et al. (2020), the existing damage measurement techniques (e.g., laser profiling system, rocks counting) present some criticalities.
In the first place, there is a substantial lack of shared standard procedures for damage measurement, which lead to a difficult comparison of data, especially in terms of

damage parameter descriptors, from experimental campaigns realized in different laboratories and with different measurement instrumentation. Another aspect concerns the intrusiveness of mechanical profiles, due to physical contact with the structure, and profiles physical limitation related to the diameter of the equipped circular foot, which performs the data acquisition, neglecting stones smaller than its size. In addition, most of the existing techniques are mainly based on 2D information. Whereas, the damage progression along a sloping coastal structure is a 3D process, in which it is important to consider also the surface distribution of damage.

In recent years, with the continuous development of digital technologies for image processing and remote sensing, other alternatives for damage evaluation have been proposed. They are mainly based on reality-capture 3D models (e.g., dense point clouds, polygonal meshes), obtained through the application of range-based methods (e.g., laser scanning, structured-light scanning) or image-based techniques (photogrammetry). Remote sensing and 3D modeling through reality capture are growing in many sectors, as industrial manufacturing (Guerra et al. (2019); Jovančević et al. (2017); Lavecchia et al. (2018); Law et al. (2018)), civil infrastructures (Hallermann & Morgenthal (2012); Kasireddy & Akinci (2017); Koch et al. (2015)), building refurbishment, cultural heritage conservation (Aragón et al. (2018); Waas & Zell (2013)) and coastal monitoring (Valentini et al. (2017); Valentini & Balouin (2020)). In particular, a broad employment is related to condition assessment, surface damage detection, and the monitoring of the state of conservation of objects at different scales, from small manufacturing components to buildings, civil infrastructures or entire environments. For example, some authors propose automatic defects detection, classification and structural health monitoring of historical buildings, based on machine or deep learning algorithms on point clouds or polygonal meshes (Gong et al. (2021); Grilli et al. (2019); Mishra (2020); Musicco et al. (2021); Valero et al. (2019)). Furthermore, reality capture 3D models are employed for the extraction of quantitative

information about surface defects, starting from geometric and radiometric parameters (Galantucci et al. (2018); Guerra & Galantucci (2020); Valero et al. (2018)).
In coastal engineering the use of range or image-based techniques for the eroded area measurement is still little explored, especially when wave-structure interaction processes are investigated by means of physical modelling (Fortes et al. (2019); Musumeci et al. (2018); Puente et al. (2014); van Gent & van der Werf (2014)).
Fortes et al. (2019), applied a stereo-photogrammetric technique for evaluating the temporal evolution of a rock armour breakwater slope. They highlighted only absolute differences/displacements in two dimensions, without being able to distinguish the eroded area from the accretion one. A similar approach was adopted in van Gent & van der Werf (2014), focused on the assessment of S at breakwater toe exploiting 3D point clouds only to evaluate the erosion profiles of the breakwater toe. Indeed, the damage was assessed through the number of displaced stones. While, Puente et al. (2014) used LiDAR to acquire surface and volumetric data about the structure damage of a roundhead breakwater, made of Concrete Armour Units (CAU) cubipod elements. In this case, the evaluation of damage was performed by applying image processing pipelines to 2D binarized maps, with damaged areas and volumes retrieved from the regular pixel grid. This method proved to be effective for defence structures made of CAU, with constant and regular shapes and dimensions, and pre-determined mutual positions. However, when dealing with breakwaters made of stones, the situation drastically changes, since they have an irregular morphology, which could hardly be investigated on 2D maps. In Musumeci et al. (2018), the wave-induced damage on a slope breakwater made with accropodes was retrieved by a Red-Green-Blue and Depth (RGB-D) device equipped with a Kinect sensor, which allows detecting both emerged and submerged slopes without wave flume emptying. Nonetheless, as they stated, 3D point clouds they retrieved have a considerable absolute error, even at short distances from the object (0.5 m - 1 m), making unfeasible to detect small stones displacement (e.g. $D_{n50} = 1$ cm).

Herein the photogrammetric technique as a support within the workflow traditionally used for damage assessment of breakwaters in laboratory, with the use of cost-effective, simple, and accessible equipment, in more expeditious acquisition time. To this purpose, the outcomes of the present experimental campaign performed on a 2D small scale physical model at the EUMER Laboratory University of Salento (Lecce, Italy), performed to explore the hydraulic stability of a rubble mound breakwater under different water conditions, are used Marino et al. (2022). Before and after each test, the structure profile has been measured by a laser profiler and also derived by photogrammetric technique. Obtained results have been then compared in different configurations and boundary wave hydrodynamic conditions (as shown in Sections 3.1.3). Quantitative three-dimensional data of the eroded area have been retrieved to evaluate the damaged areas. The main goal is to demonstrate the reliability of photogrammetric 3D model with respect to laser profiler, and whether they can be considered comparable, both in terms of precision and accuracy. A methodological workflow has been proposed as reported in Figure 24, which introduces photogrammetry as an alternative measuring system, with respect to the well-known laser profiler. Digital photogrammetry enables the restitution of the spatial location (3D coordinates) of each point of an object from multiple images, according to Structure from Motion (*SfM*) and Dense Multi-View Reconstructions (*DMVR*) algorithms (Luhmann et al. (2019); Schenk (2005)). Indeed, among various reverse engineering techniques (e.g., laser or structured-light scanning), photogrammetry has been preferred, due to the availability and affordability of instrumentation (compact cameras, bridge or reflex cameras, tripods or telescopic rods, drones) and the great adaptability of the method to the order of magnitude of the elements to be investigated.

During the experimental campaign, the photogrammetric survey provides both 2D and 3D data of wave flume and structure conditions before (pre) and after (post) each test. Indeed, 2D cross-shore profiles are treated to derive the amount of damage, throughout the computation of the transversal eroded area, whose accuracy is verified against laser profiler outcomes. Whereas, 3D development of the eroded area involves the three-

dimensional damage study, through a deviation analysis. To encompass a plurality of scenarios in the investigation, the analyses have been performed in different wave conditions, with distinct layout configurations (Table 7).

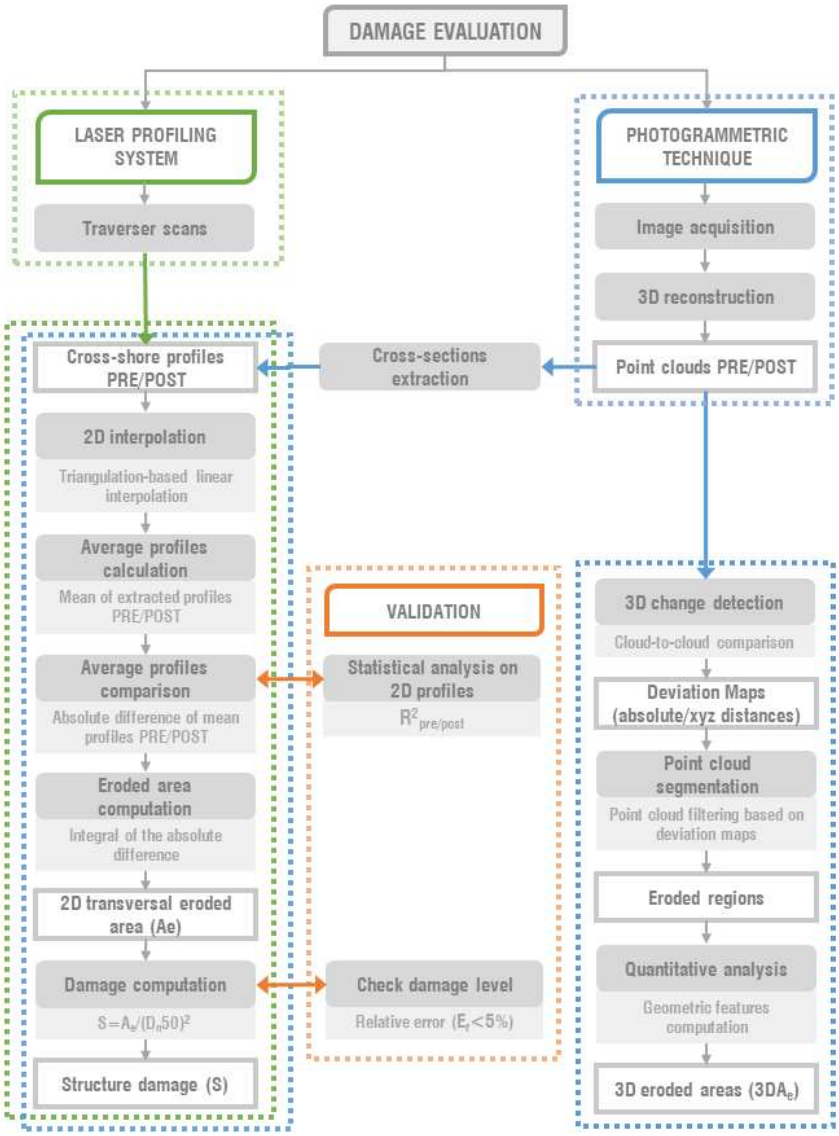

Figure 24 Methodological workflow.

3.2.4 Photogrammetric damage measurement system

3.2.4.1 Photogrammetric technique

Photogrammetric acquisitions have been performed to collect reality-based 3D data (point clouds) of the physical model, before and after each experimental test. Multiple images of the physical model are gathered from specific camera locations, characterized by the following constant set-up parameters:

- camera (sensor size, number of pixels, lens focal length);
- object to be surveyed (extension, planimetric development, volume);
- site configuration (shooting distance, presence of physical obstructions);
- scans execution (percentage of overlap between adjacent images).

In order to retrieve 3D data with comparable resolution, the Ground Sample Distance (*GSD*) of the photogrammetric outputs has been determined in advance, to guarantee the needed level of detail on 3D data, with reference to the size of the analysed elements (e.g., the smallest rock size) or phenomena Luhmann et al. (2019). The GSD is typically related to the resolution of the photogrammetric survey throughout the size, in real world, of an element represented by a single pixel. It corresponds to the distance between two consecutive pixel centres and can be expressed as a function of focal length (f), shooting distance (*k*) and pixel size (*p*), (3. 5).

$$GSD = \frac{k}{f} * p \tag{3. 5}$$

The reconstruction process furnishes scaled and oriented point clouds, namely unorganized sets of points located in three-dimensional space with known coordinates and normal vectors in the flume reference system. The point clouds are then processed to remove unvalid points which are generally characterized by a high level of

uncertainty, noise or high reprojection error (i.e. points not accurately reprojected in different images), or reproduce unnecessary objects (e.g., vertical walls, instruments, ecc.) (Lavecchia et al. (2017); Napolitano & Glisic (2017)). Then, to compare 3D data, a raw registration of pre and post point clouds is achieved by a first expeditious method, through a manual selection and association of equivalent point-pairs, in correspondence of well-known or easily recognizable points (i.e. targets). Then, the two clouds are aligned, by roto-translating the post-test cloud with respect to the pre test cloud, which is considered as reference fixed model in all the analyses. Afterward, the Iterative Closest Point (*ICP*) algorithm allows an improvement of the alignment, by the identification of the best matches minimizing the Euclidean distance between the two clouds Besl & McKay (1992). ICP reduces errors in the registration phase, by decreasing the Root Mean Square Error (*RMSE*), defined as follows (3. 6):

$$RMSE = \sqrt{\sum_{i=1}^{n} \frac{(\Gamma_{ipre} - \Gamma_{ipost})^2}{n}} \tag{3. 6}$$

where Γ_{ipre} represents *x, y* and *z*-coordinates of a point in the reference model (*pre*), Γ_{ipost} the *x, y* and *z*-coordinates of the corresponding point in the compared model (*post*) and n indicates the points number. Given that *ICP* algorithm is an iterative process, in the present work the maximum limit of iterations has been set as a function of the RMSE threshold equal to 10^{-6} m to achieve a negligible error magnitude order. In addition, the percentage of pre and post overlapping clouds has been chosen in a range of 80-90%, to avoid differences between the two models, due to rocks displacements, which could compromise the alignment.

At the end of point cloud pre-processing, the change detection between 3D data enables a direct comparison of pre/post clouds in order to identify the temporal evolution of the structure armour layer under wave action and quantify the damage

extension affecting the rock slope. Among various existing methods to evaluate 3D changing features (e.g., Multiscale Model to Model Cloud Comparison M3C2 Lague et al. (2013)), the deviation between aligned 3D data has been computed by means of Cloud-to-cloud (C2C), which has proven to be the *'simplest and fastest direct 3D comparison method of point clouds'* (Girardeau-Montaut et al. (2005)).

The algorithm is based on the Nearest Neighbour Distance analysis, where the Euclidean distance between each point of the compared cloud (*post*) and its nearest point in the reference cloud (*pre*) is calculated. The results can be evaluated either as absolute distances or *xyz* displacements, visualized through deviation maps as depicted in Figure 25.

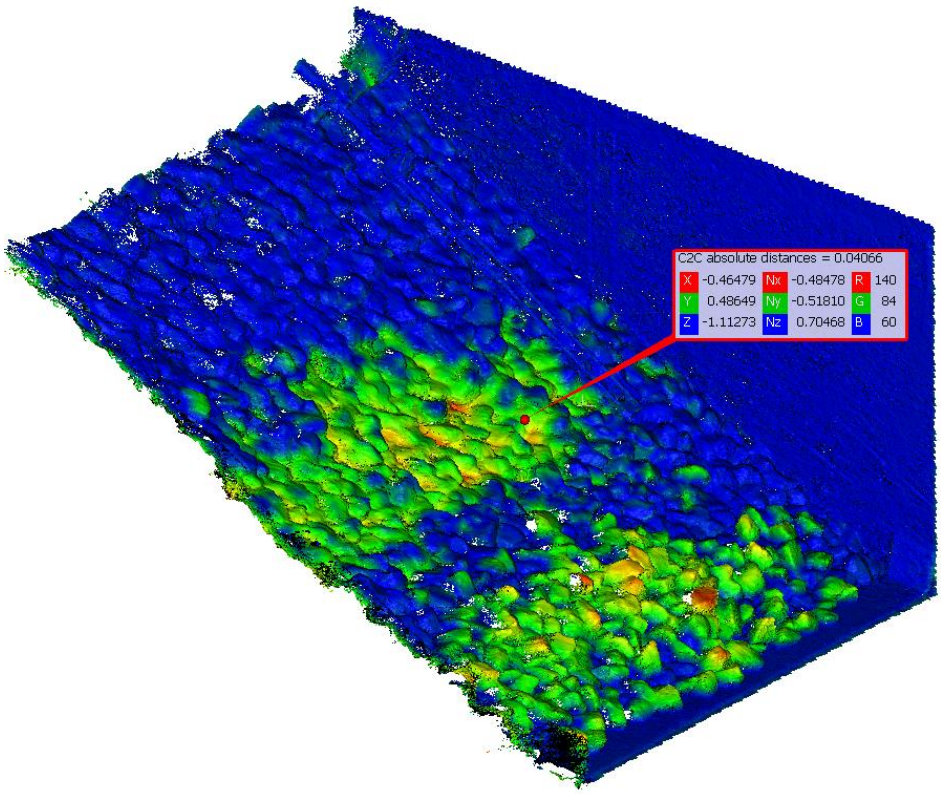

Figure 25 Deviation map reporting both absolute and relative distances between pre and post corresponding points.

The validation procedure has enabled to determine that erosion/accretion of the structure profile occurs when the vertical distance between corresponding points is within a range of approximately the rock nominal diameter and 0.01 m. This enriched point cloud is then segmented to identify the damaged regions and measure their 3D size.

3.2.4.2 Acquisition campaign and 3D structure reconstruction

Each photogrammetric scan consisted of 21-23 photos acquired from the same fixed locations to cover the entire structure in both *x* and *y* directions. The equipment entails a simple, easy-to-use and cost-effective instrumentation, including 1) a bridge digital camera, Canon PowerShot SX410 IS, with CCD 1/2,3 sensor with a resolution of 5152 px 2896 px and a zoom lens (24 mm - 960 mm), installed on a tripod support, in order to reach the required height and maintain a fixed position during the acquisition; 2) different instruments (laser distance beam, tape measure, bubble level), for the localization of the shooting position; 3) six coded targets of 3D known coordinates were placed in specific locations, not interested by wave action (e.g., flume walls), to collect landmarks for photogrammetric model scaling as well as orientation (Figure 21).
The reference coordinate system has been chosen in accordance with the one indicated in Figure 26. In the photogrammetric pipeline, the coordinate system has been defined by targets 1, 2 and 3: Targets 1 and 2 have been placed at the structure toe, having the same *y,z* coordinates and a different *x*; 3 has been placed placed at known distance from 2 along z and having the same *x,y* coordinates of targets 1 and 2. The mutual distances and heights among targets have been measured through the help of a laser distance meter. The other targets have been used as further control points, along the structure slope, for the successive model scaling.

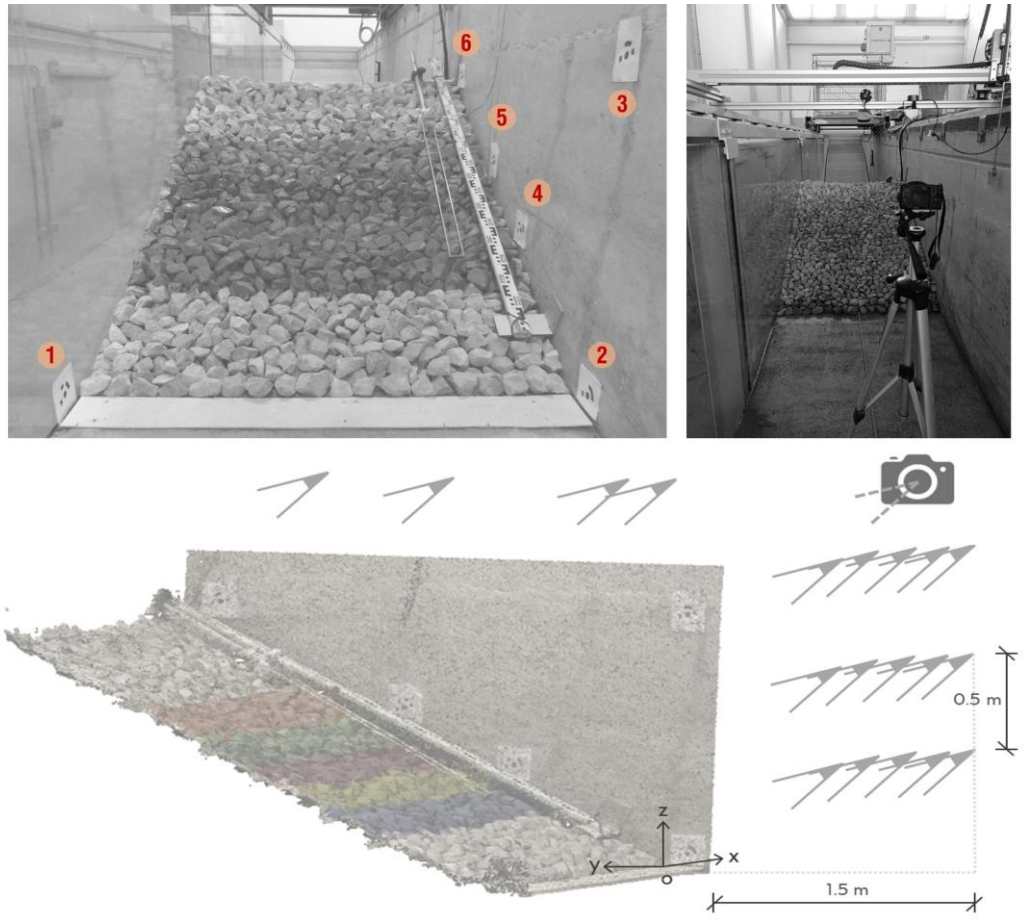

Figure 26 Photogrammetric acquisition set up.

The acquisition planning (number of images, shooting distance, camera locations, image steps) has been determined, in order to achieve 3D data with an output resolution in the order of millimetres or sub-millimetres (~ 0.5 mm in x, and ~ 1 mm in z). Therefore, images have been acquired at a mean distance of about 1.5 m from the structure toe, with spatial steps along the x-axis and z-axis, equal to 0.30 m and 0.50 m, respectively, so that an image overlapping of about 85% – 90% along x direction and 70% – 75% along z direction has been reached (Figure 26).

Furthermore, each area of the object has been acquired by more than 9 images, as it is possible to observe from one of the report photogrammetric reconstruction Figure 27.

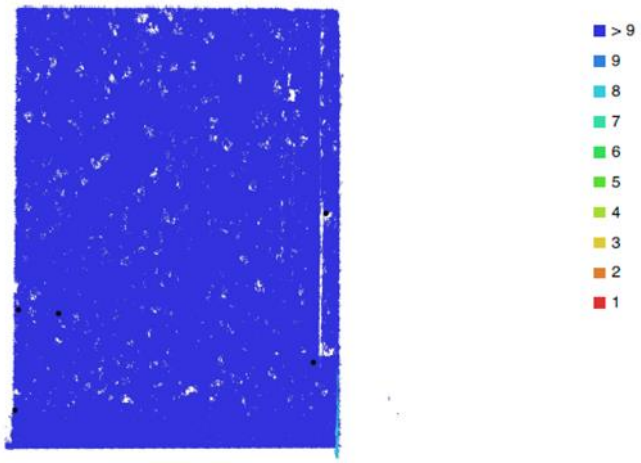

Figure 27 Result of one of the photogrammetric reconstruction report that highlight that each point of the breakwater has been acquired by > 9 images

With the aim of reducing the doming effect, the camera has been orientated both in parallel and oblique direction with respect to the structure surface James & Robson (2014).

The photogrammetric process led to the creation of 3D point clouds, representative of the structure conditions before and after the experimental tests (Figure 28). Agisoft PhotoScan and Metashape have been used, as software support, based on Structure from Motion (*SfM*) algorithms and Dense Multi-View 3D Reconstruction (*DMVR*). For the alignment of cameras and the generation of the sparse cloud, high accuracy has been chosen, to exploit all the information of the images in their original size without any compression downsizing operation.

During the dense point cloud reconstruction, the quality has been set as high, for the depth maps generation in correspondence of every image. High-quality reconstruction means a downscaling of the original images by a factor of 4 and a mild depth filtering, which implies a slight filtering of the outliers (e.g., points deriving from noisy or out-of-

focus images), without losing small scale details. It is important to specify that for the dense point cloud reconstruction, images have been downsized, in order to reach the best compromise between the desired reconstruction and the time processing. In this phase, indeed, the use of original size images requires a large amount of computation time, yet it provides a level of detail that is too high in comparison to the scale of the phenomena being investigated. Throughout the photogrammetric process, the above-mentioned parameters, related to the quality of alignment and point cloud reconstruction, have been kept identical, in order to generate comparable 3D data.

Figure 28 Example of point clouds pre and post wave test.

In Table 10 the main physical model parameters related to each structure layout and wave test are associated with the main photogrammetric features of the reconstructed point clouds, concerning: the number of points of each cloud (N_{points}); the Ground Sample Distance (GSD); the height resolution (R_h) along the perpendicular direction with respect to the plane of the image (y in the current reference system); the reprojection error (E_{rep}), namely the distance among the projections of the same point in multiple images, with respect to the projection of the point in the original image; and the average point density (d_{points}) per square centimetres of each point cloud. As can be observed, the parameters related to the resolution of the point clouds are smaller than

the rock size. It is worth to underline that a comparison and a deviation analysis between pre and post point clouds can be considered consistent only in presence of analogous 3D data. This condition is verified when the values of the photogrammetric parameters of pre/post point clouds (N_{points}, GSD, R_h, E_{rep}, d_{points}) lay within the same order of magnitude. Otherwise, results could be affected by divergences ascribable to either acquisition or elaboration process thus affecting the damage evaluation.

Table 10 Physical model parameters and photogrammetric characteristics (R_h=height resolution, E_{rep}=reprojection error, d_{points}=point density).

Test		Hm0,t	ht	Dn50	Npoints	GSD	Rh	Erep	dpoints
		[m]	[m]	[m]	[-]	[mm/px]	[mm/px]	[px]	[pt/cm2]
WL1-02	Pre	0,185	0,4	0,046	5.957.641	0,524	1,05	0,734	91,1
	Post				5.855.321	0,536	1,07	0,769	87,2
WL1-05	Pre	0,215	0,4	0,046	5.957.641	0,524	1,05	0,734	91,1
	Post				5.855.321	0,536	1,07	0,769	87,2
WL2-05	Pre	0,145	0,2	0,046	5.957.641	0,524	1,05	0,734	91,1
	Post				5.855.321	0,536	1,07	0,769	87,2
WL3-05	Pre	0,06	0,1	0,046	5.957.641	0,524	1,05	0,734	91,1
	Post				5.855.321	0,536	1,07	0,769	87,2
WL4-05	Pre	0,043	0,05	0,046	5.957.641	0,524	1,05	0,734	91,1
	Post				5.855.321	0,536	1,07	0,769	87,2

3.2.4.3 Laser profiler and photogrammetric 2D data interpolation

As far as the damage evaluation is concerned, in view of comparing the two measuring techniques, 2D equally-spaced cross-shore profiles have been extracted from the point clouds, matching the same sections measured by the laser profiler (Figure 22). Indeed, ten *0.1 m* equally-spaced profiles have been extracted from both pre and post photogrammetric point clouds, starting at *0.15 m* far from the left vertical flume wall, with a profile thickness of *1 mm*. The resulting profiles, before the interpolation phase, are made of an approximate point number ranging from 2900 and 4000. The cross section function of *CloudCompare* has been used to the scope

To make the collation feasible, it is necessary to uniform the sections extracted by both techniques, in terms of length and number of points. The scattered and non uniform sequence of points belonging to each transect has been interpolated on a 2D *xy*-grid, with a constant step and fixed axes limits in the wave flume reference system. Among other interpolation methods (e.g., cubic, natural neighbour, cubic or biharmonic spline), a triangulation-based linear interpolation has been chosen, due to the mono-directional development of the examined sections. The grid step depends on the size of the rocks under investigation (õ10^{-2} m). Since the smallest diameter of the stones was less than *0.01 m*, a grid pace of *0.001 m* has been selected and the y-grid limits set as 0 - 1.8 m, resulting in a total number of points equal to 1800 for each transect. Representative pre and post profiles of the structure are then obtained by averaging the interpolated sections. At this stage, mean initial and final profiles are overlapped and compared in order to quantify the discrepancies in *z-elevation*, by a point-to-point difference calculation, and identify erosion as well as accretion areas.

CHAPTER 4
RESULTS AND DISCUSSION

"I often say that when you can measure what you are speaking about, and express it in numbers, you know something about it; but when you cannot measure it, when you cannot express it in numbers, your knowledge is of a meagre and unsatisfactory kind."
Lord Kelvin

4. Results and discussion

4.1 Data Analysis

4.1.1 Wave analysis

Wave statistical and spectral characteristics have been estimated from the measured surface elevations (η) with and without the breakwater for all the gauges placed along the wave flume. The statistical parameters, namely, H_z and T_m , the significant wave height and the mean period in the time domain respectively, have been retrieved by means a zero up-crossing analysis (Kamphuis (2020)). The process of zero up-crossing analysis can be described as follows: i) define the reference point represented by the that passes from a negative to a positive position of water surface elevation and intercepts with the reference solid black line in Figure 29; ii) identify the wave height of the first loop as the maximum difference of water surface elevation between two consecutive zero-crossing points; iii) the wave period of the first loop is the time interval from the first zero-crossing point to the second one. These three steps along the reference line should be carried out to get the wave height and wave period of all wave loops. The red and green points respectively, represent the wave crests and throughts that have been detected with the method.

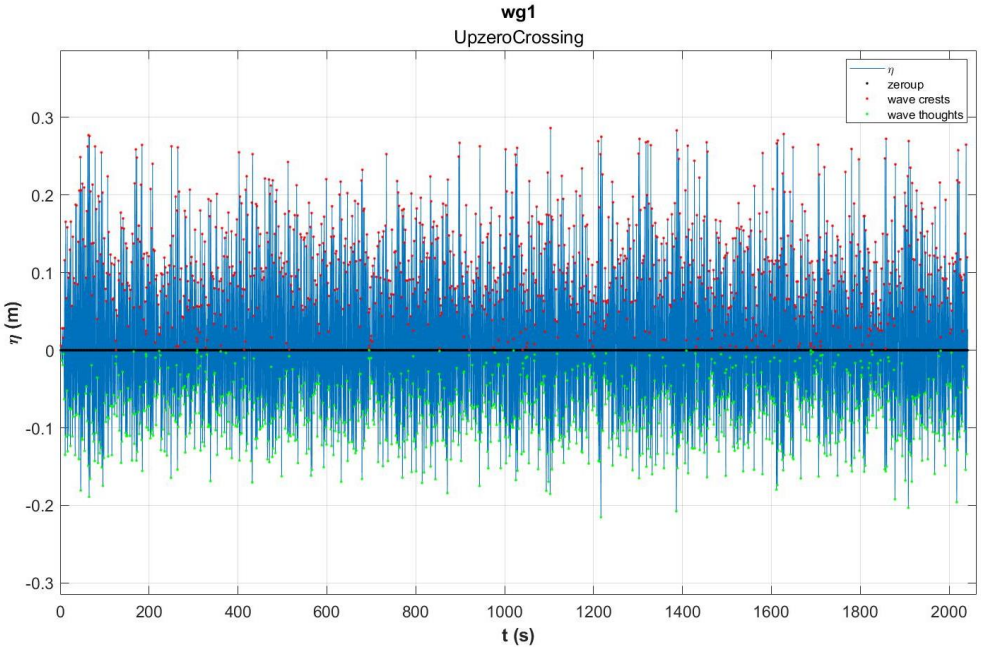

Figure 29 An example of the application of the zero-up crossing method for the test WL1-04 with Hs=0.302 m and Tm =1.795 s measured at the offshore gauge (WG1).

To the purposes of the present research, a spectral analysis of the raw wave signals acquired have been performed in order to retrieve the main spectral wave characteristics namely, the spectral wave height (H_{m0}), the spectral wave period ($T_{m-1,0}$) and the peak wave period T_p. These quantities have been determined by considering the entire spectrum acquired for each wave gauges. A filter at the low frequency has not been implemented to avoid loosing an important amount of the wave energy, especially in shallower water conditions. Only, a low pass filter at a frequency equal $3f_p$ with f_p being the peak frequency has been applied in the analysis, to depurate the signal from the noise associated with the wave probes and the acquisition chain.

The presence of the foreshore induces a heavy wave breaking, thus changing the wave behaviour considerably (Hofland et al. (2017); Suzuki et al. (2017)).The spectrum offshore (solid black line in Figure 30) shows a clear peak at the high frequency (~0.5 Hz) but moving to the structure toe, the wave breaking occurs and the peak is shifted

at the lowest frequencies. The spectral shape becomes noisy, and the single peak is not anymore recognizable. All tests show that nonlinear wave transformations (e.g., shoaling and wave breaking) occur along the foreshore. Such behaviour is revealed by the bimodal and more flattened spectrum (Figure 30) and more peaked time series at the toe of the breakwater (WG7) (Figure 30). In shallower conditions, has been encountered that the wave time series doesn't present thoughts anymore, and the spectrum reveals to have only a peak at the very low frequencies (0.02 Hz – 0.03 Hz).

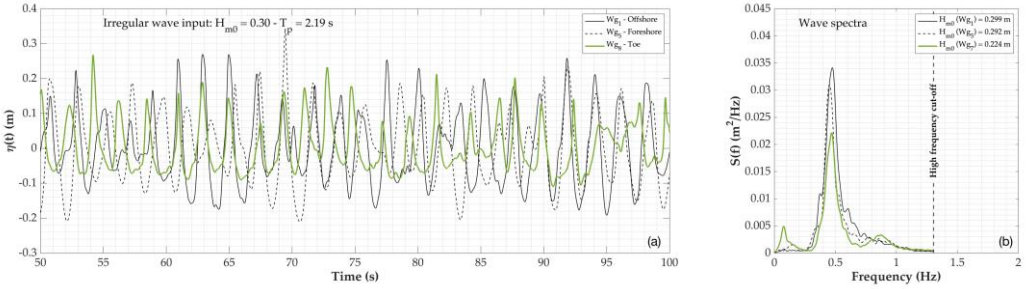

Figure 30 Temporal evolution of the free surface elevation η(t) (m); b) Wave spectra of the free surface elevation and computed at three different points along the wave flume from offshore till the structure toe (WG1-WG5-WG7).

The spectral parameters, have been evaluated as follows:

$$m_n = \int_0^{3f_p} f^n E(f) df \,,$$

$$T_{m-1,0} = \frac{m_{-1}}{m_0} \,,$$

$$H_{m0} = 4\sqrt{m_0} \qquad (4.\ 1)$$

where E is the variance energy density spectrum, f the frequency and m_n the n-th order of moment of E.

Since that it has been necessary retrieve di wave height at the breakwater toe, in order to perform hydraulic stability study of the structure, this quantities has been retrieved with and without the structure in place.

In the first case, the incident wave components has been separated from the reflected ones by means the application of the Mansard & Funke (1980) method applied at the wave gauges placed offshore (WG2-WG3-WG4 Figure 7). Then, the reflection coefficient (K_r [%]) so determined has been applied to the total wave height measured at the toe, thus deriving the effective incident height. The K_r has been found to vary for all the tests analysed in a range between 0.221 and 0.375.

Noticed that this method is valid for deep water and cannot be applied in shallow water conditions (Altomare et al. (2016)), since the linearity of the waves is not respected anymore.

Once all the stability tests have been completed, the executed tests have been repeated without structure in order to more accurately determine the incident wave height at the toe. The parameters estimated in these two flume configurations have been compared as reported in Figure 31 and the goodness of the fit in the comparison has been quantified by means the correlation coefficient (r Eq. (4. 2)) and the Root mean Square Error (RMSE Eq.(3. 6)).

$$r = \frac{\sum_{i=1}^{j}(o_i - \bar{o})(e_i - \bar{e})}{\sqrt{\sum_{i=i}^{j}(o_i - \bar{o})^2 \sum_{i=1}^{j}(e_i - \bar{e})^2}} \tag{4. 2}$$

Where *j* is the number of observations, o_i is the observed value (with the structure), e_i is the estimated value (without the structure) and $\bar{o}$, $\bar{e}$ are the average of the target and estimated values respectively. A value of $0 \leq r \leq 1$ measures the degree of correlation, an high values means a better correlation between the parameters.

The presence of the structure has a strongly influence on the wave period measured at the breakwater toe, (Figure 31b), especially when the period increase (due to wave

breaking and shallower water conditions). It has been found that the period with the presence of the structure is always greater than the other without it.

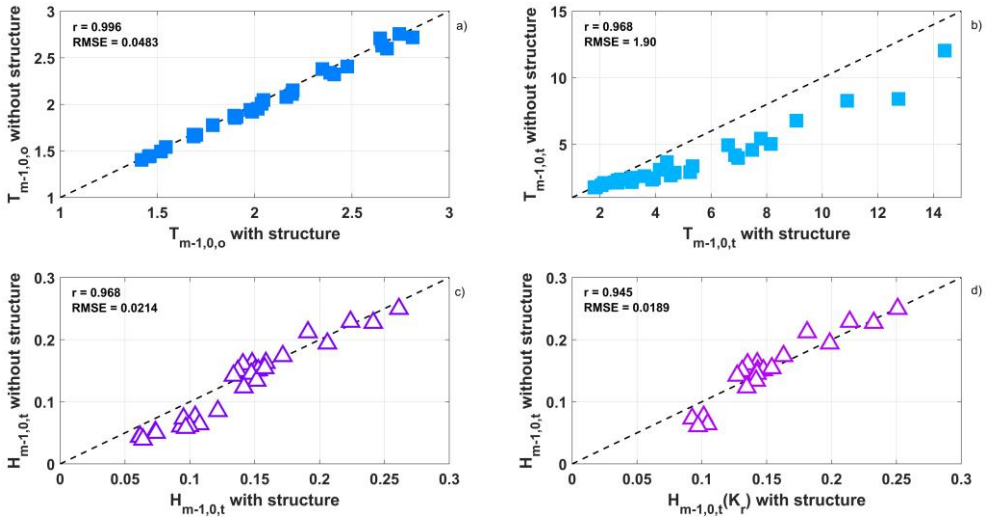

Figure 31 a) – b) Comparison between the spectral wave period with and without the structure in place, offshore ($T_{m-1,0,o}$) and at the breakwater toe ($T_{m-1,0,t}$), respectively; c) comparison between the spectral wave height at the breakwater toe ($H_{m-1,0,t}$), with and without structure; d) comparison between the height measured without the structure and the height retrieve by applying a reflection coefficient evaluated offshore.

4.1.2 Damage analysis

In Figure 32 an example of pre/post profiles acquired with laser (blue line) and photogrammetry (red line) are reported. The dashed black line represents the design profile of the structure, which slightly differs from the initial profile in of the structure built into the wave flume.

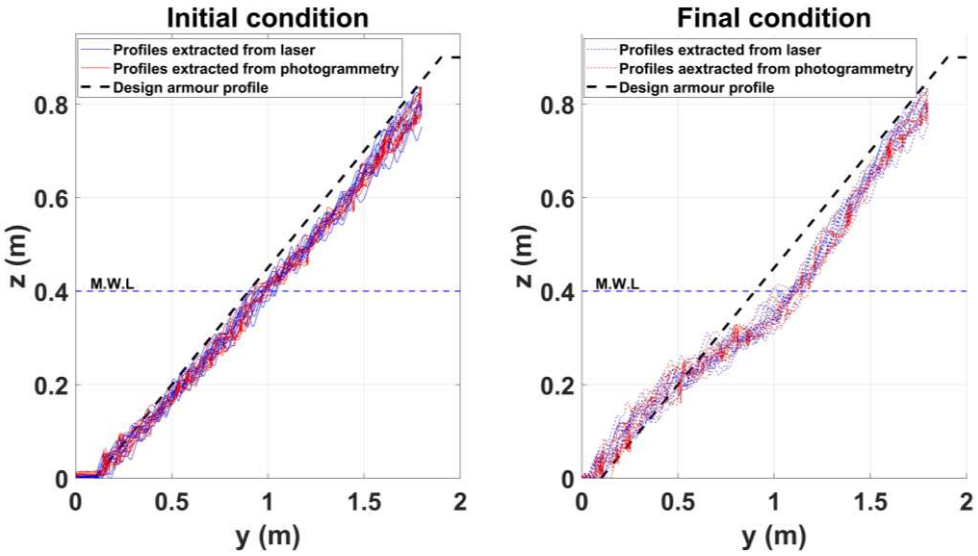

Figure 32 Example of cross shore structure profiles acquired by laser profiler (blue lines) and extracted from images (red lines) before (left panel) and after (right panel) the wave test WL1-02 (see Table 11).

Figure 33 reports an example of the mean initial (red curve) and final profiles (black curve) detected by both techniques, which can be quantitatively compared to derive the damage *S*. In the same figure, the positive and negative areas of d_z curve (blue line), correspond to the eroded (A_e) and accreted areas (A_a), respectively. For both measurement systems, it has been stressed that the difference between the accretion and the eroded areas is not equal to 0, unlike what would be expected, since many stones have been dragged by waves outside the investigated areas and, as a consequence, not considered in the balance equation. Results show that

photogrammetric procedure (*ph*) well estimates the temporal evolution of the structure damage measured by the laser profiler (*lp*).

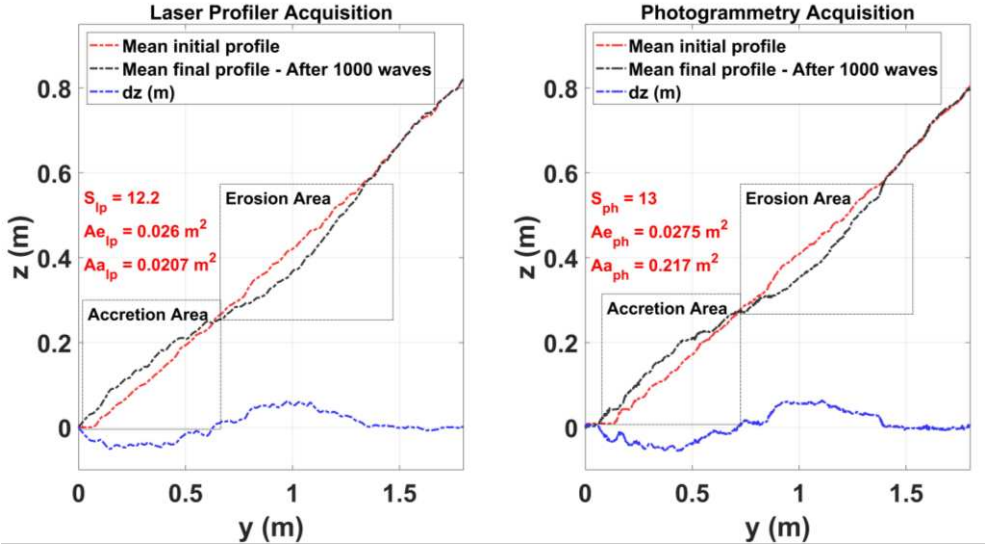

Figure 33 Example of comparison between the average profiles before (red curve) and after (black curve) the wave attack measured by the laser profile (left panel) and extracted from photogrammetry (right panel), for the test WL1-02 (see Table 11).

4.1.2.1 Validation of photogrammetric technique for damage evaluation

The validation procedure is accomplished relying on standard statistics, namely the correlation coefficient R^2 and the percentage error $E_r(\%)$, related to both pre and post single and average profiles. In Eq.(4. 3), zi(y) represents the profile elevation with respect to the flume bottom z_0 and ż is the average value of $z_i(y)$:

$$R^2_{pre/post} = 1 - \frac{\sum_{i=1}^{j}(z_{i,lp} - z_{i,ph})^2}{\sum_{i=1}^{j}(z_{i,lp} - \dot{z})^2} \tag{4. 3}$$

where *j* is the total points number of the spatial discretization grid on each cross-shore transect.

For each breakwater configuration, Table 11 shows that R^2 values are close to the unit, demonstrating the high accuracy of the photogrammetric technique with respect to the traditional laser profiler. Once the eroded areas were retrieved, the damage S was computed in all tested configurations (Table 11),according to Eq. (2. 13).

Table 11 Results from the application of both measurement techniques and relative standard statistics (E_r and R^2).

Test	D_{n50} [m]	Ae [m^2]		Aa [m^2]		3DAe [m^2]	S [-]		Er [%]		R^2 [-]
		lp	ph	lp	ph		lp	ph	lp	ph	
WL1-02	0,046	$7,5*10^{-3}$	$6,7*10^{-3}$	$8,5*10^{-3}$	$1,1*10^{-3}$	0,426	3,5	3,2	5,9	22	pre 0.998 post 0.998
WL1-05	0,046	$2,6*10^{-2}$	$2,7*10^{-2}$	$2,1*10^{-2}$	$2,2*10^{-2}$	0,962	12,2	13	3,17	4,2	pre 0.998 post 0.999
WL2-05	0,046	$5,3*10^{-3}$	$5,1*10^{-3}$	$3,5*10^{-3}$	$4,5*10^{-3}$	0,313	4,6	4,4	2,2	25	pre 0.998 post 0.998
WL3-05	0,046	$8,6*10^{-4}$	$9,6*10^{-4}$	$4,8*10^{-4}$	$9,1*10^{-4}$	0,132	1,5	1,7	5,36	61,9	pre 0.994 post 0.994
WL4-05	0,046	$4,2*10^{-4}$	$6,2*10^{-4}$	$1,2*10^{-4}$	$4,9*10^{-4}$	0,032	2,2	3,2	19,8	121	pre 0.993 post 0.993

By considering the variables A_e and S, derived from both measurement techniques, it is straightforward to deduce that they are comparable, since the S values lie within the same damage level range (Table 2), showing a relative error (E_r) less than 5%. Besides a two-dimensional damage computation, a 3D change detection analysis has been also performed, by estimating the deviation between pre and post models. The area subjected to erosion ($3DA_e$) has been detected and quantified from the segmented point clouds.

Figure 34 presents an example of the deviation maps in absolute and relative distances, as well as the variable ζ on the x-axis which is the z-difference between pre and post 3D models for each test. This variable follows a Gaussian distribution, whose probability density function $\Phi_{\mu-\sigma^2}(\zeta)$ is completely characterized by two parameters, mean μ and variance σ^2, namely the first and the second order moments of the distribution, respectively. The amount of damage has been related to the Gaussian distribution of z-displacements (ζ), showing consistency between obtained results and the actual physical damage of the structure. Accordingly, high values of the variance describe notable levels of damage, as found in the test W L1 - 02 where σ^2 is equal to 0.0172, corresponding to the maximum encountered damage ($S = 13$). It is worth specifying that the damage can be observed when the vertical distance between corresponding points is enclosed in a range varying approximately between the armour rock nominal diameter and the core size. To this end, two different ranges of exclusion have been defined, as shown in Figure 34, by dashed vertical lines, identifying the ζ range inside of which values are not considered as a z-displacement: for tests WL1 and WL2, with a nominal diameter of the armour layer equal to 0.046 m and 0.034, respectively, a range of $-0.01\ \text{m} < \zeta < 0.01\ \text{m}$ have been established, while for WL3 and WL4, as the armour dimension is in the order of 1 cm, the range of exclusion has been restricted to $-0.005\ \text{m} < \zeta < 0.005\ \text{m}$.

The mean value for all tests is equal to zero, indicating that the number of points displaced in erosion and accretion areas is equal. An increase in variance implies more dispersion of data around the mean value and a higher degree of damage. As an

example, WL1-02 had the highest level of damage (S=13), and its pdf curve is flatter than the other tests, signalling that a larger number of points were displaced along the entire slope.

Results show that the damage level S evaluated by the proposed measurement workflow falls in the same range of the damage calculated by the standard laser profile procedure (Table 2), with a mean relative error Er of 5%. It is important to underline that, for the accreted areas the outcomes are less accurate, especially when small scale objects are considered, due to the fact that many stones could be dragged away from the investigated area and, hence, not considered in the volume balance. As stated by Broderick (1984), the focus of the investigation concerns the displacement of the stones within the structure surface. Furthermore, for calculating the parameter S, which is fundamental for the design of breakwaters, it is necessary to consider only the eroded parts and not the accreted ones. Therefore, the accuracy decreasing in accretion measurements does not affect the calculation of the damage. Conversely, if there was an interest in evaluating the accreted area, it would have been possible to include also the stones dragged away from the structure toe, by simply varying the cutting point of the photogrammetric profiles.

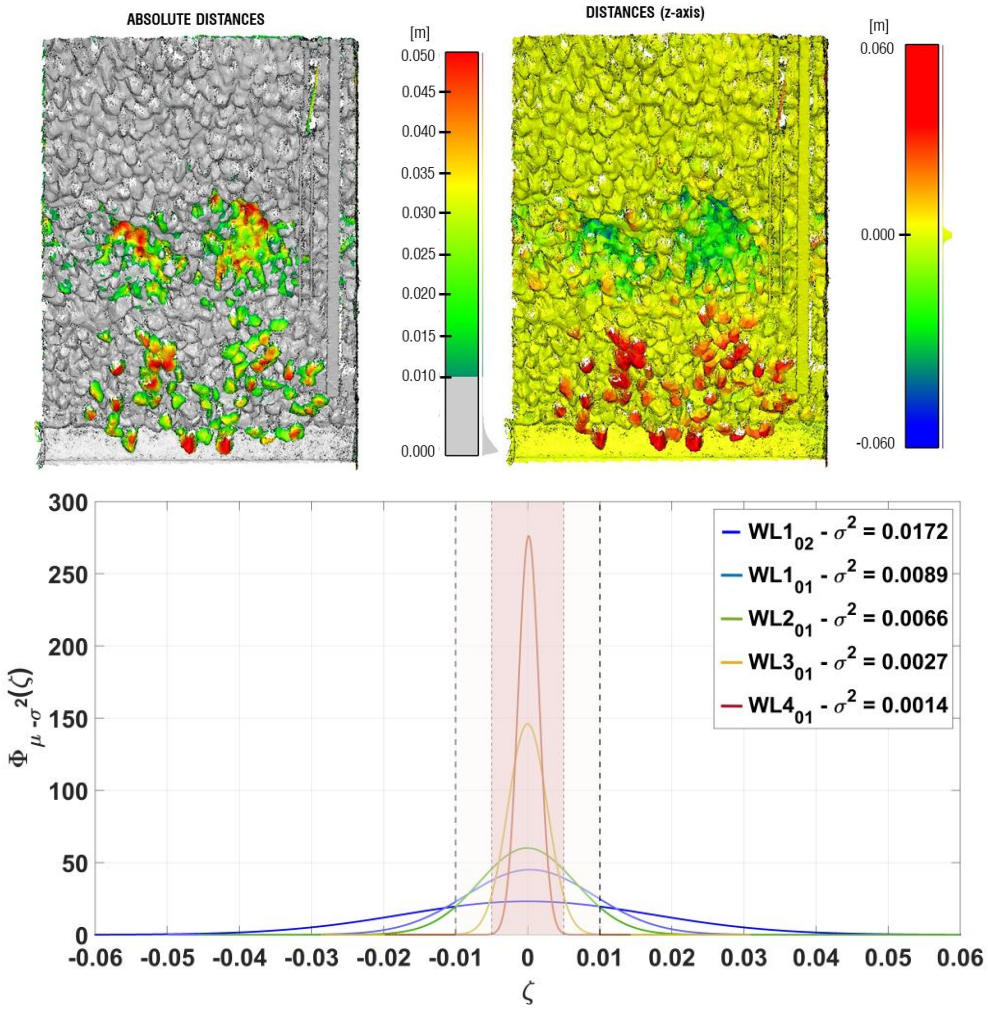

Figure 34 Top: Deviation maps, representing the absolute distances (top) and the distances computed in z (bottom), with the relative scalar fields, for the test WL1-02 ($H_{m0,o}$ = 0.25 m, $T_{m-1,0}$ = 2.57 s). Bottom: z-difference point Gaussian distribution for each test.

In conclusion, it is important to underline some aspects related to the acquisition and processing times of the photogrammetric and the laser profiler techniques. Considering the whole workflow (Figure 24), the photogrammetric procedure requires about half the time needed for the laser profiler. The greatest advantage, in terms of expeditiousness, is related to the data acquisition, which must be carried out in the laboratory, before

and after each test. Indeed, for the laser profiler, the acquisition of 10 transects took about 50 minutes, while, with the photogrammetric pipeline, the image acquisition of the entire structure took between 5 and 10 minutes. This yields to a consistent optimization of the total timing of the experimental campaign. In fact, given a test duration of 40-45 minutes, it is necessary to consider 50 additional minutes only for data acquisition before and after each test, with the laser profiler (see Table 12 for detail). Thus, the total timing for the laboratory activities reaches more than two hours, for every single test, with respect to one hour needed in the case of photogrammetry. The main consequence is related to the possibility of performing a higher number of tests within the same interval of time. In addition, it is important to underline that, with laser profiler, the data collection

is limited to 10 transects, in the present experimental campaign, because every additional cross-section, which could be useful to improve the damage measurement accuracy, would imply an increase in measurement time. While, the use of photogrammetry entails a fast image acquisition, from which the 3D model is reconstructed, providing a huge amount of data about the temporal evolution of the entire structure.

Table 12 Time estimation for retrieving the level of damage of the structure by applying both the photogrammetry and laser profiler method.

	PHOTOGRAMMETRY (ph)								
	Test	Image acquisition *pre*	Image Acquisition *post*	3D reconstruction	Profiles extraction	Profiles analysis	Deviation analysis	Total *ph*	Total
Mean time (min)	40-45	6	6	12	22	5	5	55	95-100
	LASER PROFILER (lp)								
								Total *lp*	Total
	40-45	6	6	no	no	5	no	110	150-155

4.1.3 Pressure analysis

In the following section the analysis of the pressure sensors signals placed inside the breakwater core, is reported. Hereinafter, the term 'pressure' refers to the dynamic component p' and the total pressure $p = p_0 + p'$(where p_0 is the hydrostatic pressure), namely the excess pore water pressure concerning the static initial conditions, which is solely induced by wave action. Once acquired, the pressure signal time series have been processed (e.g., depuration from the level set-up, signal denoising, data filtering, etc.) and then analysed in both time and frequency domains similar to the free surface elevation. Firstly, a sensitivity analysis through the RMSE estimator (e.g., Aristodemo et al. (2018)), has been performed to choose the best filtering method between the Savitzky-Golay filter(Savitzky & Golay (1964)), the Mexican hat Wavelet filter (Morlet et al. (1982)), and a filt-filt filter (Mitra & Kuo (2006)). Finally, the digital 'filt-filt' function has been applied to denoise and filter the pressure signals (Figure 35). The signals have been filtered in the frequency bandwidth between 0.03 Hz and 2 Hz where the high pass filter has been chosen as the natural resonant frequency of the wave laboratory flume (Rabinovich (2009); Savitzky & Golay (1964)).

During all experimental tests, the analysis of the pressure time series have experienced a high water level set-up inside the breakwater, which generally occurs when a conventional breakwater is exposed to waves (Wellens & Van Gent (2012)). In physical models, such a secondary non-linear effect is more evident, since the outflow velocity from the rear side of the breakwater is much lower than the seaside slope inflow velocity, compared to prototype conditions. This is due to laboratory constraints, mainly depending on the different hydraulic properties of the porous medium (e.g., permeability, air entrainment). In order to minimize such an effect, during the construction of the physical model, two drain pipes were placed inside the concrete bed to guarantee water circulation in the flume. Nevertheless, a residual water set-up has been observed, thus requiring signal filtering aimed to depurate the pressure measurements from the flow set-up.

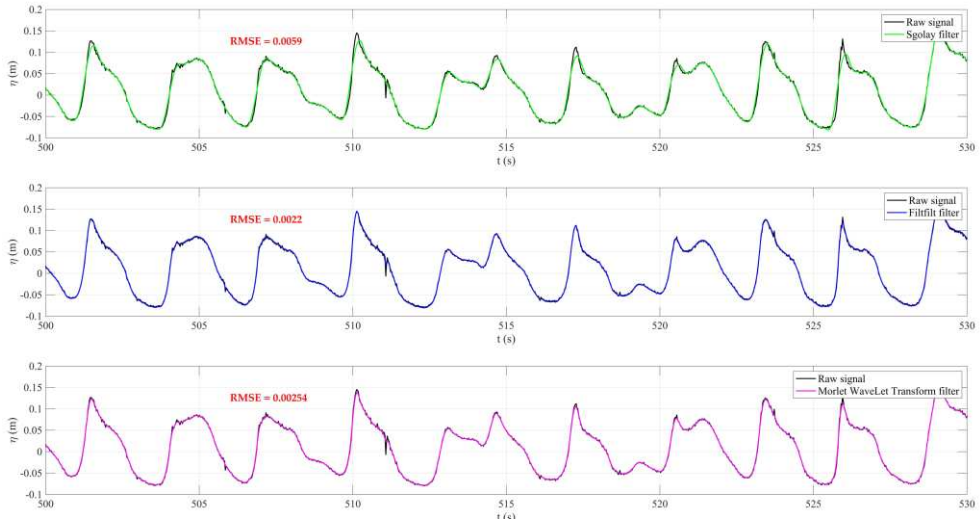

Figure 35 Sensitivity analysis with respect to the Savitzy-Golay filter (top), the Morlet filter (middle) and the Zero phase digital filter (bottom).

Consequently, the pore pressure oscillations have been corrected for all the test series, following a standard MATLAB routine by depurating the single signal from the moving average for the acquired one over a window equal to 10 waves (for the irregular tests) and 5 waves (for the regular tests). Calculated every ten (irregular tests) and five (regular tests) waves from the measured time series. The maximum measured set-up $\tilde{\eta}$ falls in a range between 0.027 m - 0.104 m. It corresponds to a relevant component that can not be neglected during the analyses, since it was about 26% - 45% of H_i and 7% - 26% of h_t, in line with previous studies, which report a magnitude of the internal set-up within 10-20 % of the water depth at the toe of the breakwater (Bürger et al. (1988)).

The internal setup is a function of the horizontal distance from the interface between the filter and the core, the material properties of the core, and the incident wave characteristics. Generally, for long tests, the set-up is more or less constant through the core of the breakwater for a given condition. When a wave approaches the slope, the water table rises rapidly (transient phase), and then reaches a plateau (stationary phase) due to a slow penetration flow induced by friction. As expected, the level of the

water table of the phreatic flow averagely increases along the x-direction in the first half of the breakwater, reaching its maximum between P_{t2} and P_{t3} whereas from the middle to the lee side of the breakwater, the water table increases with a lower velocity because the phreatic flow manages to pass the porous medium reaching the rear side of the structure through transmission (Figure 36).

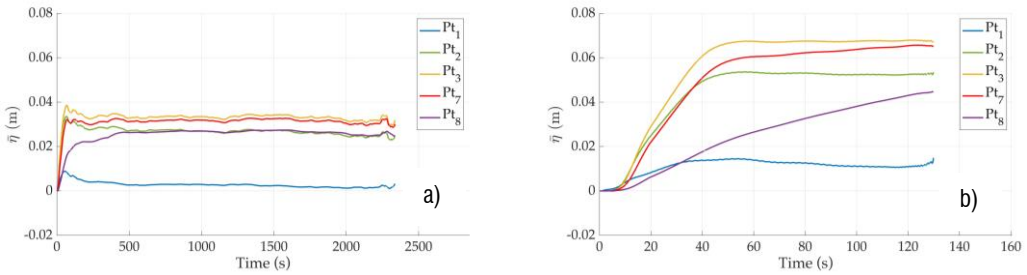

Figure 36 Example of temporal variation of the adimensionalised internal setup for: a) an irregular test b) a regular test.

Then, the filtered signal acquired by the pressure transducers has been then used to investigate both the temporal and spatial variation of the dynamic component of the pore pressure inside the structure. At this scope, the mean pressure height P_m has been derived from pressure transducer measurements, through a zero up-crossing analysis in the time domain for regular tests. For irregular waves, a spectral pressure height P'_{m0} together with the P'_m has been obtained from the pressure variance spectrum as $P'_{mo}=4\sqrt{m_o}$, where m_0 is the zeroth-order momentum of the energy spectra in the frequency bandwidth (Eq.(4. 4)).

$$m_0 = \int_{0.03}^{3f_p} E(f)df \qquad (4.\ 4)$$

The Figure 37 illustrates the temporal variation of the measured dynamic pressure oscillations for each $P_{t,i}$, which shows the pressure fluctuation damping along the

horizontal plane (from P_{t1} to P_{t8} see Figure 19) inside the breakwater (p'(t)) in meter water column, with water density $\rho_w = 1000 kg/m^3$ for a frame of 50 s). It should be noted in Figure 37, a slight phase lag $\tau = 1$ s between waves at the toe with the structure in place and the pore pressures. The phase lag can be explained by the pore fluid transferring slowly in the core with low permeability and due to the effect of the breakwater reflection. Indeed, this time shift is no more evident when the incident wave spectrum computed without the breakwater in the flume is used. In depth-limited water conditions, the surf zone is dominated by low-frequency motions closely related to the incident wave groups in which the energy of the long wave components grows as the wave approaches the structure, whereas, the energy of the short wave components decreases (Kamphuis (2001)). This process involves a complex wave energy re-organisation, which considerably influences the pressure field inside the breakwater.

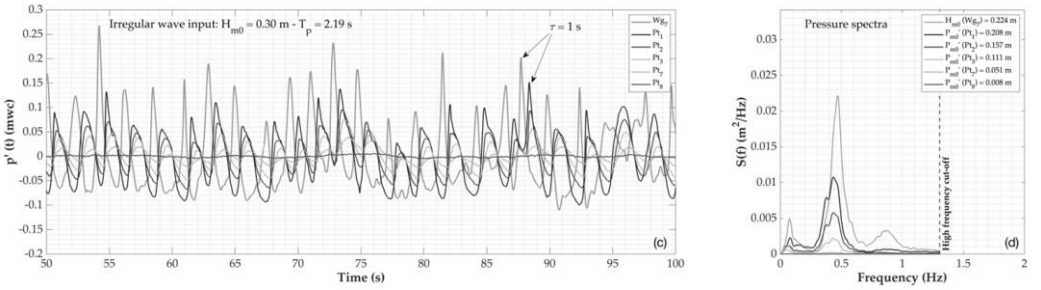

Figure 37 Left: Temporal variation p'(t) (meter of water column) of the horizontal filtered pressure signals for a time frame of 50 s for an irregular test; Right, Pressure spectra retrieved from the pressure time series for all the pressor devices placed on the same distance from the bottom.

In Figure 38 an example of the spatial variation of P'_m inside the breakwater along with the mean wave height measured at the WG6 and W G7is reported. Since data with regular and irregular waves have been acquired, in order to compare them, mean pressure heights P'_m have been taken into account in the further analysis. As expected, a larger wave period leads to larger run-up events (van Gent & Doorn (2001)). The reference pressure is, generally, affected by the wave run-up (represented by the wavelength) on the armour slope (Vanneste & Troch (2012)). After that, dissipation

through the porous media begins. Pore pressure data in Figure 38 clearly shows the friction-induced pore pressure attenuation inside the core of the breakwater. This dissipation is stronger when the whole water column has flooded the armour and filter layers and slower when the water reaches and propagates through the core. The first dissipation length is dominated by internal breaking and friction due to the armour and filter layers, whereas the second dissipation length is dominated by core friction. As can be seen in Figure 38, the dissipation decreases the P'_m just below the crest to approximately 80/90 % of the initial pressure.

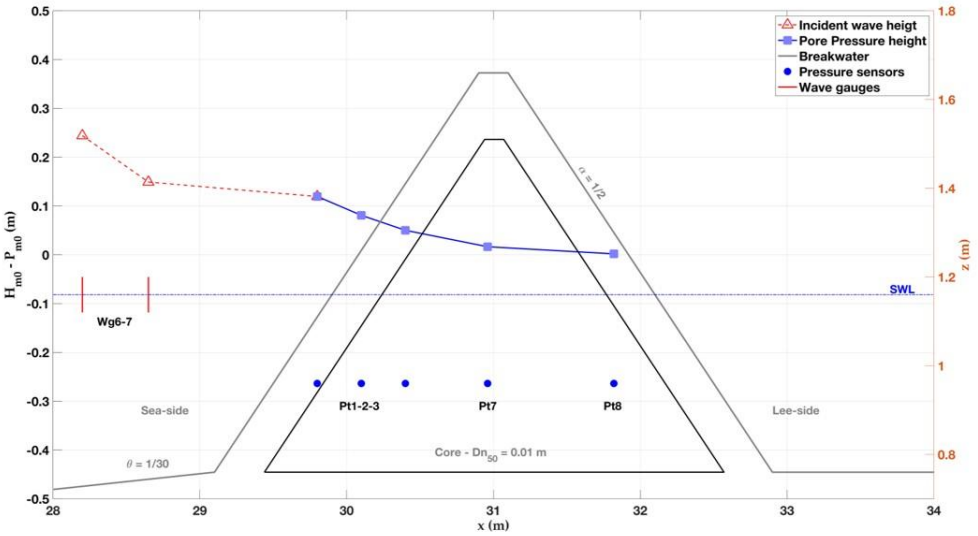

Figure 38 Example of pore pressure damping trend inside the core of the breakwater for an irregular test, together with the mean wave heights measured by the 2 wave gauges (WG6 - WG7) placed at the structure toe.

4.2 Waves in depth limited water conditions

The tests have been scheduled in order to reproduce different water depth-limited conditions, from intermediate up to extremely shallow. In Figure 39 the relative wave height ($H_{m0,t}/H_{m0,o}$) is plotted versus the relative depth ($H_{m0,o}/h_t$), showing that the relative

wave height exponentially decreases as the relative water depth increases. For the lowest tested water level, the wave height at the toe reaches values up to 20% of the deep water spectral wave height, mainly due to shoaling and breaking processes that occur over the foreshore.

A nonlinear regression analysis has allowed to estimate the coefficients β_1 and β_2 equal to 0.64 and -0.63, respectively, with a good correlation coefficient (R^2) equal to 0.97 and an RMSE of 0.0931. The Eq. (4. 5) allows to evaluate the wave height at the toe of the structure, by means of the known parameters ($H_{m0,o}$ and h_t), at least for the tested foreshore (θ= 1V:30H).

$$\frac{H_{m0,t}}{H_{m0,o}} = \beta_1 \left(\frac{H_{m0,o}}{h_t}\right)^{\beta_2} \tag{4. 5}$$

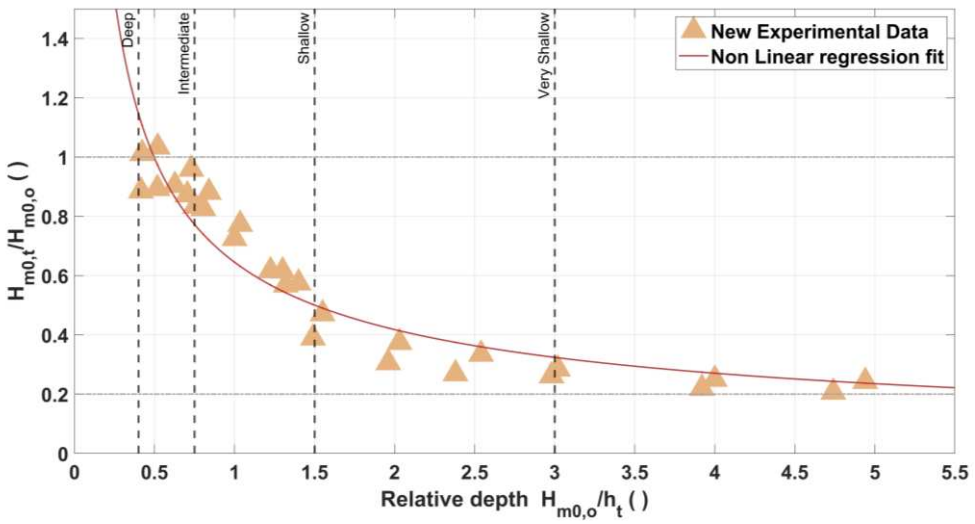

Figure 39 The effect of the water depth-limited conditions on the ratio $H_{m0,\,o}/H_{m0,\,t}$.

The spectral breaker parameter ($\xi_{m-1,0}$), has been found to be strongly dependent to the relative depth ($h_r = H_{m0,o}/h_t$). As expected, the surf similarity parameter exponentially increase as we move from intermediate toward shallow and extremely shallow water

conditions, reaching a maximum value of 30 (Figure 40). In fact, due to wave transformation occurring over the foreshore, the spectral wave period at the structure toe can become larger than 6/7 times the offshore period (Hofland et al. (2017)). Then, it is possible that breaker parameter can have an influence on the hydraulic stability of the structure.

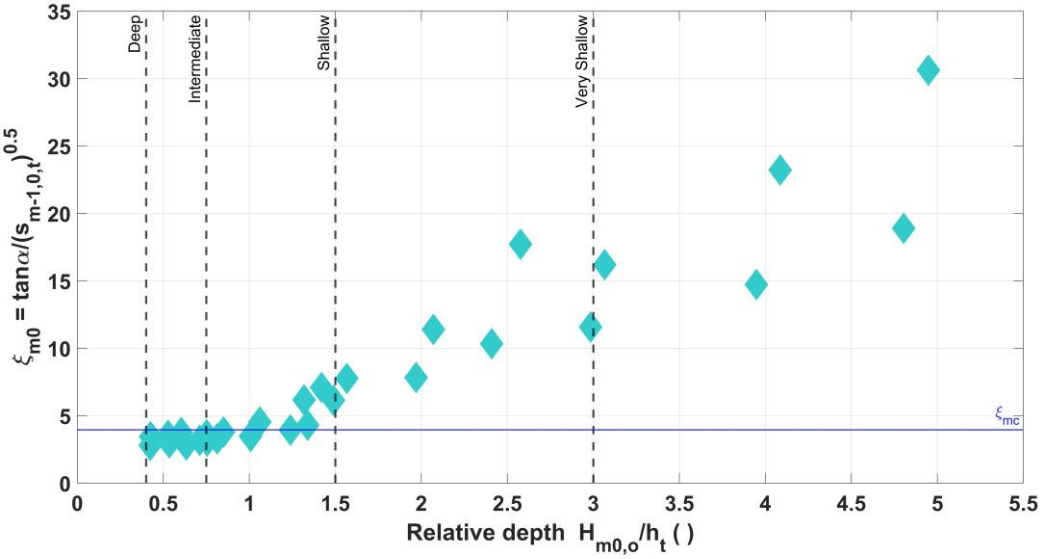

Figure 40 The influence of the relative depth in different shallowness conditions, on the spectral breaker parameter $\xi_{m-1,0}$.

In Figure 41 the ratio between the spectral wave period at the structure toe and offshore ($T_{m1-0,t}/T_{m1-0,o}$) has been reported on the y-axis along with both the relative depth and a modified relative depth ($\ddot{h}$ Eq.(2. 10)) on the x-axis. The $\ddot{h}$ parameter introduced by Hofland et al. (2017) takes into account the influence of the foreshore slope (cotθ). The experimental data (squares blue) shows a good fit with a R^2 equal to 0.91 and 0.923 without and with the slope influence, respectively. On the right in Figure 41, the present data are slightly overestimated by the empirical formulation (Eq.(2. 11)) proposed in Hofland et al. (2017). In fact, the datasets on which the formula has been calibrated (grey triangle Altomare et al. (2016); Chen et al. (2015); Van Gent (1999)), don't

present data with a foreshore slope 1V:30H. So, the formulation should be re-calibrated also considering the present data.

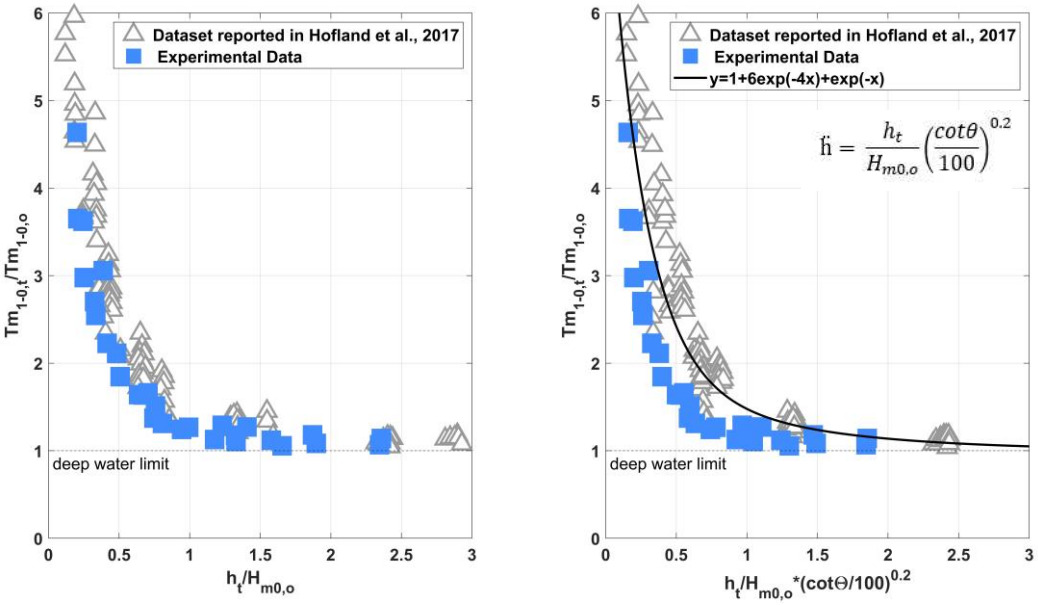

Figure 41 The measure evolution of the spectral wave period at the breakwater toe $T_{m-1,0,t}$ as a function of the relative depth (on the left) and with a slope correction (on the right) (Hofland et al. (2017)).

4.3 Comparison with the existing hydraulic stability formulae in depth limited water conditions

The tests have been carried out to investigate the rock slope stability in different water depth-limited conditions, from intermediate until extremely shallow. The slope damage has been quantified for each test by comparing, the mean initial and final slope profile. In Figure 42 the armour slope damage data (S) retrieved after tests of 1000 and 3000 waves , respectively, have been reported on the y-axis, along with the stability number (x-axis) $Ns = H/\Delta D_{n50}$, with $H = H_{m0,t}$.

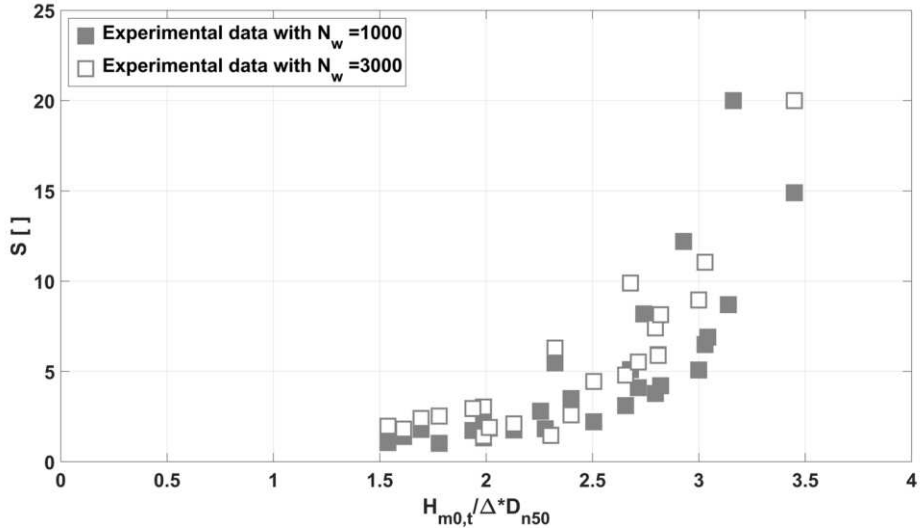

Figure 42 Slope armour damage S as a function of the stability number $Ns = H/\Delta D_{n50}$, with $H = H_{m0,t}$.

Different formulas are commonly used to estimate rock armor damage although not all of them should be used for shallow water conditions as described in Section2. Here, is shown a comparison between the armor damage measured in the present study and the predictions given by Eq.(2. 16)and Eq. (2. 17)which can be re-written in terms of armor damage, S. In order to apply the Eq.(2. 16) as reported in Smith et al. (2003), the trend of the ratio $H_{2\%,t}/H_{s,t}$ has been investigated (Figure 43). For non breaking waves this ratio is equal to 1.4 (deep water conditions) which means that they are following a Rayleigh distribution. However, with the waves approaching the foreshore they begins to break and it has been revealed that the ratio between the wave height exceed by 2% of waves and the significant wave height, starts to decrease until a value of about 1.2 (intermediate-shallow water conditions). Instead, for values of relative depth greater than 1.5 (namely, vary and extremely water conditions), the ratio between the characteristics wave heights increase, indicating that the waves are again approaching the Rayleigh distribution (Smith et al. (2003)). This analysis points out that in applying the Eq.(2. 16), the ratio $H_{2\%,t}/H_{s,t}$ has to be used instead of the fixed values 1.2-1.4.

In order to support the above statement, in Figure 44 the experimental wave heights distribution (black histogram) is plotted against the Rayleigh (solid red line) and Gaussian (blue solid line) distribution, for tests with different water conditions, extremely shallow at the top of the figure and intermediate at the bottom. It is clearly visible that the measured wave heights are well described by the Rayleigh distribution in both water conditions.

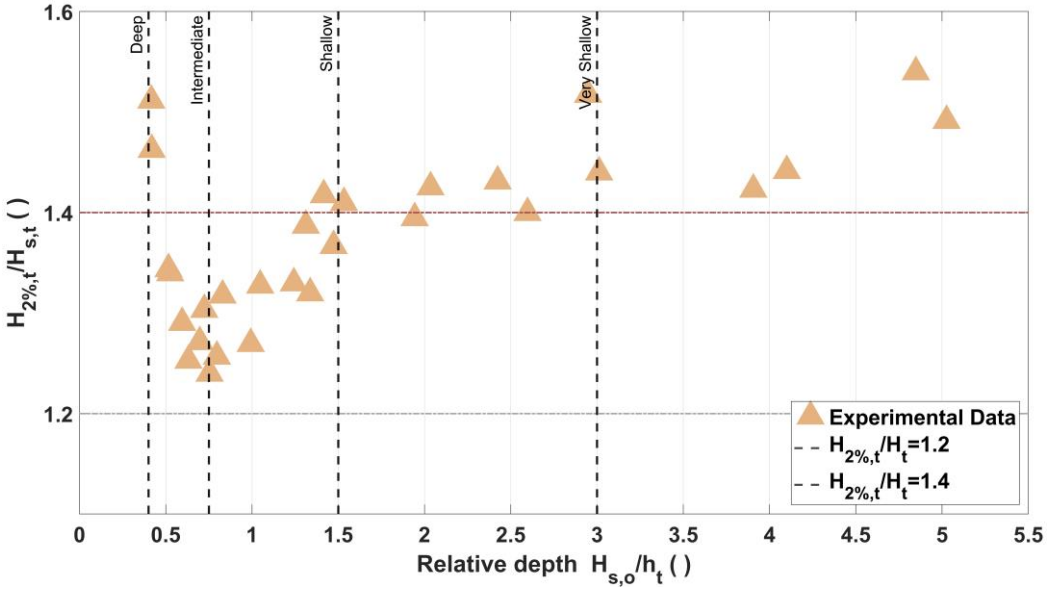

Figure 43 The influence of the shallow water conditions on the ratio $H_{2\%,t}/H_{s,t.}$

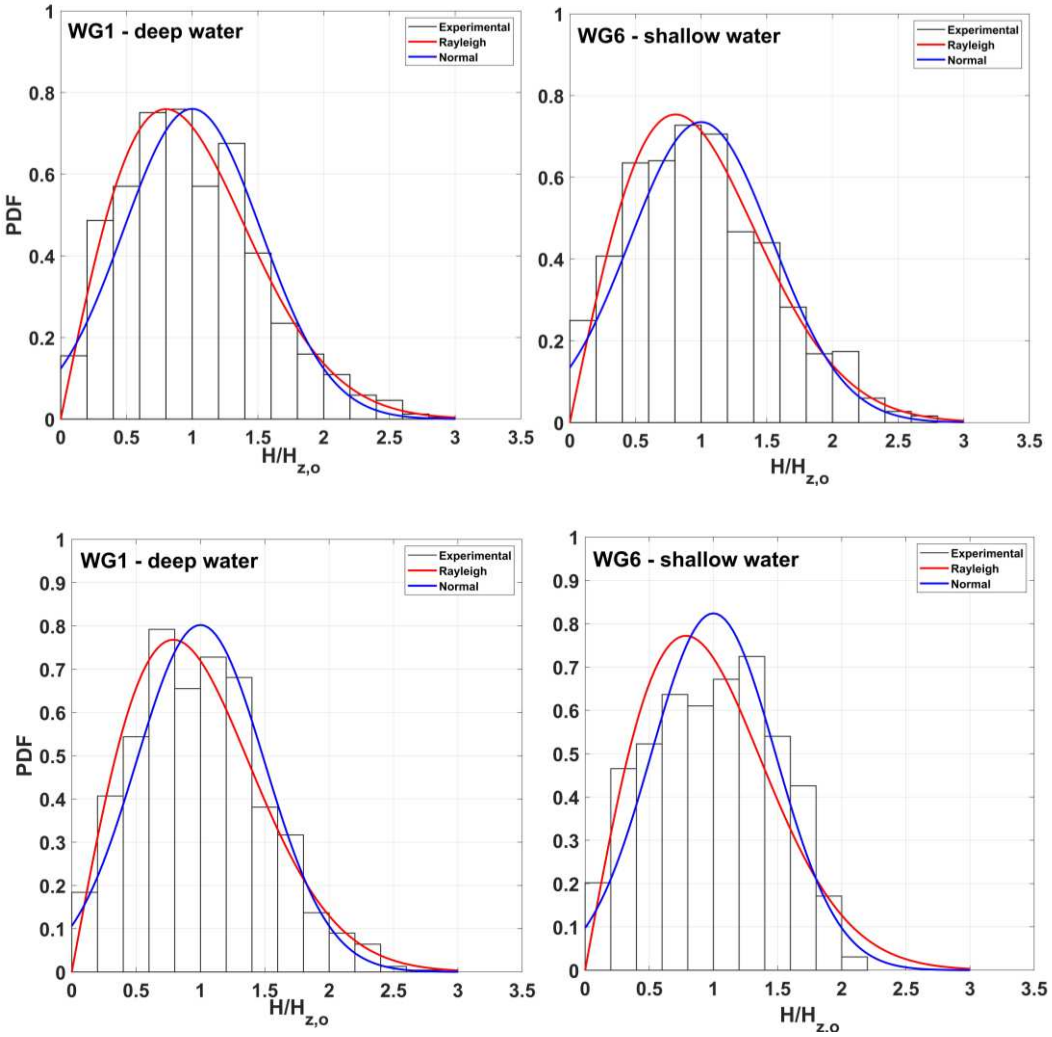

Figure 44 Top: Wave height distribution evaluated at two different locations along the wave flume for test serie WL4 with Hm0,o=0,25 m and Tp = 2,83 s; Bottom: Wave height distribution retrieved at two different locations along the wave flume for test serie WL1 with Hm0,o=0,25 m and Tp = 2,83 s.

As suggested in Eldrup & Andersen (2019), the influence of different wave height parameters, namely H_{m0}, H_s and $H_{2\%}$, on the stability numbers in depth limited water conditions has been investigated. In Figure 45 the calculated stability numbers (y-axis),

varying the characteristic wave height, have been compared with the use of the present data and with respect to the breaker parameter (x-axis). The data presents an important scatter especially when the Iribarren number becomes greater than 10. Contrarily, to what has been achieved in (Eldrup & Andersen (2019); Herrera et al. (2017)), with the present data the scatter is reduced by using H_s in the stability number.

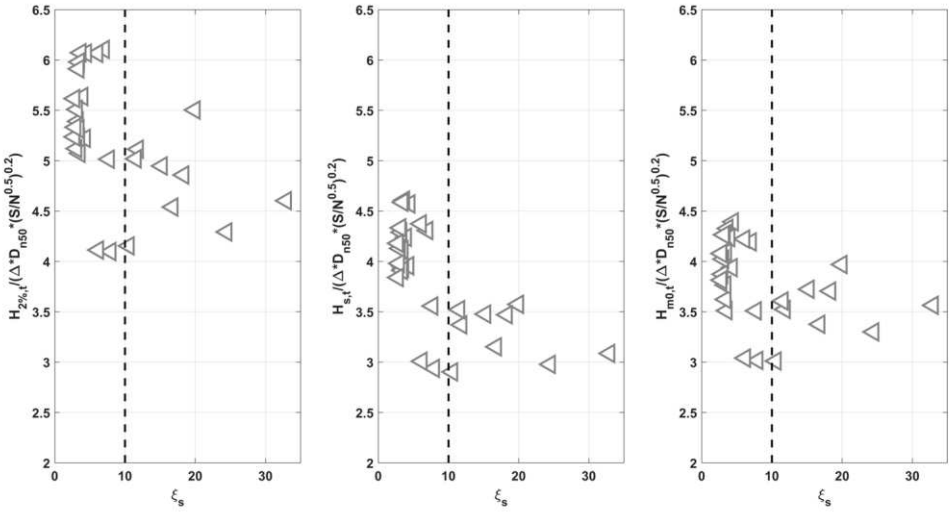

Figure 45 The experimental data compared to stability numbers with different wave characteristics, $H_{2\%}$, H_s and H_{m0}, respectively from left to the right.

A qualitative comparison of measured and predicted stability numbers by means Eq.(2. 16) is reported in Figure 45. The present data have been classified both on the basis of the number of waves (N_w) and value assumed by the mean breaker parameter (ξ_m where, the spectral wave period has been used in place of the mean one) with respect to the critical Iribarren number (ξ_{mc})(Eq. (2. 15)). The data in both the surging domain ($\xi_m > \xi_{mc}$) and the plunging domain ($\xi_m < \xi_{mc}$) are not well described by the formulation proposed in Van Gent et al. (2004). Concerning the data in the plunging domain, they are systematically underestimated, while the data in the surging domain are close to the perfect fitting line (solid black line) for low values of the stability number ($1.5 < Ns < 2$), and are totally scattered when Ns increase. A strong influence on this

behaviour can be associated with the spectral wave period at the structure toe and at the breaker parameter (Figure 40).

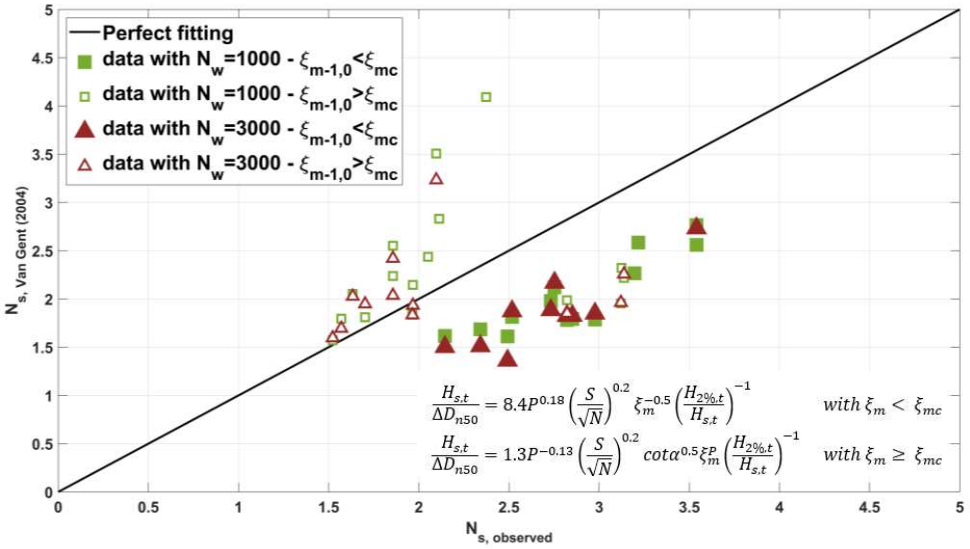

Figure 46 Comparison between observed and predicted stability numbers (Van Gent et al. (2004) Eq.(2. 16)). The solid black line represents a perfect agreement between the results.

In Figure 47 the dimensionless damage ($S/N_w^{0.5}$), has been plotted against the stability number, which has been retrieved by the Eq. (2. 17). In the analysis, the spectral wave height has been used instead of the statistical one, as suggested in Eldrup & Andersen (2019). Particularly, Figure 47 shows the data classified in terms of both water depth at the slope toe and rock armour diameter. The simple formula of Van Gent et al.(2004) doesn't match with the two higher water levels data. Nevertheless, it seems to be bias since the data for the two higher water levels (red and orange square in the graph) are on the same trendline but with another coefficient (2.3 instead of 1.75). Vice versa, the data at the lower water levels (black and blue squares) are quite well estimate from the Van Gent formulation.

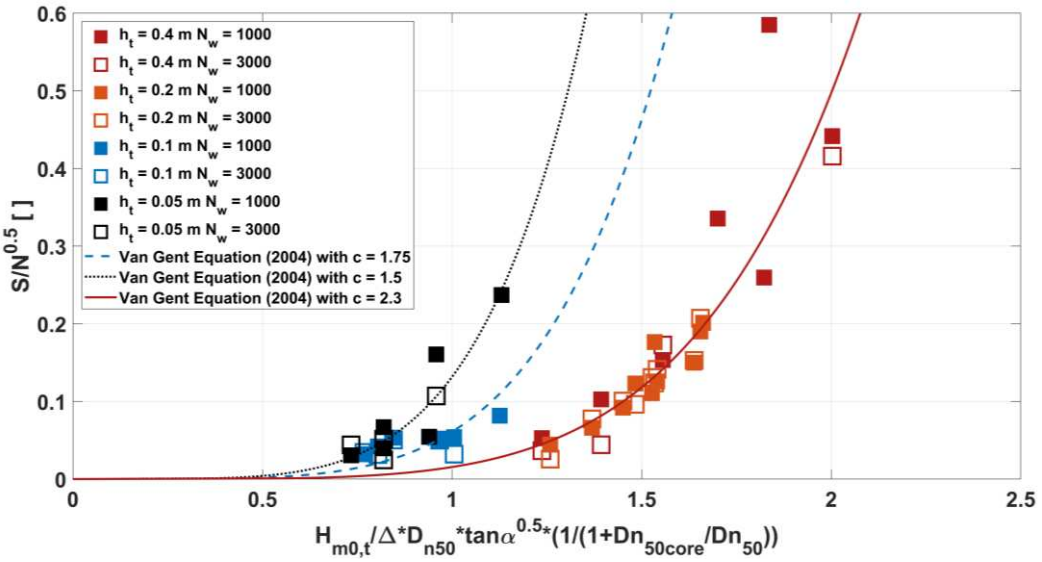

Figure 47 The experimental damage data classified in terms of water depth h_t and rock armour diameter D_{n50},plotted by using the equation (2. 17) reported in Van Gent et al. (2004).

In Figure 48 (top) the present data have been plotted together with both the data and the formula curve of Van Gent et al. (2004) (black solid line), which tends to overestimate the present dataset. In Figure 48.(bottom figure) only the data acquired in deeper water conditions have been reported, which are good correlated, but as the damage increase they are overestimated by the empirical formulation (Eq.(2. 17)).
The shape of the curve (solid black line), is governed by both an exponential (a = 0.2) and multiplying parameter (b = 1.75) (Eq.(2. 17)). Instead, the blue line shows the fitting of the present data,, with the respect to the dataset of Van Gent et al. (2004), for which the derived coefficient of determination, R^2, is 0.806 and the root mean square error (RMSE) is 0.198. The new curve parameters, *a* and *b*, have been retrieved by means a nonlinear regression analysis and they are respectively equal to 0.24 and 1.86, close to the ones reported in Eq.(2. 17).The above mentioned data overestimation can be explained due to the wave breaking that occur along the foreshore which dissipate

part of the wave energy. A greater hydraulic stability implies that the weight of individual rock armour units can be reduced for the design of a rubble mound breakwater.

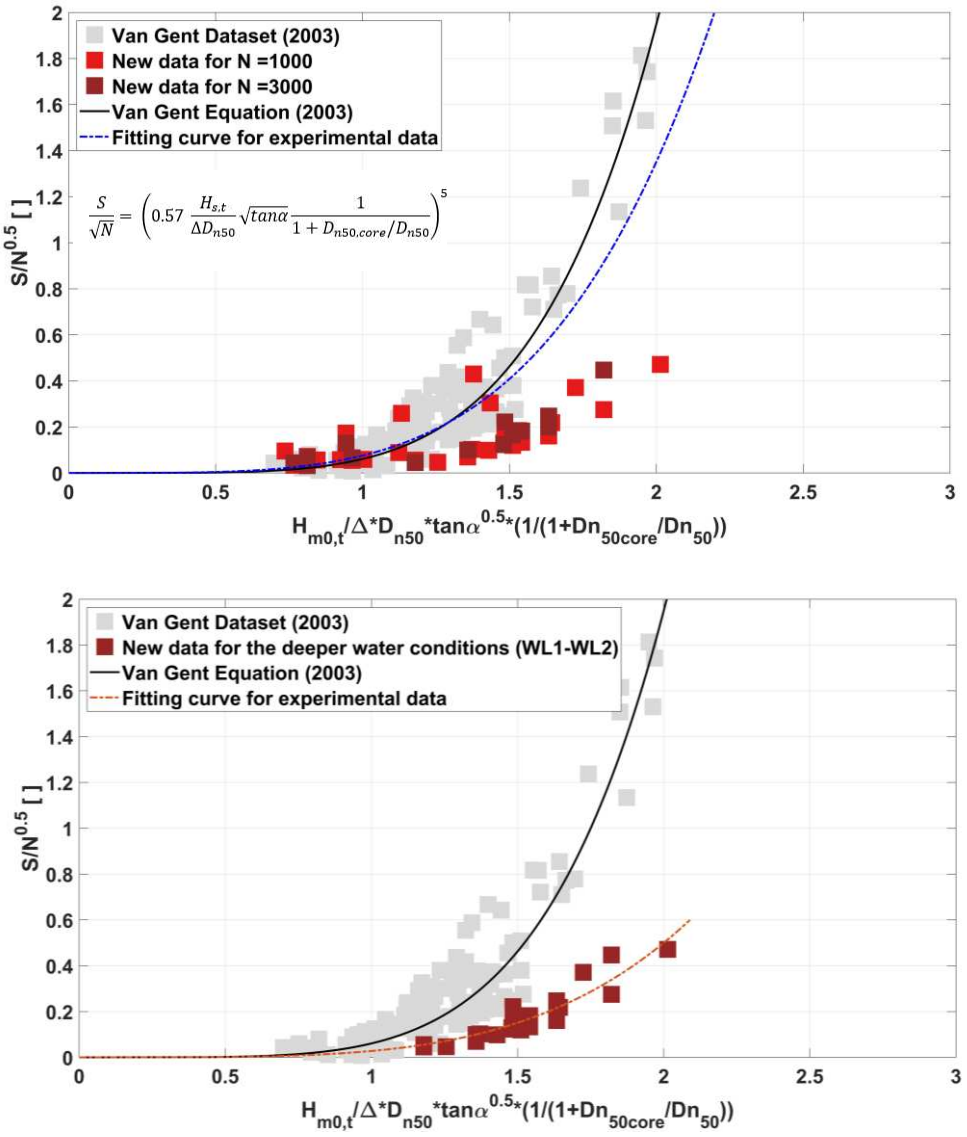

Figure 48 Top: Present data compared to design formula and data by Van Gent et al. (2004) (2. 17); Bottom: Data in the deeper water conditions tested (Test Serie WL1 and WL2), compared to design formula.

Moreover, the acquired dimensionless damage ($S/N_w^{0.5}$), has been plotted against the stability number, retrieved by using the Eq.(2. 19). For all the tests, the calculated breaker parameter has been found to be greater than the critical one reported in Eq.(2. 20), so the slope breakwater stability has been evaluated by using the equation for surging condition. Particularly, Figure 49 shows the data classified in terms of both water depth at the slope toe and rock armour diameter. The notional permeability reported in Eldrup formula has been assumed to be equal to 0.4 on the basis of the employed rocks characteristics. The formulation that has been shown in Eldrup & Andersen (2019) is really easy to use, anyway, as for the Van Gent formula, it seems to be bias, since almost all the data (for the different tested water conditions) are on the same trendline but with an higher coefficient (4 instead of 3.1).

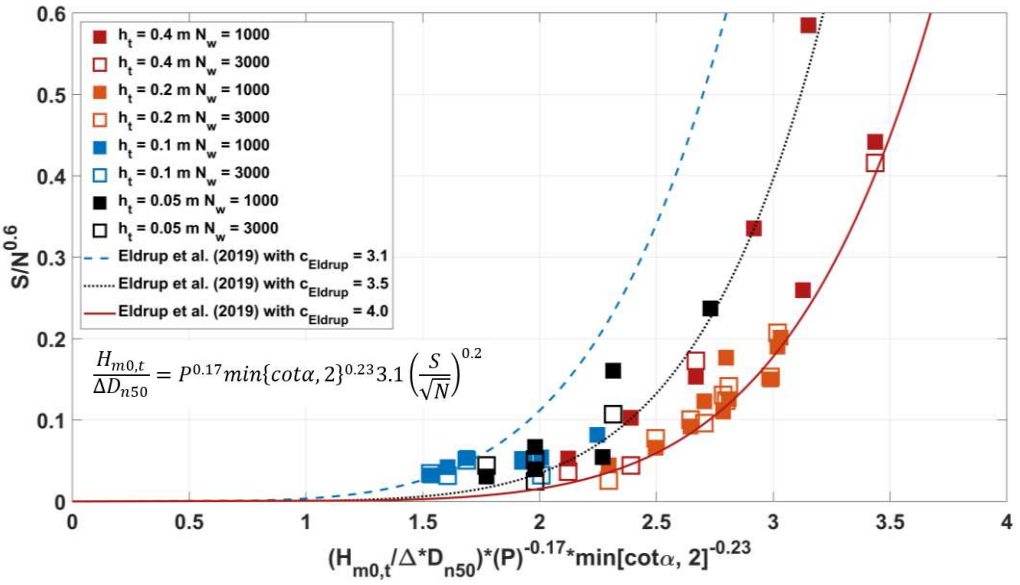

Figure 49 The experimental damage data classified in terms of water depth h_t and rock armour diameter D_{n50},plotted by using the equation (2. 19) reported in Eldrup et al. (2019).

Finally, in Figure 50 has been also checked whether there is a match with the formula by Etemad-Shahidi et al. (2020). For the highest water level ($h_t = 0.4$ m), the match is

very good (red square, while the dashed blue line represents the theoretic Eq.(2. 21)). Instead, for the lower water levels, there is a clear deviation due to the influence of the water depth, and all related parameters. The data seem highly stratified by using this formula.

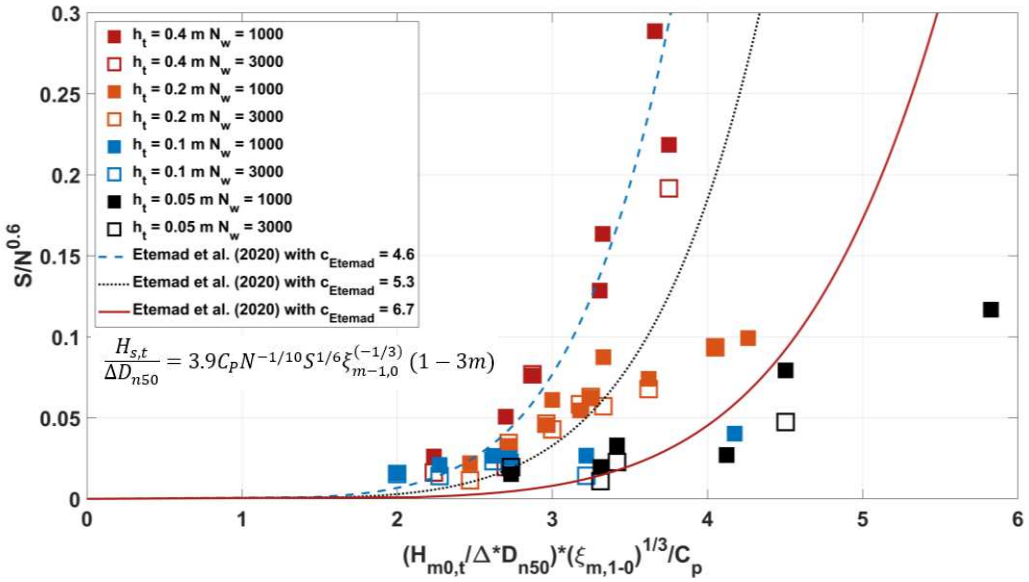

Figure 50 The experimental dam age data classified in terms of water depth h_t and rock armour diameter D_{n50},plotted by using the equation (2. 21) reported in Etemad et al. (2020).

CHAPTER 5
CONCLUSIONS AND FUTURE REMARKS

5 Conclusion and future remarks

In the present research, an alternative photogrammetry-based method for evaluating the damage of a rubble mound breakwater induced by wave action is proposed. The photogrammetric technique has been validated during the here discussed experimental campaign. During the tests, the temporal evolution of the damaged structure caused by wave action has been measured by means of both laser profiler and photogrammetry. With respect to the expensive and time-consuming profiling system, results demonstrate that the photogrammetric damage assessment can easily provide the extent as well as the magnitude of the damage, which is useful to improve the design of future defence structures with high accuracy level. Indeed, the photogrammetric survey allows to reconstruct a 3D model of the breakwater, starting from 2D images acquired with a standard digital camera.

Specifically, digital acquisitions yielded reality-based data of the physical model in the form of point clouds, before and after the execution of each test, enabling the reconstruction and analysis of 2D/3D outputs, corresponding to transversal profiles and 3D deviation maps, respectively. The effectiveness of the proposed method has been verified, by matching transects retrieved from the two techniques, for the quantification of 2D eroded and accreted areas. This approach supplies reliable data, in terms of quality, accuracy and repeatability of measurements, with readily available, easy-to-use and cost-effective instrumentation.

Moreover, 3D damaged areas have been quantified through a change detection analysis and segmentation of points clouds. The three-dimensional evolution of eroded areas could be of particular interest in the field of three-dimensional physical modelling, resulting in the computation of the exact extension of damaged regions, for example, in the presence of oblique wave attacks. Indeed, it allows to determine the long-term behaviour and stability of the structure and can provide information on the amount of material that has been removed from the structure, the rate at which the erosion is occurring, and the potential for the erosion to cause the structure to fail.

Another advantage of the photogrammetric technique is represented by its applicability and adaptability on a large scale, which makes it suitable in field monitoring applications (i.e. with unmanned aerial vehicles, UAV). In this regard, it could be valuable to further investigate 3D reconstructions also in presence of water, whose effects must be taken into account in order to produce accurate results. Water can distort the shapes of objects, cause light to be reflected in unexpected ways, and create glare that makes it difficult to see details. As future remarks, the training of a neural network with all the images collected within the photogrammetric process can be a very useful tool for the identification of different damage levels. By using all the collected images, the neural network would be able to learn the different features of each damage level and afterward be able to accurately classify them.

Dynamic pore pressure measurements inside the breakwater core have been performed during the experimental activities. Two different water levels have been tested to induce depth-limited water conditions, and 20 tests (regular and irregular) have been run. After the acquisition phase, an intensive post-processing phase (i.e., data filtering, signal denoising, depuration from the wave setup, etc.), followed by the time series analysis (in the time and frequency domains), has been performed for both free surface elevations and pore pressure fluctuations.

In conclusion, a new experimental campaign, aimed at studying the hydraulic stability of a 2D physical model of a rubble mound breakwater in water depth-limited conditions, has been carried out at EUMER laboratory (University of Salento, Lecce Italy). In accordance with the actual shallowness classification (van Gent & Doorn (2001)), new data have been obtained in extremely shallow waters ($h_r > 3$ and $\xi_{m-1,0}>10$). The observed damage level has been compared with the existing formulae suitable for shallow water conditions. The equations reported in Van Gent et al. (2004) (Eq.(2. 16)and Eq.(2. 17)) have shown that the measured stability number is overestimated by both the formulations. Eq. (2. 17) seems to carefully match the data in the shallowest condition. It is worth saying that the present data seem to be clustered in two different groups, one with a rather reasonable match with the formula (Eq.(2. 17)) (shallowest

conditions) and one showing less damage than the formula predicts (deeper-water conditions Figure 48.c). This behaviour needs to be further investigated. A slight modification of Eq. (2. 17) has been applied to fit the present data together with the hydraulic stability dataset analysed in Van Gent et al. (2004).

The formula of Etemad et al.(2020) shows that for the highest water level ($h_t = 0.4$ m), the match is very good whereas, for the lower water levels, there is a clear deviation due to the influence of the water depth, and all related parameters. The data seem highly stratified by using this formula.

The best match with the acquired data is ensured by the application of the Eldrup formula that among the other things, it is prove to be easy to apply. As for the Van Gent formula, it seems to be bias, since almost all the data (for the different tested water conditions) are on the same trendline but with an higher coefficient (4 instead of 3.1).

Then, the data acquired didn't suggest to introduce a new stability formulation but rather to re-calibrated the existing ones here analysed by taking into account both the new acquired data, which allow to widen the applicability range in relation to values of relative depth, ($h_r > 3$) and the existing hydraulic stability datasets in shallow water conditions. Further insights on the effect of the wave period on the hydraulic stability in depth-limited water conditions should be investigated by focusing on the low frequency energy spectrum.

Acknowledgments

Here we are, the last step of an important trip for my life and career.
I would thank Prof. Leonardo Damiani for all the opportunities he gave me during these three years, he supported my initiatives with effective tips.
Since the day I applied for the Ph.D. position I always said that I was doing it, among the other things, to get the opportunity to work with Alessandra. Despite some divergencies that we had, we have and will have, I consider her my mentor who followed all my steps trying to drive me through difficulties of the academic environment. She involved me in many activities, dragging me with her passion for research, and for the best that I could, I tried to be at her side.
Furthermore, I would like to thank Prof.ssa Maria Clavero who hosted me at CEAMA institution at the University of Granada, she appreciated the work that I was doing and motivated my research.
I enjoyed a lot attending the campus that besides, is the place where I met Rosella and beyond the fact she is a valuable colleague, if you are reading these lines you probably know what she represents for me. Every day, she showed me the strength of a woman, able to face the fears more than I was capable. She helped me to focus on my goals, especially when all the ways seemed insurmountable. She tolerated me and understood my dark moments, and I am sure that I wouldn't have gone so far without her. So, I am deeply thankful to you, Ros.
During these years I met new interesting friends (among the others, Giulia, Alessandro, Giulio, Virginia, Francesco, Antonella, Pasquale) that, in different ways, have been part of this "journey". Instead, sometimes I faced people whose behaviour crashes you and make you lose confidence in your abilities. Sometimes, these people makes the academic environment a gloomy place, but I learned to focus only on the nice things that the research gives you.

In the end, I have to say thank you to my parents and my sister, I am sure that not always they have totally comprehended what I was doing at the University (for my fault), but besides this, they showed me all their support. A big thanks to my brother who almost every days critically listened to my doubts or troubles, he supported my choices by trying to give me some wise tips.

Bibliography

Ahrens, J.P., 1989. Stability of Reef Breakwaters. J. Waterw. Port, Coastal, Ocean Eng. 115, 221–234. https://doi.org/10.1061/(asce)0733-950x(1989)115:2(221)

Altomare, C., Suzuki, T., Chen, X., Verwaest, T., Kortenhaus, A., 2016. Wave overtopping of sea dikes with very shallow foreshores. Coast. Eng. 116, 236–257.

Aragón, E., Munar, S., Rodr\'\iguez, J., Yamafune, K., 2018. Underwater photogrammetric monitoring techniques for mid-depth shipwrecks. J. Cult. Herit. 34, 255–260.

Argente, G., Gómez-Martín, M.E., Medina, J.R., 2018. Hydraulic stability of the armor layer of overtopped breakwaters. J. Mar. Sci. Eng. 6, 1–13. https://doi.org/10.3390/jmse6040143

Aristodemo, F., Ianchello, M., Fallico, C., 2018. Smoothing analysis of slug tests data for aquifer characterization at laboratory scale. J. Hydrol. 562, 125–139.

Atkinson, A., Baldock, T.E., 2016. A high-resolution sub-aerial and sub-aqueous laser based laboratory beach profile measurement system. Coast. Eng. 107, 28–33.

Battjes, J.A., 1974. Surf Similarity. Coast. Eng. 1974 1, 1(14), 26. https://doi.org/10.9753/icce.v14.26.

Battjes, J.A., Groenendijk, H.W., 2000. Wave height distributions on shallow foreshores. Coast. Eng. 40, 161–182.

Besl, P.J., McKay, N.D., 1992. A method for registration of 3-D shapes. IEEE Trans. Pattern Anal. Mach. Intell. 14, 239–256. https://doi.org/10.1109/34.121791

Bonakdar, L., Oumeraci, H., Etemad-Shahidi, A., 2015. Wave load formulae for prediction of wave-induced forces on a slender pile within pile groups. Coast. Eng. 102, 49–68.

Bosch, J., Staffell, I., Hawkes, A.D., 2018. Temporally explicit and spatially resolved global offshore wind energy potentials. Energy 163, 766–781. https://doi.org/10.1016/j.energy.2018.08.153

Broderick, L., 1984. Riprap stability versus monochromatic and irregular waves. Behav. Ecol. Sociobiol. 415–420.

Burcharth, H.F., Andersen, O.K., 1995. On the one-dimensional steady and unsteady porous flow equations. Coast. Eng. 24, 233–257.

Burcharth, H.F., Kramer, M., Lamberti, A., Zanuttigh, B., 2006. Structural stability of detached low crested breakwaters. Coast. Eng. 53, 381–394.

Bürger, W., Oumeraci, H., Partenscky, H.W., 1988. Ceohydraulic investigations of

rubble mound breakwaters, in: Coastal Engineering 1988. pp. 2242–2256.
Campos, Á., Molina-Sanchez, R., Castillo, C., 2020. Damage in rubble mound breakwaters. Part II: Review of the definition, parameterization, and measurement of damage. J. Mar. Sci. Eng. 8, 306.
Chen, X., Hofland, B., Altomare, C., Suzuki, T., Uijttewaal, W., 2015. Forces on a vertical wall on a dike crest due to overtopping flow. Coast. Eng. 95, 94–104.
Chen, X., Hofland, B., Uijttewaal, W., 2016. Maximum overtopping forces on a dike-mounted wall with a shallow foreshore. Coast. Eng. 116, 89–102.
CIRIA, CUR, CUTMEF, 2007. The rock manual: the use of rock in Hydraulic engineering. CIRIA.
Collins, J.I., 1970. Probabilities of breaking wave characteristics. Coast. Eng. Proc. 25.
Dai, Y. Ben, Kamel, A.M., 1969. Scale effect tests for rubble-mound breakwaters: Hydraulic model investigation. US Army Engineer Waterways Experiment Station.
Dally, W.R., 1992. Random breaking waves: Field verification of a wave-by-wave algorithm for engineering application. Coast. Eng. 16, 369–397.
Dally, W.R., 1990. Random breaking waves: a closed-form solution for planar beaches. Coast. Eng. 14, 233–263.
Dally, W.R., Dean, R.G., 1986. Transformation of random breaking waves on surf beat. Coast. Eng. Proc. 9.
Eldrup, M.R., Andersen, T.L., 2019. Extension of shallow water rock armour stability formulae to nonlinear waves. Coast. Eng. 153, 103536.
Eldrup, M.R., Lykke Andersen, T., Burcharth, H.F., 2019. Stability of rubble mound breakwaters—A study of the notional permeability factor, based on physical model tests. Water 11, 934.
Etemad-Shahidi, A., Bali, M., van Gent, M.R.A., 2020. On the stability of rock armored rubble mound structures. Coast. Eng. 158, 103655.
EurOtop, 2018. The new EurOtop Neural Network tool for an improved prediction of wave overtopping, in: Coasts, Marine Structures and Breakwaters 2017: Realising the Potential. ICE Publishing, pp. 1227–1236.
Fortes, C., Lemos, R., Mendonça, A., Reis, M.T., 2019. Damage progression in rubble-mound breakwaters scale model tests, under a climate change storm sequence. Res. Eng. Struct. Mater. 5, 415–426.
Frostick, L.E., McLelland, S.J., Mercer, T.G., 2019. Users guide to physical modelling and experimentation: Experience of the HYDRALAB network. CRC Press.
Galantucci, R.A., Fatiguso, F., Galantucci, L.M., 2018. A proposal for a new standard quantification of damages of cultural heritages, based on 3D scanning. SCIRES-

IT-SCIentific Res. Inf. Technol. 8, 121–138.
Girardeau-Montaut, D., Roux, M., Marc, R., Thibault, G., 2005. Change detection on points cloud data acquired with a ground laser scanner. Int. Arch. Photogramm. Remote Sens. Spat. Inf. Sci. 36, W19.
Glavovic, B., Dawson, R., Chow, W., 2022. CCP2 Cities and Settlements by the Sea, Climate Change 2022: Impacts, Adaptation and Vulnerability. Contribution of Working Group II to the Sixth Assessment Report of the Intergovernmental Panel on Climate Change. https://doi.org/10.1017/9781009325844.019.2163
Glukhovskiy, B.K., 1966. Investigation of sea wind waves, in: Leningrad: Proc. of Sea Climatology Conference. pp. 51–71.
Goda, Y., 2000. Random Seas and Design of Maritime Structures, Adv. Ser. Ocean Eng 15, 443.
Goda, Y., 1975. Irregular wave deformation in the surf zone. Coast. Eng. Japan 18, 13–26.
Gong, Y., Zhang, F., Jia, X., Huang, X., Li, D., Mao, Z., 2021. Deep Neural Networks for Quantitative Damage Evaluation of Building Losses Using Aerial Oblique Images: Case Study on the Great Wall (China). Remote Sens. 13, 1321.
Grilli, E., Özdemir, E., Remondino, F., 2019. APPLICATION OF MACHINE AND DEEP LEARNING STRATEGIES FOR THE CLASSIFICATION OF HERITAGE POINT CLOUDS. Int. Arch. Photogramm. Remote Sens. \& Spat. Inf. Sci.
Guerra, M.G., Galantucci, R.A., 2020. Standard quantification and measurement of damages through features characterization of surface imperfections on 3D models: an application on Architectural Heritages. Procedia CIRP 88, 515–520.
Guerra, M.G., Lavecchia, F., Maggipinto, G., Galantucci, L.M., Longo, G.A., 2019. Measuring techniques suitable for verification and repairing of industrial components: A comparison among optical systems. CIRP J. Manuf. Sci. Technol. 27, 114–123.
Hallermann, N., Morgenthal, G., 2012. The application of unmanned aerial vehicles for the inspection of structures. Proc. PLSE 1085–1095.
Herrera, M.P., Gomez-Mart\'\in, M.E., Medina, J.R., 2017. Hydraulic stability of rock armors in breaking wave conditions. Coast. Eng. 127, 55–67.
Hofland, B., Chen, X., Altomare, C., Oosterlo, P., 2017. Prediction formula for the spectral wave period Tm-1,0 on mildly sloping shallow foreshores. Coast. Eng. 123, 21–28. https://doi.org/10.1016/j.coastaleng.2017.02.005
Hudson, R.Y., 1975. Reliability of rubble-mound breakwater stability models. US Army Engineer Waterways Experiment Station.

Hudson, R.Y., 1959. Laboratory investigation of rubble-mound breakwaters. J. Waterw. Harb. Div. 85, 93–121.

Hughes, S.A., 1993. Physical models and laboratory techniques in coastal engineering. World Scientific.

Iribarren, R., 1938. Una fórmula para el cálculo de los diques de escollera. Pasajes 160.

Iribarren, R., Nogales, C., 1952. Spanish practice in harbor design. Coast. Eng. Proc. 13.

James, M.R., Robson, S., 2014. Mitigating systematic error in topographic models derived from UAV and ground-based image networks. Earth Surf. Process. Landforms 39, 1413–1420.

Jensen, B., Christensen, E.D., Sumer, B.M., 2014. Pressure-induced forces and shear stresses on rubble mound breakwater armour layers in regular waves. Coast. Eng. 91, 60–75.

Jensen, O.J., Klinting, P., 1983. Evaluation of scale effects in hydraulic models by analysis of laminar and turbulent flows. Coast. Eng. 7, 319–329.

Jovančević, I., Pham, H.-H., Orteu, J.-J., Gilblas, R., Harvent, J., Maurice, X., Brèthes, L., 2017. 3D point cloud analysis for detection and characterization of defects on airplane exterior surface. J. Nondestruct. Eval. 36, 1–17.

Kamphuis, J.W., 2020. Introduction to coastal engineering and management. World Scientific.

Kamphuis, J.W., 2001. Designing for low frequency waves, in: Coastal Engineering 2000. pp. 1434–1447.

Kasireddy, V., Akinci, B., 2017. A case study on comparative analysis of 3D point clouds from UAV mounted and terrestrial scanners for bridge condition assessment, in: Proc. Lean \& Computing in Construction Congress (LC3), CIB W.

Koch, C., Georgieva, K., Kasireddy, V., Akinci, B., Fieguth, P., 2015. A review on computer vision based defect detection and condition assessment of concrete and asphalt civil infrastructure. Adv. Eng. Informatics 29, 196–210.

Kuriyama, Y., 1996. Models of wave height and fraction of breaking waves on a barred beach. Coast. Eng. Proc.

Lague, D., Brodu, N., Leroux, J., 2013. Accurate 3D comparison of complex topography with terrestrial laser scanner: Application to the Rangitikei canyon (NZ). ISPRS J. Photogramm. Remote Sens. 82, 10–26.

Lashley, C.H., Van Der Meer, J., Bricker, J.D., Altomare, C., Suzuki, T., Hirayama, K.,

2021. Formulating wave overtopping at vertical and sloping structures with shallow foreshores using deep-water wave characteristics. J. Waterw. Port, Coastal, Ocean Eng. 147, 4021036.

Lavecchia, F., Guerra, M.G., Galantucci, L.M., 2018. Performance verification of a photogrammetric scanning system for micro-parts using a three-dimensional artifact: adjustment and calibration. Int. J. Adv. Manuf. Technol. 96, 4267–4279.

Lavecchia, F., Guerra, M.G., Galantucci, L.M., 2017. The influence of software algorithms on photogrammetric micro-feature measurement's uncertainty. Int. J. Adv. Manuf. Technol. 93, 3991–4005. https://doi.org/10.1007/s00170-017-0786-z

Law, A.C.C., Southon, N., Senin, N., Stavroulakis, P., Leach, R., Goodridge, R., Kong, Z., Team, M.M., 2018. Curvature-based Segmentation of Powder Bed Point Clouds for in-Process Monitoring.

Longuet-Higgins, M.S., 1952. On the statisticaldistribution of the height of sea waves. JMR 11, 245–266.

Losada, M.Á., 2021. Method to assess the interplay of slope, relative water depth, wave steepness, and sea state persistence in the progression of damage to the rock layer over impermeable dikes. Ocean Eng. 239, 109904.

Luhmann, T., Robson, S., Kyle, S., Boehm, J., 2019. Close-range photogrammetry and 3D imaging, in: Close-Range Photogrammetry and 3D Imaging. de Gruyter.

Mansard, E.P.D., Funke, E.R., 1980. The measurement of incident and reflected spectra using a least squares method, in: Coastal Engineering 1980. pp. 154–172.

Marcou, C., 1954. Spending beaches for a wave canal. Coast. Eng. Proc. 20.

Marino, S., Scaravaglione, G., Francone, A., Valentini, N., Saponieri, A., Damiani, L., Van Gent, M.R.A., Tomasicchio, G.R., 2022. Laboratory investigation on armour stability for extremely shallow water conditions. Proc. 39th IAHR World Congr.

Mase, H., Iwagaki, Y., 1982. Wave height distribution and wave grouping in surf zone. Coast. Eng. Proc. 4.

Miche, M., 1944. Mouvements ondulatoires de la mer en profondeur constante ou décroissante. Annales de Ponts et Chaussées.

Mishra, M., 2020. Machine learning techniques for structural health monitoring of heritage buildings: A state-of-the-art review and case studies. J. Cult. Herit.

Mitra, S.K., Kuo, Y., 2006. Digital signal processing: a computer-based approach. McGraw-Hill New York.

Morlet, J., Arens, G., Fourgeau, E., Giard, D., 1982. Wave propagation and sampling theory—Part II: Sampling theory and complex waves. Geophysics 47, 222–236.

Munk, W.H., 1951. Origin and generation of waves.

Musicco, A., Galantucci, R.A., Bruno, S., Verdoscia, C., Fatiguso, F., 2021. Automatic Point Cloud Segmentation for the Detection of Alterations on Historical Buildings Through AN Unsupervised and Clustering-Based Machine Learning Approach. ISPRS Ann. Photogramm. Remote Sens. Spat. Inf. Sci. 2, 129–136.

Musumeci, R.E., Moltisanti, D., Foti, E., Battiato, S., Farinella, G.M., 2018. 3-D monitoring of rubble mound breakwater damages. Measurement 117, 347–364.

Napolitano, R.K., Glisic, B., 2017. Minimizing the adverse effects of bias and low repeatability precision in photogrammetry software through statistical analysis. J. Cult. Herit. https://doi.org/10.1016/j.culher.2017.11.005

Pörtner, H.-O., Roberts, D.C., Adams, H., Adler, C., Aldunce, P., Ali, E., Begum, R.A., Betts, R., Kerr, R.B., Biesbroek, R., others, 2022. Climate change 2022: Impacts, adaptation and vulnerability. IPCC Geneva, Switzerland:

Puente, I., Sande, J., González-Jorge, H., Peña-González, E., Maciñeira, E., Mart\'\inez-Sánchez, J., Arias, P., 2014. Novel image analysis approach to the terrestrial LiDAR monitoring of damage in rubble mound breakwaters. Ocean Eng. 91, 273–280.

Rabinovich, A.B., 2009. Handbook of coastal and ocean engineering. Singapore. World Sci. Publ.

Saponieri, A., Valentini, N., Di Risio, M., Pasquali, D., Damiani, L., 2018. Laboratory investigation on the evolution of a sandy beach nourishment protected by a mixed soft-hard system. Water (Switzerland) 10, 1–23. https://doi.org/10.3390/w10091171

Savitzky, A., Golay, M.J.E., 1964. Smoothing and differentiation of data by simplified least squares procedures. Anal. Chem. 36, 1627–1639.

Scaravaglione, G., Marino, S., Damiani, L., Francone, A., Saponieri, A., Tomasicchio, G.R., 2022. Experimental study on pore pressure attenuation in rubble mound breakwater in depth-limited water conditions, in: 2022 IEEE International Workshop on Metrology for Living Environment (MetroLivEn). pp. 197–202.

Schenk, T., 2005. Introduction to Photogrammetry, Department of Civil and Environmental Engineering and Geodetic Science, The Ohio State University.

Smith, G., Wallast, I., van Gent, M.R.A., 2003. Rock slope stability with shallow foreshores, in: Coastal Engineering 2002: Solving Coastal Conundrums. World Scientific, pp. 1524–1536.

Suzuki, T., Altomare, C., Veale, W., Verwaest, T., Trouw, K., Troch, P., Zijlema, M., 2017. Efficient and robust wave overtopping estimation for impermeable coastal

structures in shallow foreshores using SWASH. Coast. Eng. 122, 108–123. https://doi.org/10.1016/j.coastaleng.2017.01.009

Thompson, D.M., Shuttler, R.M., 1975. Riprap design for wind-wave attack, a laboratory study in random waves. HR Wallingford report EX707, UK.

Thornton, E.B., Guza, R.T., 1983. Transformation of wave height distribution. J. Geophys. Res. Ocean. 88, 5925–5938.

Tørum, A., Mathiesen, B.J., Escutia, R., 1979. Reliability of breakwater model tests, in: Coastal Structures' 79. pp. 454–469.

Valentini, N., Balouin, Y., 2020. Assessment of a smartphone-based camera system for coastal image segmentation and sargassum monitoring. J. Mar. Sci. Eng. 8, 23.

Valentini, N., Saponieri, A., Damiani, L., 2017. A new video monitoring system in support of Coastal Zone Management at Apulia Region, Italy. Ocean \& Coast. Manag. 142, 122–135.

Valero, E., Forster, A., Bosché, F., Hyslop, E., Wilson, L., Turmel, A., 2019. Automated defect detection and classification in ashlar masonry walls using machine learning. Autom. Constr. 106, 102846.

Valero, E., Forster, A., Bosché, F., Renier, C., Hyslop, E., Wilson, L., 2018. High level-of-detail BIM and machine learning for automated masonry wall defect surveying, in: Proceedings of the International Symposium on Automation and Robotics in Construction, Berlin, Germany. pp. 20–25.

van der Meer, J., 2021. Rock Armour Slope Stability under Wave Attack; the Van der Meer Formula revisited.

van der Meer, J.W., 1988. Deterministic and probabilistic design of breakwater armor layers. J. Waterw. port, coastal, Ocean Eng. 114, 66–80.

Van Gent, M.R.A., 2000. Wave run-up on dikes with shallow foreshores. Coast. Eng. 2000 - Proc. 27th Int. Conf. Coast. Eng. ICCE 2000 276. https://doi.org/10.1061/40549(276)159

Van Gent, M.R.A., 1999. Physical model investigations on coastal structures with shallow foreshores: 2D model tests on the Petten sea-defence. H3129.

van Gent, M.R.A., Doorn, N., 2001. Numerical model simulations of wave propagation and wave run-up on dikes with shallow foreshores, in: Coastal Dynamics' 01. pp. 769–778.

Van Gent, M.R.A., Smale, A.J., Kuiper, C., 2004. Stability of rock slopes with shallow foreshores, in: Coastal Structures 2003. pp. 100–112.

Van Gent, M.R.A., Smith, G.M., 1999. Physical model investigations on coastal

structures with shallow foreshores: 2D model tests with single and double-peaked wave energy spectra.

van Gent, M.R.A., van der Werf, I.M., 2014. Rock toe stability of rubble mound breakwaters. Coast. Eng. 83, 166–176.

Vanneste, D., Troch, P., 2012. An improved calculation model for the wave-induced pore pressure distribution in a rubble-mound breakwater core. Coast. Eng. 66, 8–23.

Vidal, C., 1992. A UNIVERSAL ANALYSIS FOR THE STABILITY OF BOTH LOW-CRESTED AND SUBMERGED BREAKWATERS 1679–1692.

Vidal, C., Martin, F.L., Negro, V., Gironella, X., Madrigal, B., Garc\'\ia-Palacios, J., 2004. Measurement of armor damage on rubble mound structures: comparison between different methodologies, in: Coastal Structures 2003. pp. 189–200.

Vidal, C., Medina, R., Lomónaco, P., 2006. Wave height parameter for damage description of rubble-mound breakwaters. Coast. Eng. 53, 711–722.

Waas, M., Zell, D., 2013. Practical 3D photogrammetry for the conservation and documentation of Cultural Heritage, in: International Conference on Cultural Heritage and New Technologies, Vienna.

Wang, Y., Witten, I.H., 1996. Induction of model trees for predicting continuous classes.

Wellens, P., Van Gent, M., 2012. Wave-induced setup inside permeable structures. Coast. Eng. 2.

Annex 1 – Longitudinal sections of the wave flume

CURRICULUM VITAE

Eng. Stefano Marino

Mobile: +39 3331217384
Mail: stefano.marino@poliba.it
Skype: ste.9104

ACADEMIC BACKGROUND

Ph.D Visiting period
University of Granada (Spain) \ *Laboratorio de Dinámica de Flujos Ambientales - Instituto Interuniversitario de Investigación del Sistema Tierra en Andalucía - Sede CEAMA* supervised by Prof.ssa Maria Clavero Gilabert \ February 2022 – July 2022

Polytechnic University of Bari
Ph.D. Candidate in "Risk and Environmental, Territorial and Building development" at Polytechnic University of Bari (Italy) \ Supervisors: Prof. L. Damiani and Prof. A. Saponieri \ November 2020 – present

My research field is focused on the study of the wave structure interaction through physical and numerical modelling. I spent more than a year working in a wave Flume at EUMER Laboratory (University of Salento, Lecce Italy). I investigated the rock slope stability in extremely shallow water conditions. I am developing a numerical model in OpenFOAM aimed at the study the hydrodynamic processes (e.g., heavy wave breaking) tested.

Research Fellowship
Polytechnic University of Bari (Italy)-DICATECh \ April 2019 November 2020

Involved in the Research Project **STIMARE** (Innovative Strategies for the monitoring and analysis of the coastal erosion risk) granted by the Italian Ministry of the Environment. The research was mainly focused on remote systems for coastal zone monitoring (e.g., video

systems, UAV, satellite imagery), physical modelling on alternative coastal defence intervention and numerical modelling on wave/structure interaction.

Polytechnic University of Bari

Master Science Degree in Environmental and Territory Engineering Polytechnic University of Bari (Italy) \ April 2017

Specialized in Maritime Hydraulic with a thesis titled " **Experimental and numerical analysis of the wave overtopping**", Supervisors: Prof. L. Damiani, Prof. A. Saponieri.

University of Ghent

Research Traineeship at the Department of Civil Engineering of Gent University (Belgium)\ June 2016 - August 2016

Experimental campaign on a 2-d physical model within the research project: **"Wave overtopping and wave forces. Results from experimental campaign Raversajide – Mariakerke – Wellington West"** funded by the Flanders Hydraulics Research. Enlarged knowledge about waves impact on structure, wave overtopping laboratory instruments, laboratory measurement techniques, data acquisition and processing.

TECHNICAL and COMPUTER SKILLS

- Program for data analysis and statistical computing, Matlab;
- Programming Language, a basic knowledge of Python;
- Microsoft office package (Power Point, Excel and Word);
- LateX;
- Numerical models as **SWASH** (Simulating WAves till SHore), **CFD model as OpenFOAM, Xbeach;**
- AutoCad, QGis

SEMINARS and CONFERENCES

- OpenFOAM Introductory online course, held by Wolf Dynamics Srl, Spin off University of Genova (Italy), October-November 2021
- OpenFOAM seminar, held by Dr. Javier Blasco, University of Zaragoza

and Organized by University of L'Aquila (Italy), September 2021;
- Workshop online "Wave Loads and Marine Walls" held by Deep Excavation LLD and Prof. William Allsop, May 5, 2021;
- Ph.D. Course "Water waves for the nearshore dynamics" by Prof. Maurizio Brocchini, University of Ancona (Italy), 20/22-27/29 April 2021;
- Presentation of the work "Studio sperimentale e numerico delle portate di tracimazione per opere verticali su bassi fondali" at the 37th Edition of the Italian conference Convegno Nazione di Idraulica e Costruzioni idrauliche 14-16 June 2021;
- Presentation of the work "Approccio numerico multi-layer per valutare gli impatti derivanti da moto ondoso su una struttura tracimabile" at the Convegno Nazionale di Studi Costieri, January 28, 2021;
- Presentation of the experimental and numerical results about the project "**Low Environmental Impact Solutions for beach nourishments protection**" at the **40th Edition of Italian conference on Integrated River basin Management** at Guardia Piemontese, Calabria, Italy June 20 ,2019;
- Third **CIRN** (Coastal Imaging Research Network) Boot camp & CoastSnap Users Group Meeting at **LEGOS** (Laboratoire d'Etudes en Géophysique et Océanographie Spatiales), Toulose, France | June 17-18, 2019;

PUBLICATIONS

Conference Papers

1. Marino, S., Damiani, L., Francone, A., Saponieri, A.. "Studio Sperimentale e Numerico delle portate di tracimazione per opere verticali su bassi fondali". XXXVII Convegno Nazionale di Idraulica e Costruzione Idrauliche (IDRA) – ISBN 9788894379914
2. Marino S. "Approccio numerico multi-layer per valutare gli impatti derivanti da moto ondoso su una struttura tracimabile." Convegno Nazionale di Studi Costieri 2021 (ISSN 1129-8588);
3. Marino S., Tomasicchio G.R., Damiani L., Francone A., Scaravaglione G., Saponieri A. "The influence of extremely shallow conditions on rock slope stability." 2nd Young Professional Congress IAHR (International Association

for Hydro-Environment Engineering and Research) (in press).(ISBN: 978-90-824846-7-0)

4. Marino, S., Scaravaglione, G., Francone, A., Valentini, N., Saponieri, A., Damiani, L., Van Gent, M.R.A., Tomasicchio, G.R., 2022. Laboratory investigation on armour stability for extremely shallow water conditions. Proc. 39th IAHR World Congress. 19 24 June 2022, Granada, Spain doi://10.3850/IAHR 39WC2521716X20221364 ;
5. Scaravaglione, G., Marino, S., Damiani, L., Francone, A., Saponieri, A., Tomasicchio, G.R., 2022. Experimental study on pore pressure attenuation in rubble mound breakwater in depth-limited water conditions, in: 2022 IEEE International Workshop on Metrology for Living Environment (MetroLivEn). pp. 197–202 DOI: 10.1109/MetroLivEnv54405.2022.9826926 (awarded as Best Paper Presented by a Young Researcher);
6. Marino S., Scaravaglione G., Tomasicchio G.R., Francone A., Damiani L. Saponieri A. “Laboratory study on rock slope stability in depth limited water conditions”. XXXVIII Convegno Nazionale di Idraulica e Costruzioni Idrauliche Reggio Calabria, Settembre 2022, (in press);
7. Scaravaglione G., Marino S., Saponieri A., Francone A., Damiani L., Tomasicchio G.R. “Studio sperimentale del campo di pressioni all’interno di una diga a gettata in condizioni di acque basse”. XXXVIII Convegno Nazionale di Idraulica e Costruzioni Idrauliche Reggio Calabria, Settembre 2022,” (in press).

Journal Papers

1. Marino S., Galantucci A.R., Saponieri A. “Measuring rock slope damage on rubble mound breakwater through digital photogrammetry” Measurement, 2023, 211 doi: /10.1016/j.measurement.2023.112656 .
2. Scaravaglione G., Marino S., Francone A., Damiani L., Tomasicchio G.R., Saponieri A. “Laboratory investigation on pore pressures inside a rubble mound breakwater in depth-limited waters” Submitted on Journal of Marine Science;

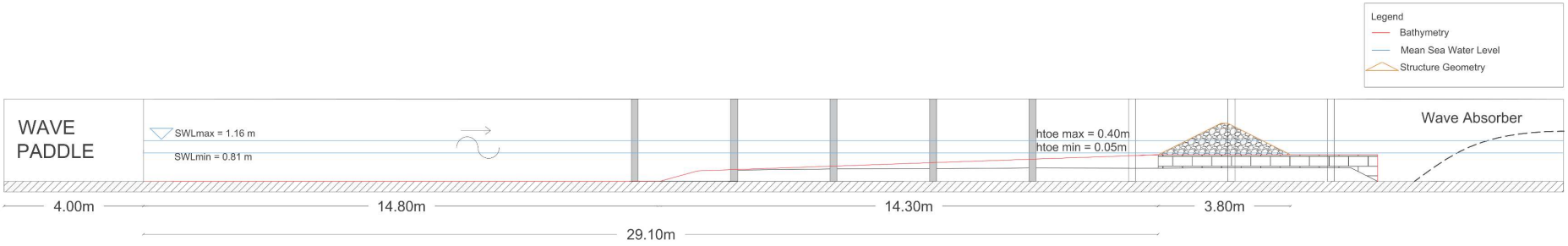
Legend
Bathymetry
Mean Sea Water Level
Structure Geometry
WAVE PADDLE
SWLmax = 1.16 m
SWLmin = 0.81 m
htoe max = 0.40m
htoe min = 0.05m
Wave Absorber
4.00m
14.80m
14.30m
3.80m
29.10m

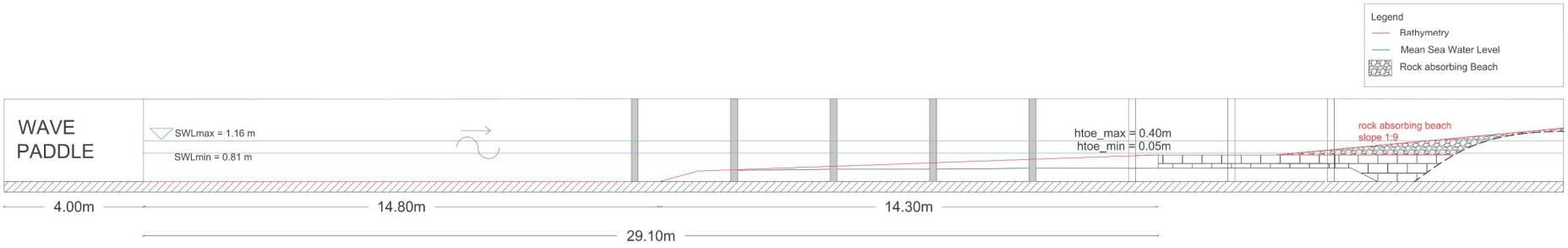
Legend
Bathymetry
Mean Sea Water Level
Rock absorbing Beach
WAVE PADDLE
SWLmax = 1.16 m
SWLmin = 0.81 m
htoe_max = 0.40m
htoe_min = 0.05m
rock absorbing beach
slope 1:9
4.00m
14.80m
14.30m
29.10m